



Hydrogel Adhesion

The Harvard community has made this article openly available. [Please share](#) how this access benefits you. Your story matters

Citation	Yang, Jiawei. 2019. Hydrogel Adhesion. Doctoral dissertation, Harvard University, Graduate School of Arts & Sciences.
Citable link	http://nrs.harvard.edu/urn-3:HUL.InstRepos:42106933
Terms of Use	This article was downloaded from Harvard University's DASH repository, and is made available under the terms and conditions applicable to Other Posted Material, as set forth at http://nrs.harvard.edu/urn-3:HUL.InstRepos:dash.current.terms-of-use#LAA

Hydrogel Adhesion

A dissertation presented

By

Jiawei Yang

to

The Harvard John A. Paulson School of
Engineering and Applied Sciences

in partial fulfillment of the requirements

for the degree of

Doctor of Philosophy

in the subject of

Engineering Science

Harvard University

Cambridge, Massachusetts

October 30, 2018

© 2018 – Jiawei Yang

All rights reserved.

Dissertation advisor:
Professor Zhigang Suo

Author:
Jiawei Yang

Hydrogel Adhesion

Abstract

Hydrogel adhesion, integrating hydrogels with a variety of materials, has advanced emerging technologies in the fields of functional materials, soft ionotronics and electronics, and biomedical applications. However, achieving strong adhesion between hydrogels and other materials is fundamentally challenging. This thesis explores various ways to develop chemistry of bonds, mechanics of dissipation, and topology of connecting materials to create strong hydrogel adhesion with diverse materials, and demonstrates potential applications in medicine and engineering.

In medical practices, strong adhesion between hydrogel and biological tissues is important. Existing adhesives are either cytotoxic, adhere weakly to tissues, or cannot be used in wet environments. We design a bio-inspired adhesives consisting of two layers: an adhesive layer made of polymer chains and a dissipative layer made of a hydrogel capable of dissipation. The polymer chains can interpenetrate into both hydrogel and tissue, and form electrostatic interactions, covalent bonds, and physical interpenetration with the polymer networks of the hydrogel and the tissue. The two layers synergistically lead to higher adhesion energy on various tissues than existing tissue adhesives. Adhesion occurs within minutes, independent of blood exposure, and compatible with *in vivo* dynamic movements.

This class of tough adhesive is promising in tissue adhesion, but the adhesion restricts to specific functional groups from both materials. To address this issue, we develop a topological adhesion that uses bio-compatible polymer chains to form a network, in topological

entanglement with the two polymer networks of the hydrogel and the tissue, stitching them together like a suture at the molecular scale. This approach does not require functional groups from both materials, and the interface is mechanically compatible with soft hydrogels and tissues. To illustrate the principle, pH is used to trigger several polymers to form networks, and strong adhesion can be created between hydrogels in full range of pH, and between hydrogels and tissues. The molecular suture can be further designed to be permanent, transient, or removable on-demand.

In developing the bonding methods so far, we realize the ways to achieve hydrogel adhesion multiply considerably by examining another aspect of adhesion: the topology of connecting materials. Topologies in existing methods are limited. Topologies of numerous varieties are possible, but have not been explored. To illustrate the potential, we delve into a specific bond-stitch topology, study its chemistry and physics, and highlight the synergy of chemistry, mechanics, *and* topology can enable strong adhesion between any hydrogels and any materials. The diversity of topologies benefits the adhesion to accommodate different materials and manufacturing processes, and also facilitates functional adhesion for various purposes.

We study the mechanics of adhesion. We conduct slow crack tests to identify the failure mechanism in the debonding of stitch-stitch topology. We also show that the hysteresis in the hydrogels greatly amplifies the energy release rate at high crack speed, but contributes negligibly to the energy release rate at low crack speed.

Hydrogel adhesion brings unprecedented capabilities and new opportunities. The field of innovation is wide open.

Table of Contents

Title page	i
Copyright page	ii
Abstract	iii
Table of Contents	v
Acknowledgements	ix
Chapter 1 Introduction	1
1.1 Diverse functions enabled by hydrogel adhesion	2
1.1.1 Hydrogel-tissue adhesion.....	2
1.1.2 Hydrogel-elastomer adhesion.....	3
1.1.3 Hydrogel adhesion with other materials	4
1.2 Manufacturing processes.....	6
1.3 Fundamental challenges in hydrogel adhesion.....	8
1.4 Topologies in hydrogel adhesion.....	11
1.5 The origin of adhesion energy	13
1.6 Hydrogel-tissue adhesion.....	18
1.6.1 Coating	18
1.6.2 Attaching.....	20
1.6.3 Piercing	21
1.7 Hydrogel-elastomer adhesion	27
1.7.1 Casting	28
1.7.2 Silane coupling method for casting, coating, printing and attaching.....	30
1.7.3 Gluing.....	31
1.8 Adhesion between hydrogels and other materials.....	34
1.8.1 Casting and coating.....	34

1.9 Design hydrogel adhesion for various purposes	36
1.10 Outline of the thesis	38
Chapter 2 Topological Adhesion of Wet Materials.....	40
2.1 Introduction.....	40
2.2 Results and discussion	41
2.3 Conclusion.....	52
Chapter 3 Tough Adhesives for Diverse Wet Surfaces	54
3.1 Introduction.....	54
3.2 Results and discussion	55
3.3 Conclusion.....	63
Chapter 4 Topologies of Wet Adhesion	64
4.1 Introduction.....	64
4.2 Results and discussion	66
4.3 Conclusion.....	75
Chapter 5 Conclusion and Outlook.....	77
Appendix A. Supporting information for Chapter 2	81
Materials.....	81
Methods.....	82
Figures	88
Tables	91
Movies	93
Appendix B. Supporting information for Chapter 3	94
Materials.....	94
Methods.....	95
Figures	106
Movies	122

Appendix C. Supporting information for Chapter 4	123
Materials.....	123
Methods.....	124
Figures	133
Tables	143
Movies	146
Bibliography	147

Dedicated to my beloved family

Acknowledgements

Please first allow me to turn back the clock to 7 years ago. At the time in 2011, I was a second-year graduate student in Tongji University, Shanghai, China. My research focused on solving the Eshelby's inclusion problem with imperfect interface between the inclusion and the body. The problem was not hard to me, and I quickly wrapped up and moved forward. During the time, two questions persisted hovering around my mind and puzzled me. What kind of research is worth doing? What can I do for the real world? With these two questions, I came to Harvard as visiting student in the fall of 2011, started to study the mechanics of instability in Prof. Zhigang Suo's group. I was always appreciated this beginning. My deepest gratitude is to my advisor Prof. Zhigang Suo, who offered me the opportunity and accepted me in 2011, and also, my gratitude goes to my advisor in Tongji University, Prof. Guohua Nie, who was supportive and understandable to my decision. In the two years, I was indulged in the rich academic environment, and learned a lot through working on several projects. When visiting ended, I was again deeply indebted to Prof. Zhigang Suo and Prof. John Hutchinson, who brought me back again to Harvard as a graduate student in 2014. Without them, I cannot be shaped as a real researcher and present the work in this dissertation.

Prof. Zhigang Suo is a critical-thinking researcher, remarkable teacher, and enthusiastic and patient mentor. He teaches me how to see the broader view of scientific problems, how to choose meaningful research topics, how to do research, and how to become an excellent researcher. He gives me freedom and encouragement to explore new field, without fear. Most importantly, he imparts the strength and faith to me and let me believe *we do research to change the world*. His creative-thinking, interactive teaching style, personality, passion and energy always motivate me, and I am very fortunate to carry those characteristics through my entire life.

I would thank Prof. John Hutchinson, who guides me in my early time at Harvard. His

deep and rich knowledge of mechanics is like a gold mine, which consistently prompts me to keep digging. He is kind and patient, and encourages me when I get lost in the research. I am grateful that he and Prof. Zhigang Suo guide me to finish my first project.

I would thank Prof. David Mooney, who provides me opportunities to closely interact with his students and postdocs, and attend his group seminars. I truly learn many aspects of tissue engineering through the group seminars, talking with peoples, and working together on several projects. Specifically, through the collaborative project (Chapter 3), I realize how mechanics can be used in the tissue engineering. Now I believe there must be many other fields that mechanics can play a role.

I am also thankful to Prof. Joost Vlassak, Prof. Ryan Hayward, and Prof. David Clarke, with whom I have the opportunity to work on many different projects, from finite element simulation to experiments. In talking with them, I really appreciate their wisdoms and scholarly.

I thank Prof. David Mooney, Prof. Joost Vlassak, Prof. John Hutchinson and Prof. James Rice for kindly agreeing to be on my PhD defense committee.

I have the privilege to work with many talented students and postdocs both in the group and outside the group, and we together produce many excellent research. In the work presented in this dissertation, I specially thank Ruobing Bai and Quansan Yang, who have devoted a great amount of effort, energy and patience into our projects. We have spent hundreds of days and nights together, working tirelessly in the laboratory. All the fruitful discussions as well as intense arguments we had in these years are precious treasures that make this work shining, and make me toward a real scholar. I also thank Jianyu Li, Adam Celiz, Canhui Yang, Xi Yao, Qihan Liu and Yujia Wang for their remarkable contributions to this work. In other projects, I thank Lihua Jin, Widusha Illeperuma, Tetsu Ouchi, Anesia Auguste, Yecheng Wang, Jiangshui Huang, Xavier Morelle, Baohong Chen, Xuxu Yang, Chenghai Li, Hang Yang, Jingda Tang, Guoyong Mao and Stephanie McNamara. I would also like to thank all the group members and group alumni: Yuhang Hu, Kejie Zhao, Matt Pharr, Philipp Rothemund, Christoph Keplinger,

Tongqing Lu, Jianguo Li, Weixu Zhang, Chao Chen, Zhengjin Wang, Paul Le Floch, Kai Luo, Junjie Liu, Sibao Chen, Junsoo Kim, Peijian Chen, Chunping Xiang, Shuang Zhou, Guodong Nie, Zheng Jia and Kevin Tian, for all the discussions and suggestions throughout these years.

The last piece of warm gratitude belongs to my beloved family: my wife Sisi Zhuang, my daughter Jill Yang, my 5-month old unborn baby, and my parents. Their unconditional love and consistent support are the origin of strength to accompany me through this long journey, and with that my accomplishment becomes meaningful.

Chapter 1

Introduction

Adhesion is an ancient practice that allows two dissimilar materials to be intimately joined together to sustain mechanical forces [1]. Unlike traditional materials like glass, ceramics, plastics and metals that are dry and hard, hydrogels are new materials that are wet and soft. Hydrogels are matters of life, as most body parts of animals and plants are hydrogels. A hydrogel is a three-dimensional hydrophilic polymer network embedded in a water-rich environment. Synthetic hydrogels start from 1960s [2], and since then a variety of hydrogels are subsequently developed [3]. The polymer network in a hydrogel is sparse, and its mesh size is typically on the order of 10 nm, much larger than the size of a water molecule. The water molecules in a hydrogel are dense, and can transport through the polymer network. They retain their chemical and physical properties like those in liquid water. Within a mesh, polymer chains move freely relative to each other, and the hydrogel is liquid-like; Beyond a mesh, those movements are restrained by the crosslinks, and the hydrogel is solid-like. This unique combination of liquid and solid properties endows hydrogels usefulness in many aspects, from contact lenses [4, 5], superabsorbent diapers [6], to cell culture [7, 8], tissue adhesives [9-11], and drug delivery [12-14].

The polymer network of a hydrogel is chemically tunable. It can be designed to be self-healing, and the hydrogel can autonomously heal itself after damage, and restore its mechanical properties [15, 16]. It can be decorated with functional groups, and the hydrogel can respond to stimuli (e.g., temperature, pH, humidity, mechanical forces, light, electromagnetic field, and chemicals), and change its volume, transparency, color, or physical and chemical properties [17-21]. Those “smart” hydrogels are used to make actuators [22, 23], sensors [24, 25], drug carriers [13, 18] and functional surfaces [26]. It also can be incorporated with degradable moieties, and the hydrogel can spontaneously degrade over time upon exposing to triggers (e.g., ions,

chemicals, enzymes and ultraviolet light). This feature is useful in wound-care, and in controlling the release of therapeutics and cells from the hydrogel [27-29]. In addition, the water molecules in the hydrogel are ionically conductive, which enables soft and stretchable ionotronics of various kinds [30-33]. Furthermore, 3D-printing technology uncovers more potentials of hydrogels. 3D-printed hydrogels can replicate complex structures of organs [34], build vascular networks [35, 36] and aortic valves [37, 38], and fabricate miniaturized wearable devices [39, 40]. As a new material, hydrogel itself is still under intense research and rapid development.

Recent innovations have integrated hydrogels with various materials to manifest novel functions and advance emerging technologies. To introduce this active and exciting field thoroughly and conveniently, we divide hydrogel adhesion in three categories: hydrogel-tissue adhesion, hydrogel-elastomer adhesion, and hydrogel adhesion with other materials, and list the current state of art in each category. Applications are developed in different manufacturing processes, but all call for strong, compatible and reliable adhesion. Despite the importance of hydrogel adhesion, the exploration of hydrogel adhesion, however, is still in the nascent stage. Hydrogels adhere poorly to most materials, either hydrophobic or hydrophilic. We will elucidate the origin of weakness of hydrogel adhesion. We propose ways to achieve strong adhesion, and elucidate how different fracture events determine the adhesion energy. We examine the existing adhesion strategies in different manufacturing processes, and summarize their advantages and limitations. We also discuss how the hydrogel adhesion can be molecularly designed to build functions into adhesion. Lastly, we outline the structure of this thesis.

1.1 Diverse functions enabled by hydrogel adhesion

1.1.1 Hydrogel-tissue adhesion

A biological tissue is an assembly of cells and their extracellular matrix [41]. Most tissues (e.g., skin, brain and muscle) in the human body are like hydrogels, wet and soft. Hydrogels

should be biologically and mechanically compatible with tissues, so that they are used in wound dressings [9-11, 29, 42], tissue repair [29, 43-47], drug delivery [12-14, 48] and implantable devices [14, 49, 50]. Using hydrogels possesses many advantages over traditional materials in practical applications. For example, suturing and stapling are common practices to close a wound. However, they usually need long preparation time, bring discomfort to the patients, inflict additional damage to the surrounding tissues, and possibly cause inflammatory response and post-surgical complications [51-53]. Hydrogels that strongly adhere to tissues largely alleviate these adverse effects. They can be applied on the tissue to rapidly seal the wound and attain hemostasis, with no constraint to the tissues (Figure 1.1(a)).

Hydrogels also can serve as tissue replacements. They can be made mechanically as stiff and tough as load bearing tissues like cartilage and tendon. Hydrogels can contain drugs, which is an appealing material for drug delivery system of many kinds (Figure 1.1(b)) [13].

High-water content of hydrogel can easily encapsulate hydrophilic drugs, while the crosslinked hydrogel network can protect bioactive drugs or cells from premature degradation due to inwardly diffusing enzymes [54]. Hydrogels can be further engineered with different mesh size and functional groups to regulate the diffusion of drugs and provide controlled drug release in space and time.

1.1.2 Hydrogel-elastomer adhesion

An elastomer is a three-dimensional polymer network formed by hydrophobic polymer chains. Most elastomers are highly stretchable and optically transparent. The integration of hydrogel and elastomer leads to the invention of hydrogel ionotronics (Figure 1.1(c)). Compared to traditional ionotronics that involve rigid components such as metals [55-57], the essence of hydrogel ionotronics is soft and stretchable [30, 32, 33]. In the design of hydrogel ionotronics, hydrogels are ionic conductors, and elastomers are dielectrics. The first-generation of hydrogel ionotronics mimics neuromuscular and neurosensory systems [30, 32], and later, different

varieties are developed. Examples include artificial muscles [30, 58-61], artificial skins [31, 62, 63], artificial axons [32, 64], ionotronic luminescent devices [65-67], liquid crystal devices [68], touchpads [69], triboelectric and ionotronic generators [70-72], hydrophilic coating of biomedical devices [73], and wearable and washable active textiles [64].

Hydrogel-elastomer adhesion also enables stretchable seal (Figure 1.1(d)). An elastomer coated hydrogel retards dehydration when exposed in an open air, and prevents mass exchange between the hydrogel and environment [64, 74]; In turn, a hydrogel coated elastomer microfluidic channels serves as a semi-permeable membrane, which encapsulates the embedded bacteria in the channels, while allows chemicals from the environment to diffuse through, so that the bacteria can detect these chemicals [40, 74, 75]. The stretchable seal enables real-time sensing of environment and remains functional while being stretched.

1.1.3 Hydrogel adhesion with other materials

By utilizing the excellent mechanical properties of traditional materials, one can incorporate them into hydrogels to create water matrix composites (WMCs), which combine both rigidity and flexibility into one material (Figure 1.1(e)). A WMC is much stiffer and stronger than the hydrogel matrix itself: the elastic modulus can be orders of magnitude higher, the breaking strength are dramatically increased, and the fracture energy can be many times larger [76-81]. Typical WMCs include hydrogel-fabrics composites [82], hydrogel-glass composites [76], hydrogel-metal composites [77, 78, 83] and hydrogel-plastics composites [79-81, 83-86]. The WMCs are of critical importance in a wide range of applications that require combination of toughness, strength and stiffness to achieve resilience, energy absorption and load bearing, such as impact-resistant helmet [87] and load-bearing tissues [88].

When a hydrogel is coated on an implantable medical device, the hydrogel provides hydrophilicity biocompatibility and mechanical compatibility to the tissue [89, 90].

Rigid electronic circuit integrated of various components (e.g., conductors, transducers,

resistors, capacitors and chips) can glue on a hydrogel substrate to develop hydrogel electronics [91-93] (Figure 1.1(f)), where the hydrogel serves as soft and biocompatible substrate that directly attaches to tissues. The hydrogel electronics are soft, flexible and wearable, and used as real-time bio-data collection, processing, and readout.

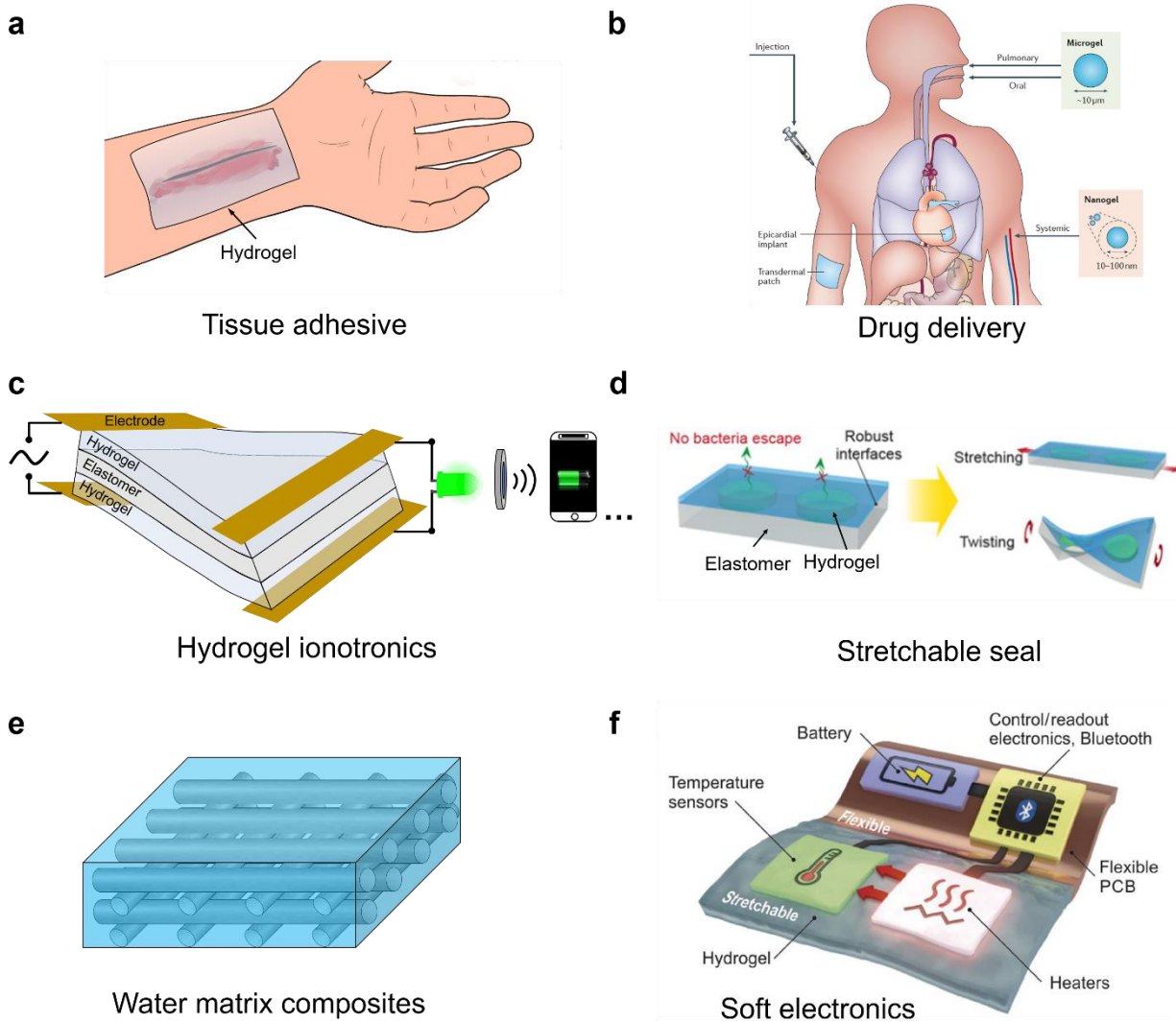


Figure 1.1. Versatile applications enabled by hydrogel adhesion. (a) Hydrogels for wound dressings. (b) Hydrogels for drug delivery [13]. (c) Hydrogel ionotronics with integrative functions of sensing, actuating and signaling. (d) Hydrogel stretchable seals for interactive microfluidic devices [75]. (e) Water matrix composites for enhancing mechanical properties of water. (f) Soft electronics for health monitoring [91].

1.2 Manufacturing processes

Performing adhesion between hydrogels and other materials (to be called adherend) should accommodate various manufacturing process: casting, coating, printing, attaching, piercing and gluing (Table 1.1).

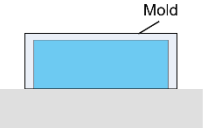
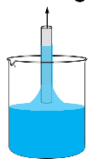
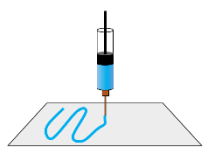

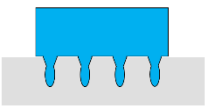
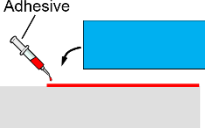
Casting, coating, and printing are processes in which a hydrogel precursor is *in situ* polymerized and form bonds with the adherend. Such processes are usually facilitated by ultraviolet irradiation, chemical reactions or physical interactions. Casting requires a mold. The hydrogel precursor is placed in the mold, in contact with the adherend, and subsequently cured in the mold, and simultaneously form bonds with the adherend. Coating and printing do not require mold, but they need careful tuning of their rheologies, which are typically done by adding polymer chains, clays, or chain transfer agents [34, 39, 40, 94-96]. The precursor is shear-thinning, liquid-like during the processes, and solid-like to maintain its shape when depositing on the adherend. Coating is conducted through spin coating, dip coating and spray coating. Spin coating deposits a thin hydrogel film onto a flat surface with well-controlled thickness, while dip coating and spray coating can deposit hydrogel film on objects of arbitrary geometries, but with a less well-controlled film thickness. Printing uses nozzles to inject hydrogel precursors on the adherend to generate complex structures in a high precise and controlled manner.

Attaching allows a pre-formed hydrogel to directly form bonds with the adherend. In this case, the polymer network of the hydrogel should have matching functional groups with the surface of the adherend.

Piercing uses rigid microneedles coated with dehydrated hydrogel to perforate into a water-rich material (i.e., hydrogel or tissue). The initially dehydrated hydrogel coating absorbs water and swells, which exerts pressure to the surrounding materials and mechanically interlocks inside the material [97].

Gluing uses an adhesive solution to bond pre-formed hydrogels and adherend. The adhesives can be monomers, polymers, and nanoparticles. Among them, monomers usually first *in situ* polymerized to become polymer and subsequently participate in bonding. As the adhesive is spread at the interface, the adhesion is realized by physical interactions [91, 98, 99], covalent bonds [29], topological entanglements [100], or their combinations [101].

Table 1.1 Hydrogel adhesion in different manufacturing processes.

Manufacturing processes	Material X	Tissues	Elastomers	Glass, ceramics, metals and plastics
Hydrogel precursors	Casting 	NA	Surface modification and <i>in situ</i> polymerization ^{32, 72, 183, 184}	<ul style="list-style-type: none"> Topological interlocking^{74-80, 194} Surface modification and <i>in situ</i> polymerization⁹⁰
	Coating 	<i>In situ</i> polymerization ⁹⁻¹¹	Silane coupling method ^{62, 92}	Surface modification and <i>in situ</i> polymerization ²⁰
	Printing 	NA	Silane coupling method ⁹²	NA
Preformed hydrogel	Attaching 	Functionalized hydrogel ¹⁵⁵	Silane coupling method ⁹²	NA
	Piercing 	Swellable microneedles ⁹⁵	NA	NA
	Gluing 	<ul style="list-style-type: none"> Nanoparticle solution⁹⁶ Cyanoacrylate^{9,10} Bridging polymers⁴⁰ Topological adhesion⁹⁸ 	<ul style="list-style-type: none"> Nanoparticle solution⁹⁷ Cyanoacrylate⁸⁹ Topological adhesion¹⁰⁴ 	<ul style="list-style-type: none"> Cyanoacrylate⁸⁹ Topological adhesion¹⁰⁴

Each manufacturing process presents its unique capability of fabricating hydrogel hybrids of various shapes and structures to meet specific purposes. For example, to make a hydrogel circuit, printing ensures high resolution and precision [39, 94]; to make a hydrogel hybrid of complex geometry, dip coating is an accessible and simple process [64, 94]; to make multi-layered hydrogel ionotronic devices, casting, attaching and gluing can be used [31, 32, 74, 91]. On the other hand, the nature of the adherend place restrictions to the type of hydrogel precursors, the mechanical properties of the adhesive layer, and the manufacture processes. Take casting as an example, if the adherend is a biological tissue, the hydrogel precursor and polymerization process should be biocompatible, and the formed hydrogel and adhesive layer should be as soft and stretchable as the tissue, so that the tissue movement is not restricted. In contrast, if the adherend is metal, above restrictions are no longer enforced.

1.3 Fundamental challenges in hydrogel adhesion

To illustrate the fundamental challenges in hydrogel adhesion, we first review bonding strategies that have been maturely and routinely used to bond traditional materials (Figure 1.2).

Wafer bonding: Two wafers with clean and little misfit surfaces are lightly pressed. The inter-atomic attraction accommodates the elasticity at the interface and allows them to adhere spontaneously.

Diffusion bonding: Ceramics or metals are pressed and heated, which allows the materials at the interface to undergo plastic deformation and creep to fill all gaps at the interface. In the same time, atoms from each material can diffuse across the interface and create new atomic bonds.

Surface activation and crosslinking: Two materials (rubber, glass and metals) are surface activated with functional groups. Upon contact or add crosslinkers, they form chemical bonds at the interface.

Polymer chains entanglements: In bonding rubber or plastics, diblock copolymers are applied at the interface at the temperature above the glass-transition temperatures of both materials. Each side of the diblock copolymer should be compatible with one of the bulk material. One segment of diblock copolymers diffuses unidirectionally into one material while the other diffuses unidirectionally into the other material, and thus physically entangles with both polymer networks of rubber or plastics. In this process, the gap between two materials must be at least smaller than the chain length of the diblock copolymer to ensure them to reach both sides of the materials and create sufficient entanglements [102-105];

Topological adhesion: In bonding rubber or plastics, monomers are applied at the interface and permeate into both polymer networks and subsequently form a new polymer network. The new polymer network is in topological entanglements with both polymer networks. Heating is needed to initiate the polymerization.

Mechanical interlocking: A liquid-form adhesive is applied at the interface of two materials and infiltrates into the asperities of the surfaces of both materials and then solidifies to a rigid adhesive layer that locks the two materials. In this process, strong adhesion is fulfilled only when the adhesive layer and both materials are stiff enough to call for a large force to separate them.

Adhesive bonding: A liquid-form adhesive is applied at the interface of two materials and solidifies. The adhesive forms physical interactions, chemical bonds, or some combinations with them. Even with non-covalent bonds, the adhesion is still appreciable due to high bonding density and well-packing.

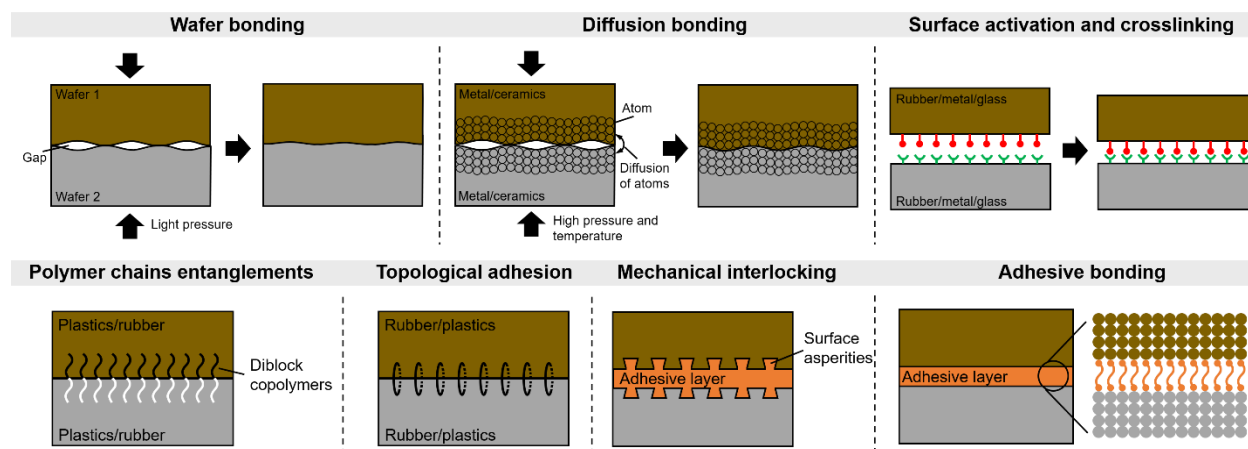


Figure 1.2 Traditional adhesion strategies: wafer bonding, diffusion bonding, surface activation and crosslinking, polymer chains entanglement, topological adhesion, mechanical interlocking and adhesive bonding.

All these common adhesion methods, however, are inapplicable or particularly weak in the adhesion with hydrogels. A hydrogel aggregates sparse polymers and dense water molecules. The sparse polymers contribute little interactions with the adherend, while the dense water molecules are same as those in liquid water and transmit little load [33]. If the surface of the adherend is hydrophobic, the water molecules in the hydrogel bond with the surface through van der Waals interactions, and the adhesion is weak. If the surface of the adherend is hydrophilic, a monolayer of water molecules forms hydrogen bonding with the surface, and beyond this monolayer, the water molecules in the bulk of the hydrogel still interact as weakly as in liquid water. The high-water content of a hydrogel is the major challenge that leads to intrinsically weak adhesion with other materials, regardless of the surface property of the adherend.

We can simply estimate the adhesion energy through the work of separation. The adhesion energy is determined by the work to separate the interface (water/adherend interface) and create two new interfaces (water/air interface and adherend/air interface). If the adherend is hydrophobic, e.g., polydimethylsiloxane (PDMS), the interfacial energies of water/PDMS,

water/air and PDMS/air are ~ 0.04 J/m², ~ 0.07 J/m² and ~ 0.02 J/m² [106]. The adhesion energy is estimated as ~ 0.05 J/m². If the adherend is hydrophilic, e.g., glass, the adhesion energy is estimated as ~ 0.14 J/m². These estimates account for the interfacial physical interactions, and no effects of chain scission and bulk hysteresis are involved.

1.4 Topologies in hydrogel adhesion

Strong adhesion relies on the minority constitute of the hydrogel: the polymer network. a sparse polymer network of strong bonds in a hydrogel can transmit significant load through the strong bonds, and elicit dissipation in the bulk [74, 92, 107, 108]. The abundance of water in a hydrogel also offers a particular opportunity to its adhesion to various materials: the fluidity and chemistry of water makes the hydrogel an ideal host for diverse topologies. By a topology of adhesion we mean a type of connectivity through bonds, chains, particles, networks, or their combinations. We discuss topologies in macroscopic scale and microscopic scale.

Topological interlocking is a topology in macroscopic scale. For most materials, they have close pores on the surface. When hydrogel precursors are casted on the surface, they only fill the pores on the surface. The hydrogel and the adherend form a key-lock structure (Figure 1.3(a)). To separate, the external force overcomes the friction between them the hydrogel and the adherend, as well as the elasticity of deforming the hydrogel. Fracture usually does not occur in this process. The key-lock design is not useful for hydrogels since they are soft (elastic modulus \sim kPa) and deformable, so the debonding force is small and the adhesion is weak. For porous materials, they have open pores in bulk. When hydrogel precursors are casted on the surface, they infiltrate into the porous material, fill all the inter-connected pores. The hydrogel and the adherend form a thread-hole structure (Figure 1.3(b)). To separate, the topologically interlocked structure must fracture—that is, at least one of the materials must break, and the adhesion is strong.

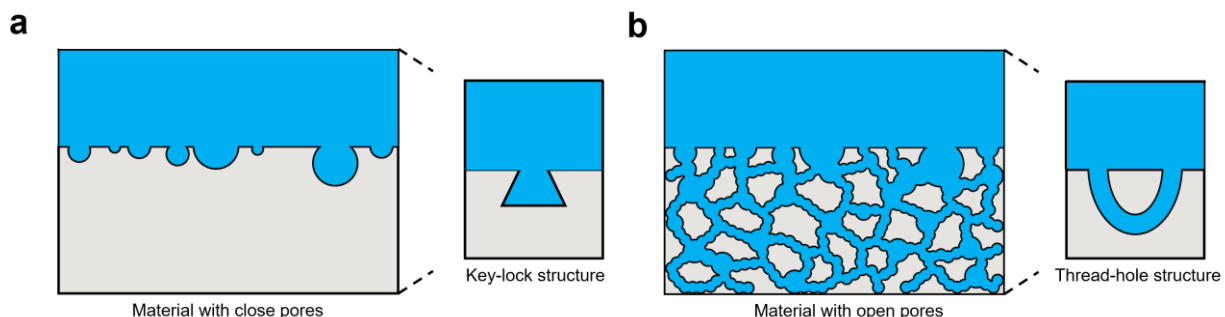


Figure 1.3 Topological interlocking. (a) When the adherend has close pores, the hydrogel precursor fills the pores on the surface. The hydrogel and the adherend form a key-lock structure. (b) When the adherend has open pores, the hydrogel infiltrates into the bulk, and fills all the interconnected pores. The hydrogel and the adherend form a thread-hole structure.

Two polymer networks or a polymer network and a nonporous solid can form direct bonds through matching functional groups (Figure 1.4(a)). Some materials naturally have reactive groups. For example, tissues have amine, thiol and carboxylic acid groups, glass has hydroxyl groups, and VHB elastomers have carboxylic acid and ketone groups [101]. If the adherend lacks reactive groups (e.g., PDMS and ceramics), chemical modification is used to introduce reactive groups on the surface. To separate, either the bonds or one of the materials must break.

Two polymer networks or a polymer network and a nonporous solid can adhere through bonding with polymer chains (Figure 1.4(b)). The polymer chains should carry matching functional groups with both materials, and can diffuse into the hydrogel. Debonding requires breaking of either such bonds, the polymer chains, hydrogel or adherend.

When two polymer network do not have matching functional groups, polymer chains are used to form a polymer network, in topological entanglement with the polymer networks of the hydrogels. That is, the new polymer network stitches the two existing polymer networks, acting as a molecular suture (Figure 1.4(c)). Hydrogels in topological entanglement have strong

adhesion, because separation requires at least one of the three polymer networks to rupture. When polymer chains cannot penetrate into the adherend, they can form bonds on the surface of the adherend and stitch with the polymer network of the hydrogel (Figure 1.4(c)).

Importantly, to attain strong adhesion, the density of topologies just needs to match the crosslink density of the hydrogel. Lower density is weaker, while higher density is in general useless, because a crack at the interface may simply kink into the hydrogel and fracture the hydrogel. In addition, high density reduces interfacial stretchability and transparency. This is particularly vital in hydrogel adhesion with tissues and elastomers, where the interface should retain softness and stretchability to conform the mechanical properties of soft materials.

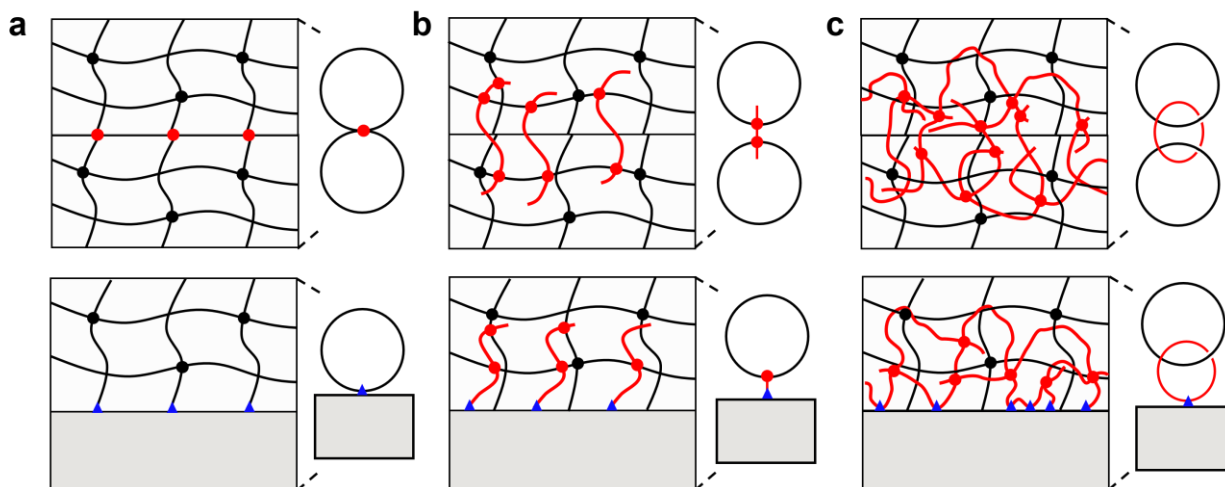


Figure 1.4 Topologies of hydrogel adhesion. (a) Formation of bonds at the interface. (b) Formation of bonds through polymer chains. (c) Stitch-stitch topology and bond-stitch topology.

1.5 The origin of adhesion energy

To separate two bonded materials, the crack needs to break the topology, and transmit the intense stress at the front of the separation into the bulk of the two materials, and may cause inelastic deformation in the bulk. Therefore, the adhesion energy not only depends on the strength of topology but also depends on the adherends. Adherends capable of large hysteresis lead to high adhesion energy. In this section, we use three cascading events of fracture to

illustrate this principle.

In the bonding of two brittle solids, such as glass, the bonds at the interface are atomic bonds. As an interfacial crack propagates, the crack only breaks one layer of atomic bonds and releases the energy stored in the layer, since all atoms in the glass are strongly bonded. The remaining bonds undergo small elastic deformation and do not dissipate energy. Taking the energy of rupture of an atomic bond as ~ 1 eV ($\sim 10^{-19}$ J), and the area of a single bond as $\sim 10^{-20}$ m², the adhesion energy is estimated about ~ 1 J/m². This estimation is consistent with experimentally measured value. This picture of fracture is known as Griffith bond breaking [109] (Figure 1.5(a)).

In the bonding of two polymer networks, the bonds at the interface are covalent bonds. Each polymer chain is comprised of many repeated monomer units. Along each polymer chain, the monomer units bind strongly, through covalent bonds similar to those in solids, but between polymer chains, monomer units interact weakly, through physical interactions similar to those in liquids. Thus, at the molecular scale, an elastomer or a hydrogel is inherently a hybrid of solid and liquid. When an interfacial crack propagates, at the crack tip, every atom—within the polymer chain or at the interface—carries the same force near the strength of the covalent bond. Upon fracture of single covalent bond, the entire polymer chain is relaxed, and the stored energy in the entire chain is dissipated. Consequently, the energy released is the covalent energy of a layer of polymer chains per unit area. Longer polymer chain leads to more dissipative energy. The adhesion energy is amplified by a factor of the number of the monomer units in the chain. Taking the typical number of 10-100 monomer units in the chain, and the covalent bond energy as $\sim 10^{-19}$ J, the adhesion energy is estimated as 10-100 J/m². This picture of fracture is known as Lake-Thomas amplification [110] (Figure 1.5(b)).

When a polymer network is interpenetrated with another sacrificial polymer network, the adhesion energy can be further amplified. The deformation of one polymer network causes the deformation of the other polymer network. As a crack propagates along the interface, the

stretchy polymer chains at the crack tip is highly stretched and is strong enough to break the brittle polymer network in a large region surrounding the crack tip, thus dissipating a great amount of energy. This picture of fracture is referred as Irwin-Orowan amplification [111, 112] (Figure 1.5(c)). The adhesion energy can be amplified as high as $\sim 1,000-10,000$ J/m². The Irwin-Orowan amplifications are essential to toughening materials of all types. Well-known examples include ductile metals, tough ceramics, ceramic matrix composites, and rubber-filled plastics [113-116], where the background hysteresis is originated from various inelastic processes such as atomic separation, twinning, phase transformation and dislocation motion.

To elicit hysteresis, the topology consisting of bonds should be sufficiently strong (the bond strengths are listed in Table 1.2). Topology consisting of weak bonds can achieve strong adhesion as well, so long as these weak bonds are high density and well-packed. Moreover, the obtained adhesion energy cannot exceed the fracture energy of both materials.

Hydrogels exhibit rate-dependent mechanical properties (i.e., viscoelasticity, viscoplasticity, and distributed damages) due to the existence of weak and reversible interactions in the hydrogels (i.e., polymer chain entanglement, dynamic covalent bonds, metal–ligand coordination, hydrogen bonds, electrostatic and hydrophobic interactions, and host–guest interaction). These interactions may be spontaneously dissociated under a constant force. For example, the chain entanglements can be slowly disentangled [117], and the electrostatic interaction can be slowly disrupted [118], under a constant stretch. At high crack speed, these interactions do not have sufficient time to dissociate, and the hysteresis in the hydrogel is elicited; while at low crack speed, they have sufficient time to dissociate, and the hysteresis in the hydrogel is much less elicited. This rate-dependent fracture has been observed in many hydrogel systems [100, 119, 120]. Furthermore, when these hydrogels are used in the adhesion, the adhesion energy is also rate-dependent. The hysteresis in the hydrogel greatly amplifies the adhesion energy at high crack speed, but contributes negligibly at low crack speed (Figure 1.5(d)). For example, in bonding two pieces of alg-PAAM hydrogels (the hysteresis is provided

by electrostatic interactions in the alginate network), the adhesion energy reaches $\sim 3000 \text{ J/m}^2$ at a crack speed of 10 mm/s , but reduces to $\sim 400 \text{ J/m}^2$ at $1 \text{ }\mu\text{m/s}$ [100]. Other types of weak and reversible interactions should play similar roles in rate-dependent adhesion energy.

Table 1.2 Examples of bonding energy of different interactions.

Interactions	Bonding energy (kT)
Covalent bond	80-320 [121]
Hydrogen bond	1-50 [122, 123]
Electrostatic interaction	1-10 [124, 125]
Hydrophobic interaction	1-10 [126]
π - π stacking	1-10 [127]
Host-guest interaction	1-10 [128]
van der Waals interaction	~ 1 [98, 122]

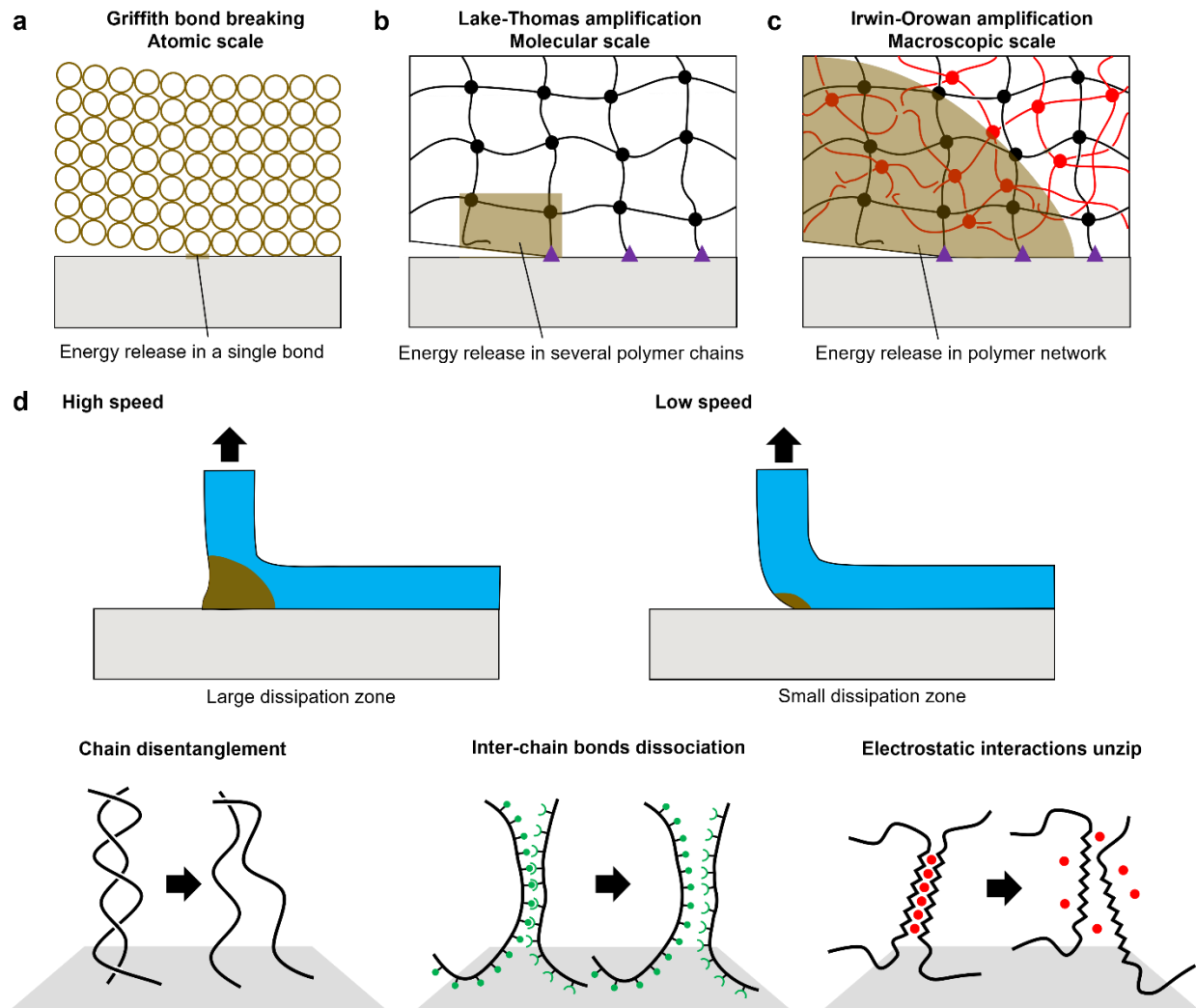


Figure 1.5 Origin of adhesion energy. (a) Griffith bond breaking at atomic scale. The debonding releases the energy stored in a layer of atomic bonds. The adhesion energy is $\sim 1 \text{ J/m}^2$. (b) Lake-Thomas amplification at molecular scale. The debonding releases energy stored in a single atomic bond and the energy stored in all bonds in the polymer chains. The adhesion energy is $\sim 10\text{-}100 \text{ J/m}^2$. (c) Irwin-Orowan amplification at macroscopic scale. In addition to Lake-Thomas amplification, sacrificial bonds in a large region surrounding the bonding front break and dissipate a great amount of energy. The adhesion energy can achieve $\sim 1,000\text{-}10,000 \text{ J/m}^2$. (d) Adhesion energy is rate-dependent. The hysteresis in the hydrogel greatly amplifies the adhesion energy at high debond speed but contributes negligibly to the adhesion energy at low debond speed. Typical rate-dependent polymer interactions: chain disentanglement, interchain

(Continued) dissociation and electrostatic interactions unzip.

1.6 Hydrogel-tissue adhesion

Hydrogel-tissue adhesion is being intensively studied for about a century, but with newly developed hydrogels and adhesion strategies, this field keeps advancing. The adhesion between a hydrogel and tissue requires biocompatible manufacturing processes, and the formed hydrogel and the adhesive layer are mechanically compatible with soft tissues so that the motion of the tissue is unrestricted, e.g., beating of a heart. Coating, attaching, piercing and gluing are used and show both advantages and limitations. In the following, we review the existing bonding principles in each manufacturing process. Interested readers can find comprehensive reviews on traditional hydrogel-tissue adhesion in the literature [9-11, 53].

1.6.1 Coating

Various types of hydrogels—synthetic and natural—have been used to polymerize *in vivo* in contact with tissues. They are categorized into protein-based hydrogels, polysaccharide-based hydrogels and synthetic hydrogels [9, 10, 46, 129, 130]. They possess many merits, such as biocompatibility, biodegradability, and minimal immune responses. Here we review the principle of adhesion in each category.

Protein-based hydrogels closely resemble biological tissues. They include fibrin gels, gelatin and collagen gels, and albumin-based tissue adhesives. The fibrin gel is commonly applied in clinical practice for tissue regeneration and local hemostats [131, 132]. The formation of fibrin gel mimics the last stage of blood clotting [133]. The fibrin gel is formed from two major components: the enriched fibrinogen with factor XIII and the thrombin with calcium chloride. When the two components are mixed and coated on a tissue, the thrombin cleaves fibrinogens by removing two fibrinogen peptides, and generate fibrin monomers with reactive polymerization sites. The fibrin monomers subsequently self-assemble to form fibrin polymers

through hydrogen bonding. At the same time, the thrombin activates factor XIII to factor XIIIa, and catalyzes the formation of amide bonds within the fibrin polymers between the glutamine and lysine amino acids, thus producing a stable fibrin network [134, 135]. The reactive sites of fibrin monomers can also bind collagen and endothelial cells in the tissue via factor XIIIa [136] (Figure 1.5(a)). Tisseel (Baxter) and Evicel (Ethicon) are commercially available fibrin sealants. In addition, due to the mechanical weakness of fibrin gel, many other modified fibrin gels are being developed with enhanced mechanical properties [137-139].

Polysaccharides are composed of naturally occurring sugar building blocks. Typical polysaccharide hydrogels are processed from chitin, chitosan, dextran, chondroitin and hyaluronic acid. These biopolymers cannot be covalently crosslinked by themselves, and chemical modification is usually introduced to graft certain reactive groups onto the polymer chains. For example, chitosan can be chemically modified with lactobionic acid and 4-azidobenzoic acid [140, 141], succinic anhydride [142], PEG oligomers [143] and N-acetylcysteine [144] at the amine site; dextran can be oxidized to dextran aldehyde, which can react with amine groups [145]; chondroitin sulfate can be chemically modified with methacrylate groups [146], aldehyde groups [147], and NHS-activated ester groups [148]; hyaluronic acid can be chemically modified with methacrylate groups [149]. Depending on the types of these reactive groups, polysaccharide hydrogels are polymerized by chemical reactions or UV irradiation, to form covalent bonds or chain entanglements with the polymer networks of tissues. To illustrate one example, methacrylated hyaluronic acid is cured under UV irradiation with a photo-initiator, the polymer chains and initiators can infiltrate into the tissue network, and physical entangle with the tissue network [149] (Figure 1.6(a)).

Among the synthetic hydrogels, the polyethylene glycol (PEG) hydrogel is FDA approved and broadly used hydrogel, which is known biocompatible, nontoxic and nonimmunogenic [150, 151]. PEG are inert polymers, and synthesis of PEG gel needs to decorate reactive groups to both ends of inert chains. Three major methods are commonly used: photopolymerization [152, 153],

amine-NHS reaction [154] and thiol-NHS reaction [155]. The crosslinking mechanism varies with different reactive groups. In the thiol-NHS reaction [155], the PEG gel is prepared by 4-arm starPEG with N-hydroxysuccinimide (NHS)-ester terminal groups and 4-arm starPEG with thiol terminal groups. When two starPEGs are mixed and sprayed on the tissue, the thiol groups react with the NHS-ester groups, and crosslink into a PEG network. Meanwhile, the amine groups on the tissue can react with the NHS-ester groups from one starPEG to form amide bonds, which allows the PEG gel to be covalently bonded with the tissue (Figure 1.6(a)). Other types of synthetic hydrogels are fabricated in the similar route and form weak bonds or chain entanglements with the tissues [46, 129, 130].

All three types of hydrogels used in clinics are typically weak in their mechanical properties. The cohesive failure of the hydrogel prohibits strong adhesion. For example, the weak hydrogen bonding between self-assembled fibrin monomers, or the small mesh size of polysaccharide and PEG polymer networks, induce negligible Lake-Thomas amplification. The adhesion energy is about 1-10 J/m², while the fracture energies of most tissues range from ~100-1000 J/m² [156, 157]. Generally, those hydrogels cannot be applied in the environments when high pressure is present, such as those inside the cardiac chambers and major blood vessels [53]. Other drawbacks include (i) the requirement of sophisticated chemical modification to the polymer chain to introduce reactive groups; (ii) the polymerization by UV irradiation is not always feasible in every place in the body, and the generated free radicals may cause damage to the healthy tissues; (iii) the fibrin and the protein gels may be easily washed out under *in vivo* dynamic conditions.

1.6.2 Attaching

Mussels can attach to various surfaces under water. This ability motivates extensive studies to understand its mechanism and develop mussel adhesives [158, 159]. Proteins that secreted by mussel are rich in lysine and 3,4-dihydroxyphenyl-L-alanine (DOPA), which

contains catechol groups that can form multiple bonds with diverse surfaces [160, 161]. A hydrogel can be functionalized with catechol groups by either modifying its polymer chains with catechol groups or mixing with polydopamine (PDA) chains [162, 163]. When a pre-formed PDA-containing hydrogel attaches on the tissue, the catechol groups on the PDA forms hydrogen bonds with the amine groups on the tissue [163] (Figure 1.6(b)). Because hydrogen bonds are reversible, the hydrogel can be repetitively attached and detached. However, the adhesion is weak due to the weak hydrogen bonding, and the hydrogel sacrifices its transparency.

1.6.3 Piercing

Endoparasitic worm uses a proboscis to penetrate into a tissue and expands a bulb using retractor muscles so that they can securely anchor on the surface of the tissue [164]. Inspired by the adaptable morphology change of the worm proboscis, an array of cone-shaped microneedles with a swellable tip are fabricated [97]. Each microneedle is made of a non-swellable polystyrene (PS) core coated with a water swellable polystyrene-poly(acrylic acid) (PS-*b*-PAA) hydrogel. Before piercing, the hydrogel coating is dry. Upon piercing into the tissue, the hydrogel coating absorbs water from tissues and swells, which exerts normal force to the surrounding tissue. This normal force generates friction between the hydrogel and the tissue, thus provides mechanical interlocking (Figure 1.6(c)). To unlock, the external force applied to pluck out the microneedles should overcome the friction between the hydrogel and the tissue, and the elastic energy stored in the deformed hydrogel layer. This bonding approach is reversible, universal to all tissues and does not involve any chemistry. However, the fabrication of the microneedles is costly and sophisticated. Because the friction between the hydrogel and tissue is typically small, and they are soft, the force required to remove a single microneedle is small, and the adhesion is weak. To achieve strong adhesion, a high density of microneedles is needed.

1.6.4 Gluing

Gluing uses suitable adhesives to bond a pre-formed hydrogel on a tissue. The adhesive is in the form of liquid, which can be a solution of nanoparticles, monomers and polymers. After the adhesives being spread at the interface, it forms chemical bonds, physical interactions, topological entanglements, or some combinations, with the polymer networks of the hydrogel and tissue. Compared to other manufacturing process, gluing is generally facile and convenient, requiring less preparation time, and can be biocompatible. Here we review the major gluing strategies that have been recently developed as well as already widely adopted.

Gluing with nanoparticle solutions has been reported to improve adhesion between hydrogels and tissues [50, 98, 165] (Figure 1.6(d)). The diameter of a silica nanoparticle is about 10 nm, comparable to the mesh size of hydrogels and tissues. When the silica nanoparticles are spread at the interface, the dangling polymer chains from the hydrogel and tissue adsorb onto the surface of the nanoparticles through van der Waals interaction. A single polymer chain can have multiple sites of adsorption. The nanoparticles act as giant crosslinks, and the adsorbed polymer chains act as bridges between them and between hydrogels and tissues. Upon debonding, the anchored polymer chains sequentially detach from the particles, and releases the energy of breaking anchors and the elastic energy from the relaxation of the adsorbed polymer chains. This detaching process resembles the Lake-Thomas picture. Since the van der Waals interaction is weak, it cannot elicit the hysteresis from both materials. Thus the detaching gives adhesion energy of 10 J/m^2 . To obtain appreciable adhesion, both the hydrogel and tissue should have dangling polymer chains in sufficient number and length on the surface to create more anchors. Additionally, nanoparticles have also been used in gluing hydrogels and elastomers following the similar bonding mechanism. The adhesion energy is measured less than 10 J/m^2 [99].

Many other variables may affect the adhesion energy. For example, the size of the particle [166]. If the size of the nanoparticle is comparable to the mesh size of the hydrogel and

tissue, the nanoparticles stay at the interface and bridge the two materials. If the nanoparticles are too small, they may submerge into one of the polymer networks, and the adhesion is weak. If the nanoparticles are too large, they may create large gaps at the interface, and the effective contact areas between the particles and the polymer chains are reduced, and the adhesion is also weak.

The commonly used super glue, cyanoacrylate, has been prevalently used in hemostasis and wound closure, owing to its fast and strong adhesion [167-169]. The cyanoacrylate monomer is highly reactive. The electron-withdrawing nature of the nitrile group polarizes the acrylate bond, making it susceptible to nucleophilic attack even by traces of weak bases like water and amines [170-172]. When the cyanoacrylate is spread at the interface of the hydrogel and tissue, the polymerization of monomers is instantaneously initiated by the abundant water molecules as well as the primary amines on the tissue, and form poly(cyanoacrylate) chains via anionic polymerization. The adhesion is established within seconds. The adhesive layer is stiff and brittle, and is covalently bonded to the underlying tissue (Figure 1.6(d)). The mechanism of adhesion between cyanoacrylate and the hydrogel is still unclear, possibly by topological entanglements. Adhesion energy is high by eliciting the Lake-Thomas and Irwin-Orowan amplifications, typically same as the fracture energies of the hydrogel or the tissue. The disadvantages of cyanoacrylate are: (i) cytotoxic [173, 174], (ii) the stiff adhesive layer is mechanically incompatible with the soft tissues, (iii) cyanoacrylate works poorly in the presence of blood, as it quickly cures before bonding with the tissues, (iv) poly(cyanoacrylate) can be hydrolyzed and degraded over time [175]. Nonetheless, cyanoacrylate is also widely used in bonding hydrogels with other materials such as elastomers, plastics, glass and metals.

To address the issues described above, biocompatible polymers has been recently invented to attain strong adhesion and meanwhile retain compliant interface [29, 47]. Bifunctional chondroitin sulphate (CS) with aldehyde groups and methacrylate groups can react with amine groups on the tissue surface to form covalent bonds, while grafting on the hydrogel

surface on the other side through *in vivo* photopolymerization [47]. This adhesion strategy is successfully applied in cartilage repair [45]. Even though the interface is compliant, the hydrogel is mechanically much weaker than the cartilage, so it readily suffers fracture. One apparent improvement is to use hydrogel that has mechanical properties close to that of cartilage.

Recently developed tough adhesives have shown strong adhesion with many tissues, even in the presence of blood [29]. The tough adhesive consists of two layers: a positively charged bridging polymer layer and a tough hydrogel layer. The bridging polymers bear primary amine groups, such as chitosan, poly(allylamine) (PAA) and poly(ethylenimine) (PEI), and are mixed with two coupling reagents, 1-ethyl-3-(3-dimethylaminopropyl)carbodiimide (EDC) and N-hydroxysulfosuccinimide (NHS). The tough hydrogel is formed by alginate-polyacrylamide (alg-PAAM), with a covalently crosslinked PAAM network and an ionically crosslinked alginate network. The bridging polymers interpenetrate into both the alg-PAAM hydrogel and the tissue, and form amide bonds by coupling the amine groups from the bridging polymers and the carboxylic acid groups from the hydrogel and the tissue through EDC chemistry [176, 177] (Figure 1.6(d)). Under deformation, the alg-PAAM hydrogel dissipates energy by unzipping ionic bonds in the alginate network. This synergy of interfacial bridging and background hysteresis triggers the Lake-Thomas and Irwin-Orowan amplifications. The adhesion energy exceeds 1,000 J/m² is obtained, while the bonding interface maintains stretchable. The limitation of this method is (i) the adhesion relies on the specific functional groups (i.e., carboxylic acid groups and amine groups in this case), and cannot bond hydrogels without the suitable functional groups; (ii) the alg-PAAM hydrogel is unstable in the physiological fluids, and the adhesion weakens over time; (iii) the alg-PAAM is relatively stiff compared to most soft tissues, so it may restrain the natural movement of certain tissues.

To resolve the above issues, an approach called topological adhesion is reported [100] (Figure 1.6(d)). The approach uses biocompatible polymers to achieve strong adhesion between hydrogel and tissues without requiring any functional groups from both materials, and

meanwhile retain interfacial softness. The biocompatible polymers can form a polymer network, in response to a trigger (i.e., pH, temperature, light, salt, and solvent), topological entangles with both polymer networks of the hydrogel and tissue, stitching them together like a suture at the molecular scale. To illustrate one example, chitosan is used as stitching polymers, and pH is used as a trigger. The chitosan chain has pKa \sim 6.5. It is soluble in water when pH < 6.5 and form a polymer network crosslinked by NH₂-OH hydrogen bonds when pH > 6.5 [178, 179]. An aqueous solution of chitosan of pH = 5 is placed between hydrogel and tissue, both of pH = 7. The chitosan chains diffuse into both materials, in response to the pH change, form a third network through hydrogen bonds, which is localized at the interface, in topological entanglement with both polymer networks of hydrogel and tissue. It is noticed that even though the chitosan network is physically crosslinked, it is mechanically stable like a covalent network, possibly owing to the dense and well-packed hydrogen bonds between chitosan chains. The chitosan network is flexible enough to retain a soft and elastomeric interface, and yet strong enough to elicit the Lake-Thomas and Irwin-Orowan amplifications. The adhesion energy is attained comparable to the fracture energy of the hydrogel, and can be as high as 1,000 J/m². In addition, benefiting from the pH-triggering mechanism, several other species of stitching polymers of different pKa can be used to create strong adhesion in full range of pH. Upon adjusting the pH back to the soluble range of pKa, the adhesion can be on-demand deactivated. The approach poses limitations. The topological adhesion requires a certain period of time to reach equilibrium, which may not be suitable for time-sensitive applications. The establishment of strong adhesion needs a consistent mechanical compression, which may be impractical for tissues that are difficult to access or to apply compression.

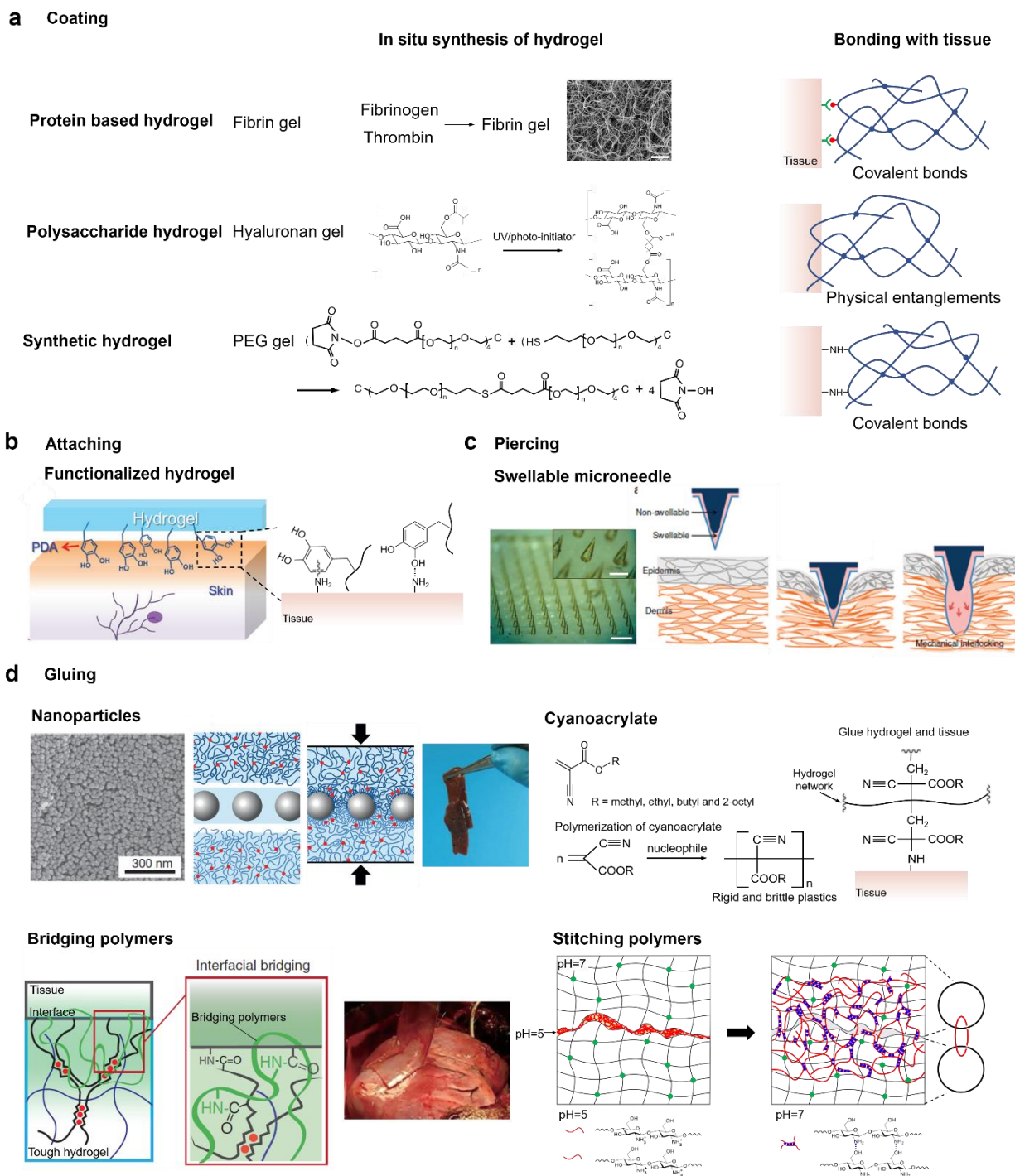


Figure 1.6 Hydrogel-tissue adhesion. (a) Coating. Three representative hydrogels: protein hydrogel, polysaccharide hydrogel and synthetic PEG hydrogel are demonstrated. Those hydrogels are all *in vivo* polymerized in contact with tissues through chemical reaction or free radical polymerization. Fibrin gel and PEG gel form covalent bonds with the underlying tissue,

(Continued) and hyaluronan hydrogel form physical entanglements with the network of the tissue. The scanning electron micrograph shows the structure of a fibrin gel. The scale bar is 10 μm . (b) Attaching. A hydrogel containing polydopamine forms hydrogen bonds with the amine groups on the tissue upon contact [163]. (c) Piercing. Microneedles with dehydrated hydrogel coating pierce into the tissue, and the hydrogel coating swells and mechanically interlocks with the surrounding tissue [97]. The image shows an array of microneedles. The scale bar is 1 mm. (d) Gluing. *Nanoparticles*: polymer chains from both hydrogel and tissue adsorb on the nanoparticles [98]. *Cyanoacrylate*: Cyanoacrylate rapidly polymerizes in the wet environment and form covalent bonds with the tissue and topological entanglements with the hydrogel. *Bridging polymers*: polymers diffuse into both hydrogel and tissue, and form bonds with their polymer networks [29]. *Stitching polymers*: polymers diffuse into both hydrogel and tissue and form a new network, in topological entanglement with the polymer networks of two materials. The example shown is the mechanism of using chitosan to bond two pieces of hydrogels [100].

1.7 Hydrogel-elastomer adhesion

Elastomers are dry, hydrophobic and stretchable, and many of them are transparent. VHB (3M), polydimethylsiloxane (PDMS, Dow Corning), and Ecoflex (Smooth-on) are mostly used elastomers in hydrogel-elastomer adhesion. The VHB elastomer is highly stretchable (stretch ~ 9), transparent ($> 90\%$, 4910), and relatively tough ($\sim 1,000 \text{ J/m}^2$). However, the VHB elastomer is crosslinked as received, and cannot be reshaped into other geometries or reprocessed with different mechanical properties [180]. PDMS has a stretchability of about 3, good transparency ($> 90\%$), but lower fracture toughness ($\sim 100 \text{ J/m}^2$). Ecoflex has a stretchability of about 7, but the transparency decreases as the thickness increases, and becomes opaque when the thickness is larger than 1 mm. Both PDMS and Ecoflex can be synthesized from precursors, so that they can be produced with tunable mechanical properties, and fabricated into complex geometries. We review the strategies of bonding hydrogels with these

elastomers.

1.7.1 Casting

Chemical modification of elastomers is often employed in the casting method. The elastomer surface is modified with functional groups such as hydroxyl groups, amine groups, acrylic groups and silanol groups. However, this method has two challenges. First, many elastomers are highly permeable to oxygen, which induces inhibition effect to the polymerization of hydrogel. Second, the functionalized elastomer surface experiences surface aging or hydrophobic recovery, and will gradually lose the introduced functional groups.

Hydroxyl groups can be generated by treating the elastomer surface with oxygen plasma or UV/ozone [181-183] (Figure 1.7(a)). This treatment modifies the hydrophobic elastomer with a hydrophilic surface layer of 10-100 nanometer thickness [183-186]. The hydrophilic layer recovers hydrophobicity easily in the air, but can be well postponed in aqueous environment [187]. The hydrophilic polymer chains of the hydrogel form hydrogen bonds with the hydroxyl groups on the elastomer. The adhesion energy is measured $\sim 1-10 \text{ J/m}^2$. Mixing a large amount of uncrosslinked hydrophilic polymer chains into the hydrogel can largely increase the number of hydrogen bonds [39], and can enhance the adhesion energy up to $\sim 50 \text{ J/m}^2$.

Creating covalent bonds between the hydrogel and the elastomer can greatly improve adhesion energy. The elastomer surface is modified with functional silanes (Figure 1.7(a)). Silane is a bi-functional molecule with reactive groups (e.g., vinyl, epoxy, amine) on one end, and hydrolysable alkoxy-silyl groups on the other end [188]. During the silane modification, an elastomer is first plasma treated to exhibit hydroxyl groups on the surface. As the silane solution is casted on it, the alkoxy-silyl groups are hydrolyzed to silanol groups, which further condense with hydroxyl groups and form siloxane bonds, thus modifying the elastomer surface with the reactive groups of silanes [189, 190]. The silane reactive groups form direct bonds with the matching functional groups on the polymer network of the hydrogel [191, 192]. As an example,

we illustrate the procedure to bond an alginate hydrogel to PDMS. The alginate hydrogel can be either ionically crosslinked by calcium ions or chemically crosslinked by adipic acid dihydrazide (AAD). The PDMS is first oxidized in hydrogen peroxide or sulfuric acid solution to obtain hydroxyl groups on its surface (OH-PDMS). The surface is then treated with 3-aminopropyltriethoxysilane (APTES). The APTES molecules covalently bond the OH-PDMS surface through silane condensation, and modify the OH-PDMS to NH₂-PDMS. The amine groups react with the carboxylic acid groups on the alginate chains through the EDC chemistry and form amide bonds [176, 177]. The bonded hydrogel-elastomer is robust, and the adhesion energy reaches the fracture energy of the alginate hydrogel itself. Due to the brittleness of the alginate hydrogel, the interfacial covalent bonds elicit little Lake-Thomas amplification.

Generating radicals on the surface of elastomer can bond hydrogels that are free-radical polymerized (Figure 1.7(a)). Benzophenone is one of the chemicals that can activate the elastomer surface with radicals, and alleviate the oxygen inhibition during *in situ* polymerization of hydrogels [193]. During the process, benzophenone is first adsorbed to the surface of an elastomer, and the hydrogel precursor is subsequently casted on the surface. Under UV irradiation, the benzophenone is excited into a singlet state and converted to a triplet state through intersystem crossing. The triplet-state benzophenone abstracts a hydrogen atom from the surrounding unreactive C-H bonds of the elastomer polymer chains and generates surface radicals [193, 194]. Consequently, the polymer network of the hydrogel is grafted on the reactive sites of the elastomer surface. This method requires oxygen-free environment. The covalent bonds at the interface can elicit the Lake-Thomas and Irwin-Orowan amplifications. Adhesion energy exceeds 1,000 J/m² can be obtained [74].

The surface modification methods can create strong adhesion, but they are hardly applicable in bonding hydrogels and elastomers of complex geometries. In addition, they often involve toxic chemicals, multiple steps of reaction and sophisticated environment control. Furthermore, we note that casting elastomer precursors on a pre-formed hydrogel is rarely

achieved, mostly because surface modification of a hydrogel with hydrophobic groups is difficult.

1.7.2 Silane coupling method for casting, coating, printing and attaching

The silane coupling method attempts to solve the challenges encountered in the above casting methods [94] (Figure 1.7(b)). Silane molecules are mixed into the precursors of both hydrogel and elastomer, and are copolymerized into their networks. The silane coupling agents hydrolyze before condensation, which allows time for a manufacturing process before bonding. After a manufacturing process, the silane coupling agent condenses, forming additional crosslinks in the networks of both hydrogel and elastomer, as well as covalent bonds between the two networks at the interface. This approach is oxygen-tolerant, independent of the sequence of forming the networks. Therefore, it unlocks many manufacturing processes including casting, coating, printing and attaching. The bonding can trigger the Lake-Thomas and Irwin-Orowan amplifications, and the adhesion energy can approach the fracture energy of either material. The bonding kinetics can be tuned by temperature, pH, and surfactants. A higher temperature speeds up the kinetics and reduces the amount of required coupling agents. The pH of the hydrogel affects the bonding speed, and lowest speed is observed around pH = 4. The surfactant serves as an adhesion promoter. It adsorbs at the hydrogel-elastomer interface and helps the silane coupling agents on the elastomer chains get solvated for hydrolysis. The drawbacks of this method include (i) invasive: incorporating silane into both materials changes their mechanical and chemical properties; (ii) the method requires a post-condensation time to reach equilibrium of the adhesion, which is inapplicable for time-sensitive applications; (iii) the method is limited to certain elastomers that can be copolymerized with the silane coupling agent.

1.7.3 Gluing

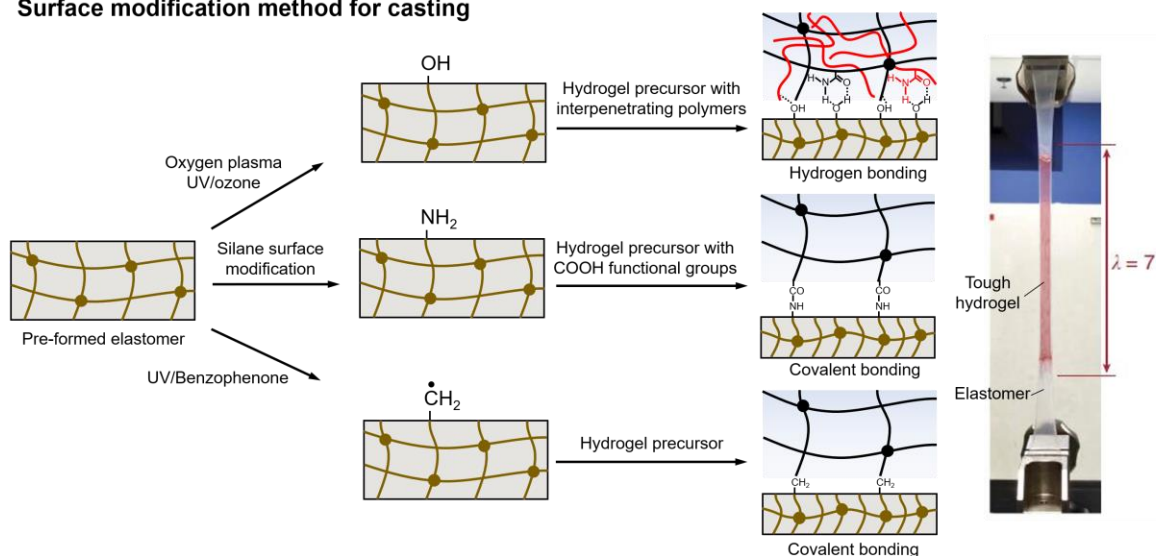
It has been described in the previous section that cyanoacrylate forms a stiff and brittle adhesive layer, which is mechanically incompatible with hydrogels and elastomers, and also sacrifices the transparency of the interface. To address this issue, cyanoacrylate is diluted in an organic solvent to prevent forming glassy phase [91] (Figure 1.7(c)). The bonding mechanism is not well studied yet. The polymerized, non-glassy cyanoacrylate network possibly forms topological entanglements with the networks of both materials. The adhesion is strong enough to elicit the Lake-Thomas and Irwin-Orowon amplifications, with an adhesion energy reaching the fracture energy of either material. The merit of cyanoacrylate is attributed to its facile preparation and instant bonding, which is important in time-critical applications such as rapid prototyping and high-throughput manufacturing. The diluted cyanoacrylate can also be used to bond hydrogels with plastics and metals.

It is known that if a material has a low interfacial energy (i.e., PDMS and polyethylene (PE)) with cyanoacrylate, the adhesion is weak due to the poor wettability of cyanoacrylate on the surface of the material. To improve the wettability, wet chemical treatment [195, 196], plasma treatment [197, 198], and metallization [91, 199] are usually used, and metallization is a general and effective method among them [91, 199]. The low surface energy material is deposited with a thin layer of chromium (Cr) through physical vapor deposition (PVD), and the surface energy can be increased by two orders of magnitude. In addition to this inconvenience, cyanoacrylate along with its organic solvent are toxic, and the application is limited to near-neutral-pH environment.

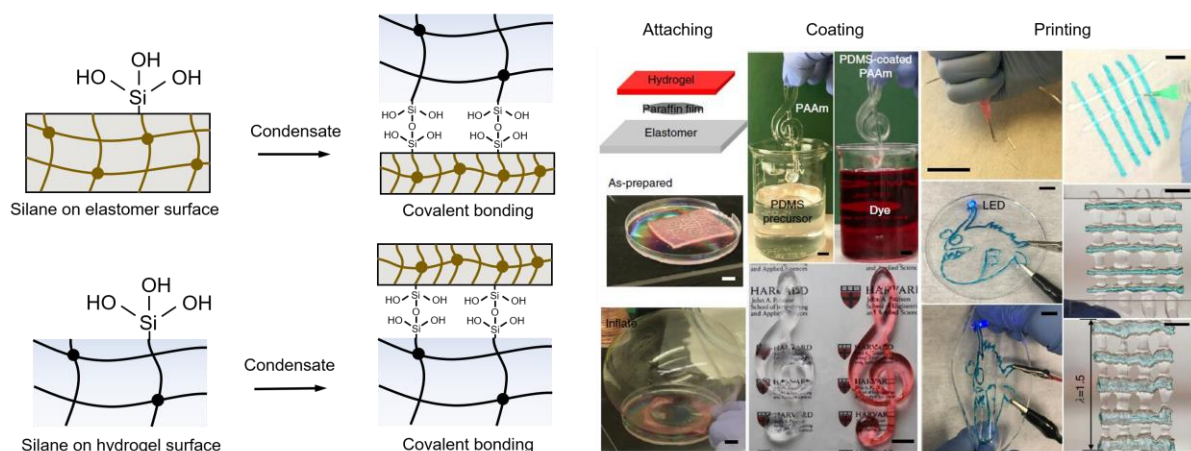
A bond-stitch topology is applicable in adhering hydrogel with metals, glass and plastics, where the hydrogel is pre-form with no functional groups, and the adherends have functional groups. Polymer chains are used to form a network, which bonds on the adherend through matching functional groups, and stitches with the polymer network of the hydrogel [101] (Figure 1.7(c)). As an example, a chitosan solution of $\text{pH} = 5$ is prepared and spread at the interface of a

hydrogel (pH = 7) and VHB elastomer. Some chitosan chains bond on the surface of the VHB elastomer through imine bonds and ionic bonds [200, 201], and other chitosan chains remain mobile. The mobile chitosan chains diffuse into the hydrogel and crosslink into a network by $\text{NH}_2\text{-OH}$ hydrogen bonds in response to the pH change [178, 179], in topological entanglement with the hydrogel network. For the elastomers without a specific functional group (e.g., PDMS), they should be surface-modified with functional groups (i.e., carboxylic acid groups on PDMS surface), and the polymers can form bonds with the modified surface of the elastomer. The bond-stitch topology can elicit the Lake-Thomas and Irwin-Orowan amplifications, and the adhesion energy is on the same order of the fracture energy of hydrogel. This approach provides strong adhesion yet retains interfacial stretchability. However, the kinetics of adhesion is slow, and creating functional groups on the elastomer surface may be complicated.

a Surface modification method for casting



b Silane coupling method for casting, coating, printing and attaching



c Gluing

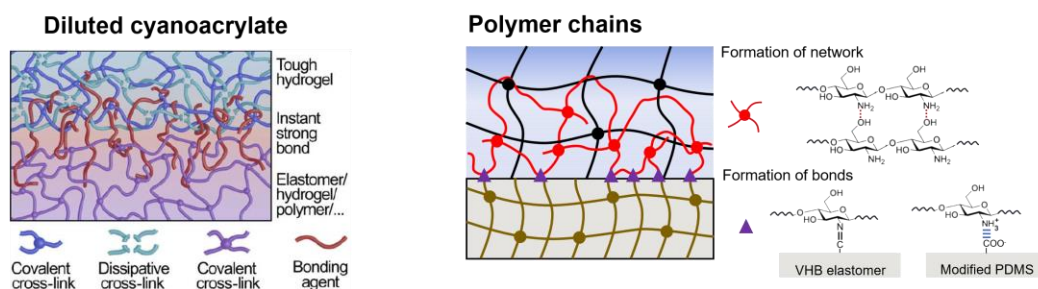


Figure 1.7 Hydrogel-elastomer adhesion. (a) Surface modification method for casting. The surface of an elastomer is chemically modified with OH groups, NH₂ groups and radicals. A hydrogel precursor is then casted on it, polymerized and form bonds on the surface of the

(Continued) elastomer. The photo shows the bonded alg-PAAM hydrogel and Ecoflex elastomer can sustain large deformation (stretch ~ 7) without debonding [74]. (b) Silane coupling method for casting, coating, printing and attaching [94]. Silane coupling agents are added into the precursors of hydrogel and elastomer, and subsequently hydrolyze. When they contact, the hydrolyzed silanes condense and form siloxane bonds between the two networks. This approach is independent of the sequence of forming the networks. The photo shows coating, printing and attaching [94]. (c) Gluing. *Diluted cyanoacrylate*: cyanoacrylate is diluted in an organic solvent, and then applied at the interface. The cyanoacrylate monomers polymerize and form a third network which topologically entangles with the polymer networks of both materials [91]. *Polymer chains*: polymer chains diffuse into the hydrogel and form a polymer network in response to a trigger, which form bonds on the surface of the elastomer and in topological entanglement with the hydrogel network. One example shown is the chemistry of using chitosan to bond hydrogel on VHB elastomer and modified PDMS [101].

1.8 Adhesion between hydrogels and other materials

Bonding hydrogels with stiff materials (i.e., glass, plastics and metals) creates novel composite materials. The unique soft-rigid combination integrates both material properties into one composite and gives rise to properties beyond individual constituent. The stiff materials are mostly lacking reactive groups for forming bonds with hydrogels. If the materials are porous, topological interlocking can be used for bonding. If the materials are nonporous, surface chemical modification is required before bonding.

1.8.1 Casting and coating

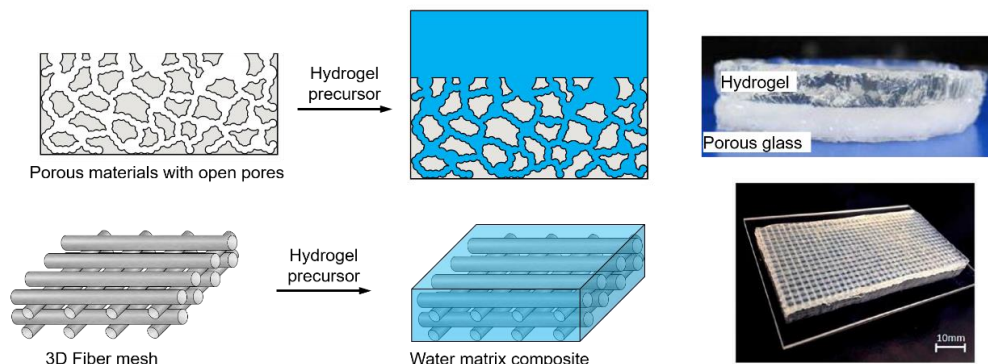
For a porous material, we have shown that the adhesion can be strong when the material has inter-connected open pores. The pores constitute a three-dimensional inter-connected porous medium. When a hydrogel precursor is casted on the material, it infiltrates into the pores

inside the material until filling all the pores. The precursor is subsequently polymerized and form a hydrogel within the porous medium as well as in the bulk material above the surface (Figure 1.8(a)). The hydrogel and the porous material are in topological interlocking at the macroscopic scale [202]. This mechanism is also valid in the case when a three-dimensional mesh composed of nonporous materials is directly immersed in the hydrogel precursor (Figure 1.8(a)). The hydrogel itself does not form strong bonds with the porous material. This simple bonding process is independent of types of hydrogels and stiff materials. To separate, the topologically interlocked hydrogel is usually ruptured.

To bond hydrogels with nonporous materials, surface modification is required [20, 92]. Nonporous materials like glass, ceramics and some metals naturally have a thin oxidized layer on the surface. The first step of surface modification is to create a hydroxyl-activated surface by oxygen plasma or UV/ozone treatment. Functional silane 3-(Trimethoxysilyl)propyl methacrylate (TMSPMA) is then grafted onto the hydroxyl-activated surface through silane condensation. In this reaction, the methoxy groups in TMSPMA first hydrolyze to silanols, and then form chemically stable siloxane bonds with the hydroxyl-activated surface upon removal of water [190, 203]. Surface-grafted TMSPMA has a methacrylate-terminal group, which can copolymerize with the monomers in a hydrogel precursor under free radical polymerization, and thus chemically anchor the hydrogel network on the surface (Figure 1.8(b)). This method can bond any type of hydrogel that is synthesized from free radical polymerization. The adhesion energy obtained is as high as the fracture energy of the hydrogel. However, toxic chemicals and multiple steps of chemical treatment are involved during the preparation. In addition, this method may not work well for materials that are inert to oxidization, such as gold, or difficult to be hydroxyl-activated, such as plastics.

a Casting

Topological interlocking



b Surface modification for casting and coating

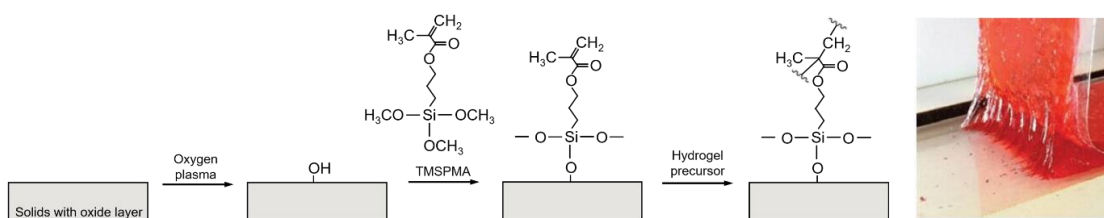


Figure 1.8 Hydrogel adhesion with other materials. (a) Casting. *Topological interlocking*: hydrogel precursors infiltrate into all inter-connected pores inside a porous material, or a three-dimensional material mesh, and polymerize to form topological interlocking with them. The photos show topological interlocking of a hydrogel and a porous glass [202], and a three-dimensional plastic mesh embedded WMC [80]. (b) Surface modification for casting and coating. A solid with oxide layer is oxygen plasma treated and chemically modified with methacrylate groups on the surface, which are used to graft hydrogel network. The photo shows the strong adhesion between a alg-PAAM hydrogel (colored red) and a glass substrate, and multiple fingers are observed in the peeling test [92].

1.9 Design hydrogel adhesion for various purposes

The diversity of topology enables building functions into adhesion for various purposes. Three types of post-adhesion—permanent, transient and triggerable—can be achieved.

Permanent adhesion is crucial in providing stable and reliable functions during the

course of adhesion. For example, hydrogel ionotronic devices need to consistently function; the WMCs need to maintain the mechanical properties over a long time; the stretchable seals need to prevent leakage permanently; some hydrogel implants need to stay in the patient's body for the lifetime. To fulfill this mission, permanently stable hydrogels and adhesion topology should be used. Permanent hydrogels include polyacrylamide (PAAM), polyethylene glycol (PEG), poly(isopropylacrylamide) (PNIPAM) and poly(dimethylacrylamide) (PDMA). The stable topology should be created with polymer chains and bonds that are inert with environment change.

Transient adhesion is especially useful in biomedical applications. For example, hydrogel adhesives and sealants capable of spontaneous degradation or detachment after a healing period is highly desirable in the post-surgery recovery. A hydrogel with a tunable degree of degradation enables the control of the drug release kinetics. Transient adhesion requires either the hydrogel itself or the topology of bonds and polymers to be transient. Typical transient elements are degradable moieties like anhydrides, esters, thioesters and certain peptide sequences. Hydrogels made of degradable polymers can be natural polymers (e.g., protein and polysaccharide), and some synthetic polymers (e.g., poly(lactide acid) (PLA), poly(caprolactone) (PCL), and poly(lactic acid-co-glycolic acid) (PLGA)). Degradation of a transient hydrogel can occur at the polymer chains or the crosslinks, by hydrolysis or enzyme activity [27]. For example, a synthetic PEG-b-PLA copolymer hydrogel is susceptible to hydrolytic cleavage at the ester bonds of the PLA segments [204]. A mildly oxidized alginate hydrogel can hydrolytically degrade through the cleavage of labile bonds [205]. A hydrogel synthesized from the copolymer of PEG and short oligopeptides can specifically cleavage by collagenase and plasmin proteases [206]. Similar degradable moieties can be incorporated in the topology to make transient topology.

Triggerable adhesion allows adhesion and de-adhesion in a controlled manner. The adhesion stays stable and permanent if the surrounding environment is stable, but becomes unstable or diminishes if a trigger is present. In response to triggers (e.g., chemicals, pH, heat,

light, ultrasound and ultraviolet light), moieties like physical bonds (e.g., ionic bonds, hydrogen bonds, or host-guest interaction) and cleavable covalent linkages (e.g., ester bonds, disulfide bonds) can be dissociated. Either a triggerable hydrogel or topology can generate triggerable adhesion. As an example, an ionically crosslinked alginate hydrogel accelerates the drug release in response to ultrasound, due to the disruption of calcium crosslinks and thus changes its molecular structure [207]. As another example, the alg-PAAM hydrogel crosslinked by disulfide bonds and ionic bonds can on-demand dissociate by chelator ethylenediaminetetraacetic acid (EDTA) and the reducing agent glutathione (GSH) [28]. Similarly, these physical bonds and cleavable covalent linkages are commonly used to make triggerable topology.

Different types of hydrogels and topologies can be combined to build even more complex functions into adhesion. For example, a transient hydrogel and a triggerable adhesion topology give rise to both characteristics of transient and triggerable adhesion. The adhesion depends on two concurrent kinetic processes: the degradation of hydrogel and the deactivation of the adhesion topology. The rates of these two processes may vary greatly among different types of bonds and triggers. It is conceived that the adhesion can be carefully and precisely programmed, and would enable much broader and versatile applications.

1.10 Outline of the thesis

In Chapter 2, we use stitch-stitch topology to strongly adhere two wet materials (i.e., hydrogels and tissues) using polymer chains, without requiring functional groups from both wet materials, and the interface maintains softness. In response to a trigger, the polymer chains form a network, in topological entanglement with the two polymer networks of the wet materials, stitching them together like a suture at the molecular scale. The adhesion energy above 1000 J/m^2 can be obtained. The molecular suture can be designed to be permanent, transient, or removable on-demand.

In Chapter 3, we use bridging topology to develop a class of strong tissue adhesive

consisting of alginate-polyacrylamide (alg-PAAM) hydrogel and biocompatible polymer chains. The alg-PAAM hydrogel provides large energy dissipation during deformation, and the polymer chains can form bond with both polymer network of hydrogel and tissue. A new record of tissue adhesion exceeding 1000 J/m^2 is measured. Adhesion occurs within minutes, independent of blood exposure and compatible with *in vivo* dynamic movements. This family of adhesives may be useful in many areas of application, including tissue adhesives, wound dressings, and tissue repair.

In Chapter 4, we examine a new aspect in hydrogel adhesion: topology of connecting materials. We realize topologies of numerous varieties have not been used, and their potential applications are unexplored. To highlight the potential, we delve a specific bond-stitch topology. We aim to adhere a pre-formed hydrogel with no functional groups to diverse materials with functional groups on the surface. We trigger polymer chains to form a polymer network, which forms bonds on the surface of the material, and stitches with the polymer network of the hydrogel. Through the synergy of chemistry, mechanics and topology, we can achieve adhesion energy over $1,000 \text{ J/m}^2$. We further use topologies to demonstrate a series applications in medicine and engineering.

In Chapter 5, we outlook the future directions of hydrogel adhesion from the aspects of design, control, industrial translations and scientific opportunities, as well as potential challenges.

Chapter 2

Topological Adhesion of Wet Materials

Abstract: Achieve strong adhesion between wet materials (i.e., tissues and hydrogels) is challenging. Existing adhesives are weak, toxic, incompatible with wet and soft surfaces, or restricted to specific functional groups from the wet materials. The approach reported here uses biocompatible polymer chains to achieve strong adhesion and retain softness, but requires no functional groups from the wet materials. In response to a trigger, the polymer chains form a network, in topological entanglement with the two polymer networks of the wet materials, stitching them together like a suture at the molecular scale. To illustrate topological adhesion, pH is used as a trigger. The stitching polymers are soluble in water in one pH range but form a polymer network in another pH range. Several stitching polymers are selected to create strong adhesion between hydrogels in full range of pH, as well as between hydrogels and various porcine tissues (liver, heart, artery, skin, and stomach). The adhesion energy above $1,000 \text{ Jm}^{-2}$ is achieved when the stitching polymer network elicits the hysteresis in the wet materials. The molecular suture can be designed to be permanent, transient, or removable on-demand. The topological adhesion may open many opportunities in complex and diverse environments.

2.1 Introduction

Existing and emerging medical practices have posed a persistent, fundamental challenge: creating strong adhesion between wet materials—living tissues and synthetic hydrogels—under physiological conditions. Applications include tissue repair [29, 46], wound dressing [29, 208], and drug delivery [13]. Also under intense development are implantable devices for energy harvesting [209], neural stimulation and recording [210], sensing [14], and actuation [49]. Existing adhesives are weak, or toxic, or incompatible with wet and soft surfaces, or restricted to specific functional groups from the wet materials. For example, cyanoacrylate is a strong

adhesive, but is cytotoxic, and forms a glassy phase and hardens the interface [211]. Nanoparticles [98], bridging polymers [212], fibrin [136] and polyethylene glycol gels [11] are facile, but the adhesion energy is low ($1-10 \text{ Jm}^{-2}$), due to either weak bonds or fragile materials. A family of recently developed adhesives achieve adhesion energy of $1,000 \text{ Jm}^{-2}$, but the adhesion relies on functional groups from the tissues and hydrogels, and cannot bond hydrogels without suitable functional groups [29].

2.2 Results and discussion

Here we report an approach that molecularly stitches wet materials. Each wet material, to be called an *adherend*, has a pre-existing polymer network. The molecular stitch uses polymer chains to form a new polymer network, in response to a trigger. This new polymer network is localized at the interface between the two adherends, and in topological entanglement with the network of the adherend on either side. It is through this topological entanglement that the new polymer network stitches the two pre-existing polymer networks. To debond, the topologically entangled networks must disentangle—that is, at least one of the three networks must break. We call the polymer chains the *stitching polymers*, and their network the *stitching polymer network*. We call this bonding method *topological adhesion*, or *topohesion* for brevity, and call the solution of the stitching polymers the *topohesive*. The stitching polymer network functions as a *molecular suture*.

Our hypothesis is twofold. First, polymer chains can be triggered to form a network, localized at the interface of two adherends, and in topological entanglement with the pre-existing networks of the adherends. Second, the stitching polymer network can be flexible enough to retain the softness of the adherends, and yet strong enough to achieve adhesion energy comparable to the bulk toughness of the adherends by eliciting the hysteresis in the adherends, without requiring any functional groups from the adherends. (Functional groups may exist in tissues and hydrogels for other reasons, but need not form any bonds with the

stitching polymers.)

Topological entanglement has played fundamental roles in polymers [213]. It has in recent decades led to hydrogels and elastomers of exceptional modulus, strength, and toughness [107, 108, 214, 215]. Topological entanglement has also been used to achieve adhesion by diffusing monomers into adherends and polymerizing *in-situ* [202, 216]. Such a bonding method starts with monomers, and often involves invasive and toxic chemical reactions, as well as ultraviolet irradiation. No attempt has been reported to trigger polymer chains to form a stitching network and achieve strong adhesion between hydrogels and tissues.

We illustrate topological adhesion by using pH as a trigger. This pH-triggered topological adhesion mimics the formation of strong byssal threads by a mussel (*Mytilus californianus* Conrad 1837) [161]. When a foot of the mussel attaches to a surface, the distal depression of the foot secretes an aqueous solution of proteins at pH ~ 3 . When the foot lifts off, the surrounding seawater of pH ~ 8 flows in, and the proteins form a strong network.

To formulate a topohesive, we use polymer chains that dissolve in water in one pH range and form a polymer network in another pH range. We prepare an aqueous solution of the stitching polymer chains at one value of pH. The two adherends have another value of pH, representative of that in a physiological environment. We place the solution of the stitching polymer chains between the two adherends. In response to the pH in the adherends, the polymer chains form a third network. We readily achieve adhesion energy above $1,000 \text{ Jm}^{-2}$ when the stitching polymer network elicits hysteresis in the wet materials. By choosing different species of stitching polymers, we achieve strong adhesion in full range of pH. We bond hydrogels to various porcine tissues (liver, heart, artery, skin, and stomach). Furthermore, the molecular suture is removable, on-demand, by changing the pH back to the soluble range of the polymer chains.

To ascertain our hypothesis, we first bond two pieces of hydrogels using chitosan chains. Hydrogels are relatively simple and well-characterized systems, and structurally similar to living

tissues and extensively used in medicine [12, 14]. Chitosan chains are biopolymers widely used in bioengineering [217]. The amine groups on chitosan are responsive to changes in pH [178]. The dissociation $[\text{NH}_3^+] \rightleftharpoons [\text{NH}_2] + [\text{H}^+]$ has the equilibrium constant $K_a = [\text{NH}_2][\text{H}^+]/[\text{NH}_3^+]$. By definition $\text{p}K_a = -\log[K_a]$ and $\text{pH} = -\log[\text{H}^+]$, so that $\log[\text{NH}_2] - \log[\text{NH}_3^+] = \text{pH} - \text{p}K_a$. For chitosan, $\text{p}K_a = 6.5$. When $\text{pH} < 6.5$, $[\text{NH}_2] < [\text{NH}_3^+]$, and the chitosan chains dissolve in water as a polyelectrolyte (Figure 2.1(a)). When $\text{pH} > 6.5$, $[\text{NH}_2] > [\text{NH}_3^+]$, and the $\text{NH}_2\text{--OH}$ hydrogen bond promotes the chitosan chains to form a network (Figure 2.1(b)) [178, 179].

We prepared an aqueous solution of chitosan of $\text{pH} = 5$, and placed the solution between two hydrogels of $\text{pH} = 7$ (Figure 2.1(c)). The chitosan chains diffused into the two hydrogels and, in response to the pH in the hydrogels, formed a third network (Figure 2.1(d)). We have hypothesized that the chitosan network is localized at the interface, in topological entanglement with the networks of the two hydrogels. Whether such a chitosan network will form depends on two concurrent kinetic processes: the diffusion of chitosan chains into the hydrogel, and the formation of the chitosan network.

To confirm the formation of the chitosan network localized at the interface, we labeled the chitosan chains with fluorescein isothiocyanate (FITC), and tracked their diffusion using confocal microscopy (Figure 2.1(e)). In the first hour, the chitosan chains diffused away from the interface, shown by the gradual thinning of the chitosan-rich layer and the thickening of the diffusion layer. However, fewer chitosan chains diffused away in the next few hours, and finally chitosan chains ceased to diffuse at 24 hours. As a comparison, when we placed the same chitosan solution between two hydrogels of $\text{pH} = 5$, the chitosan chains kept diffusing into the hydrogels, and no chitosan network formed (Figure A1).

According to the Rouse model [218], the diffusivity of a chitosan chain in water is $D = kT/(N\eta b)$, where kT is the temperature in the unit of energy, η is the viscosity of water, b is the size of the repeating unit of the chitosan chain, and N is the number of the repeating units. Taking $kT = 10^{-21}$ J, $\eta = 10^{-3}$ Pa·s, $b = 10^{-9}$ m, and $N = 1,000$, we obtain that $D \sim 10^{-12}$ m²s⁻¹, which

is much lower than the diffusivity of H^+ and OH^- ($\sim 10^{-9} \text{ m}^2\text{s}^{-1}$). The time scale is estimated as $h^2/D \sim \text{hours}$, where h is the diffused chitosan thickness ($\sim 100 \mu\text{m}$ from the confocal image). This estimate roughly agrees with our experimental observation.

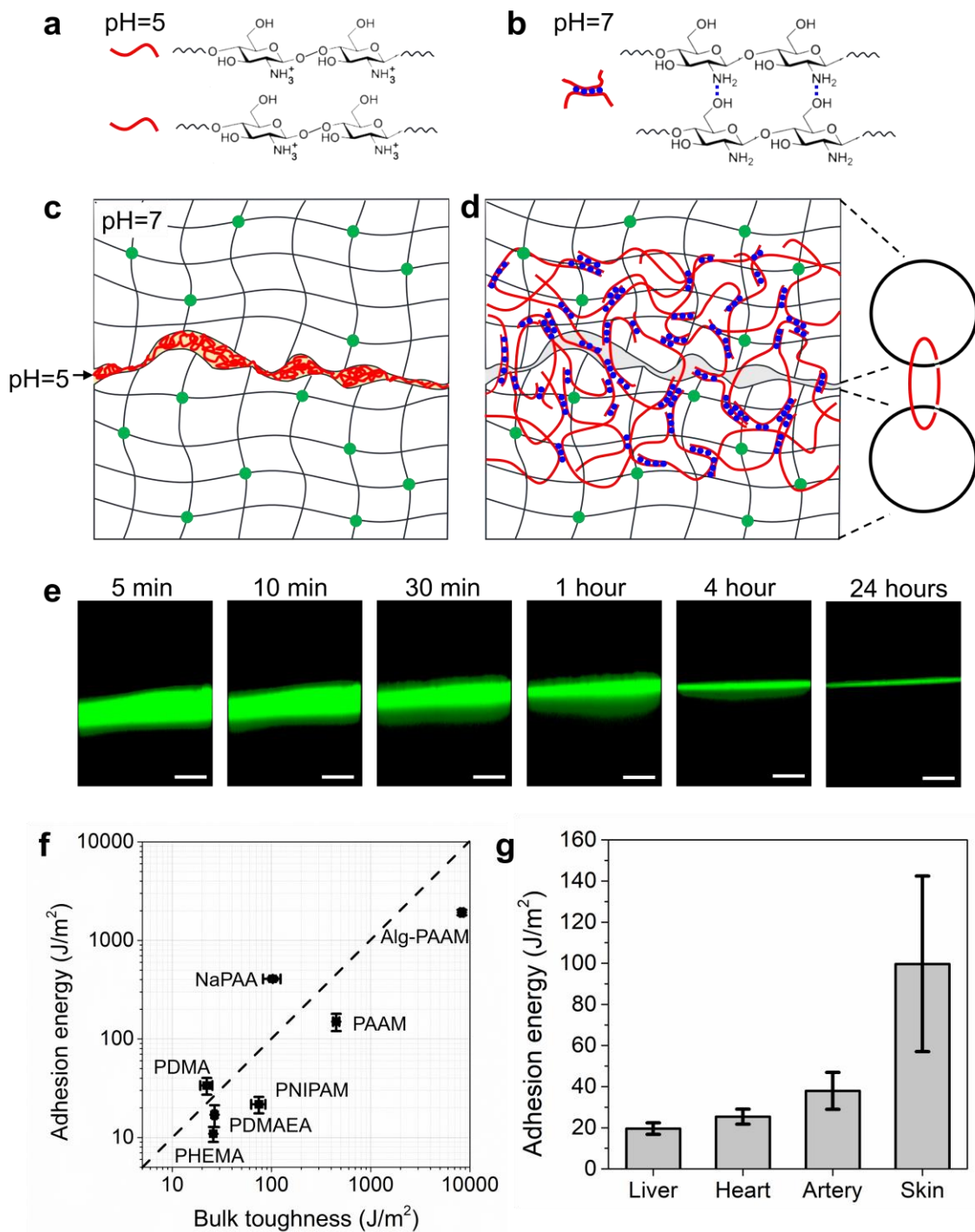


Figure 2.1 Topological adhesion. (a) Chitosan chains dissolve in water at $\text{pH} = 5$. (b) Chitosan

(Continued) chains form a network in water at pH = 7. (c) Place an aqueous solution of chitosan of pH = 5 between two hydrogels of pH = 7. (d) The chitosan chains diffuse into the two hydrogels and form a network, which topologically entangles with the networks of the two hydrogels. (e) A chitosan solution is placed between two pieces of polyacrylamide hydrogels. A sequence of confocal microscopic images show that the chitosan chains diffuse away from the interface in the first hour, diffuse less for the next few hours, and cease to diffuse at 24 hours. The scale bar is 300 μm . (f) The adhesion energy of the chitosan-stitched hydrogel is plotted against the bulk toughness of the hydrogel. The hydrogels used are listed in Table A1. (g) The adhesion energy of chitosan-stitched PAAM hydrogel and various tissues. The data represent the mean and standard deviation of 4–6 experimental results.

We further ascertain the formation of chitosan network in topological entanglement with the networks of the hydrogels by measuring the adhesion energy. The dissociation energy of a hydrogen bond is weak ($\sim 10 kT$) compared to that of a covalent bond ($\sim 140 kT$) [122, 219]. However, tens to hundreds of hydrogen bonds in aggregation result in a high bonding energy [220]. The network of pure chitosan is still fragile, but the chitosan network in topological entanglement with the network of the adherends achieves adhesion energy comparable to the bulk toughness of the adherends (Figure 2.1(f), Table A1). For example, the bulk toughness of PDMA is $\sim 22 \text{ Jm}^{-2}$, and the adhesion energy is $\sim 33 \text{ Jm}^{-2}$ the bulk toughness of alg-PAAM is $\sim 8,000 \text{ Jm}^{-2}$, and the adhesion energy is $\sim 2,000 \text{ Jm}^{-2}$. Moreover, the bonded hydrogels are stretchable and transparent (Figure A3) [221]. We also used chitosan chains to stitch PAAM hydrogel to various porcine tissues: liver, heart, artery, and skin (Figure 2.1(g)). The skin exhibits a relatively high toughness among the soft organs ($\sim 1,000 \text{ Jm}^{-2}$) [157], thus the corresponding adhesion energy is also high ($\sim 100 \text{ Jm}^{-2}$).

The procedure for preparing adhesion can greatly affect the adhesion energy. To illustrate some of the effects, we spread a chitosan solution on one piece of PAAM hydrogel,

placed another piece of PAAM hydrogel on top, and compressed the two hydrogels with a strain d/L (Figure 2.2(a)). The maximum adhesion was achieved at the combination of a solution of 500 μm thickness and a strain of 5.5 %, and the thinner chitosan layer and larger strain lead to weaker adhesion energy (Figure 2.2(b)). We monitored the change of adhesion energy over time, and found that the adhesion energy established to $\sim 50 \text{ Jm}^{-2}$ within 30 min, and then approached an equilibrium value of $\sim 150 \text{ Jm}^{-2}$ after 24 hours (Figure 2.2(c)). The slow kinetics may be associated with the slow formation of the chitosan network. Similar phenomena have been observed in the aging of PAAM-PVA hydrogels [222] and PAAM-chitosan hydrogels [221], as well as in the slow recovery of alg-PAAM hydrogels [108]. For topological adhesion, the kinetics of adhesion depend on stitching polymers. For example, poly(4-aminostyrene) (PAS) reached adhesion energy of $\sim 300 \text{ Jm}^{-2}$ within the first 15 min, and saturated to $\sim 400 \text{ Jm}^{-2}$ after 10 hours (Figure A4). The controlled kinetics of adhesion may find clinical advantages, as the initial relatively small adhesion is often sufficient to hold tissues or hydrogels [29, 98], but allows repositioning. In addition, the chitosan chains need to be sufficiently concentrated and long to ensure strong adhesion (Figure 2.2(d-e)).

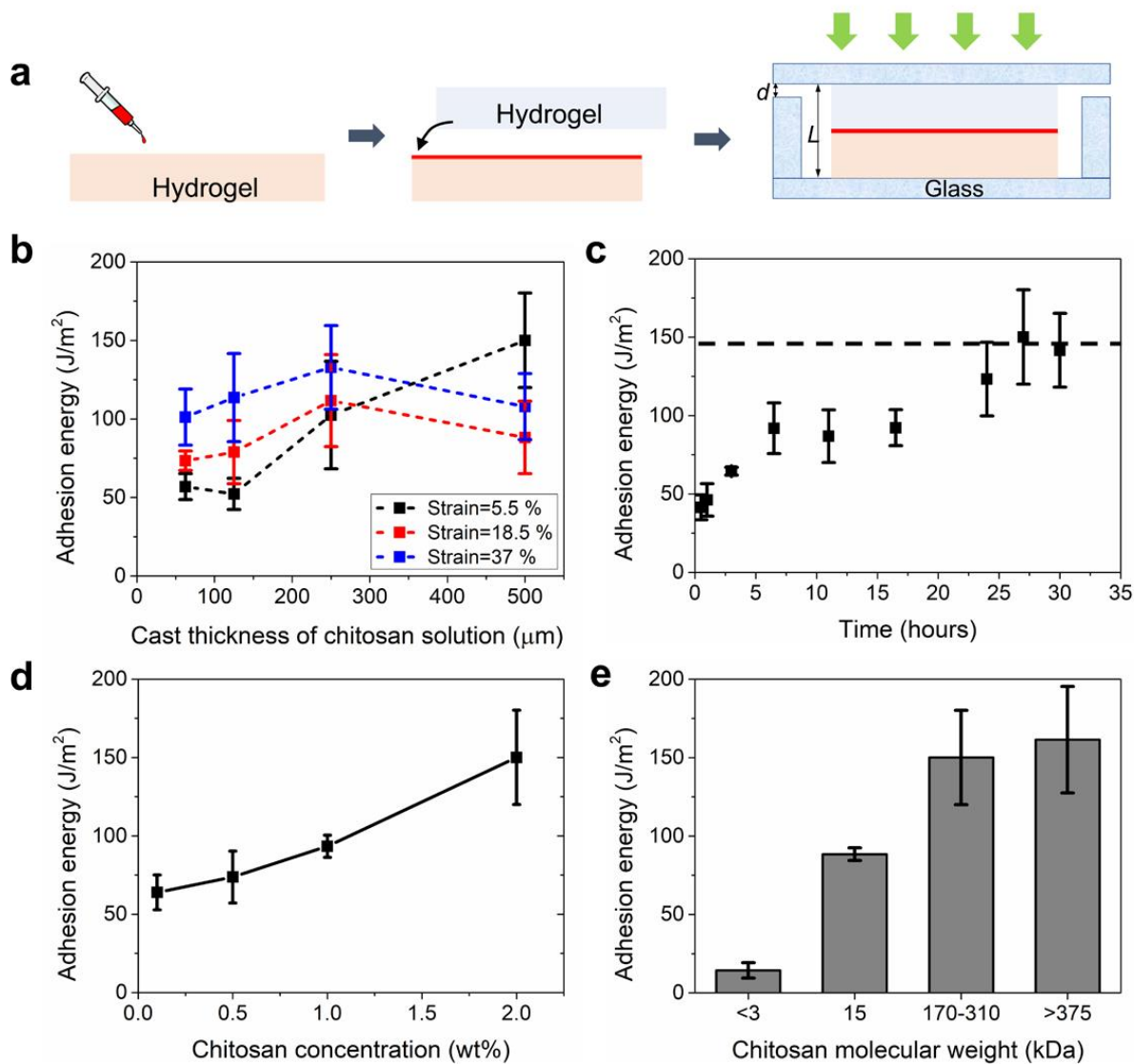


Figure 2.2 Adhesion energy as a function of several variables. (a) Schematics of the bonding procedure. Spread an aqueous solution of chitosan on the surface of one PAAM hydrogel, place the other PAAM hydrogel on top, and compress the two pieces of hydrogels with strain d/L . (b) Adhesion energy varies with the thickness of the chitosan solution and the compressive strain. (c) Adhesion energy evolves with time. (d) Adhesion energy increases with the concentration of chitosan solution. (e) Adhesion energy increases with the molecular weight of chitosan chains. All the data represent the mean and standard deviation of 4–6 experimental results.

The fluids in human tissues vary greatly in pH [223]. The blood, the cerebrospinal fluid, and the cellular fluid of muscle and skin are nearly neutral (pH = 6-7.4), the pancreatic fluid and bile are alkaline (pH = 7.6-8.8), and the gastric fluids are extremely acidic (pH = 1-3.5). We next used several species of stitching polymers to achieve strong adhesion in full range of pH. In addition to chitosan, which forms a network when $\text{pH} > 6.5$, we used three other species of stitching polymer chains: PAS forms a network when $\text{pH} > 4.6$, alginate forms a network when $\text{pH} < 3.5$, and cellulose forms a network when $\text{pH} < 13$ (Figure 2.3(a), Table A2). We used the four species of polymers to bond PAAM hydrogels of various values of pH, and confirmed that adhesion was established only when the pH of the hydrogels was in the network-forming range of each species of the stitching polymers (Figure 2.3(b-e)).

In the network-forming range of pH, the adhesion energy is low when the pH of hydrogel is either close to, or far from, the pKa of the stitching polymers, and exhibits a maximum in the middle. We interpret this finding using chitosan as an example. When the pH of hydrogel is close to pKa of chitosan, the positively charged amine NH_3^+ and neutral amine NH_2 are comparable in numbers. This may lead to insufficient number of hydrogen bonds and thus a weak chitosan network. When the pH of hydrogel far exceeds pKa, the chitosan chains at interface are neutralized to form network much faster, which impedes the diffusion of chitosan chains into both hydrogels. This may lead to insufficient topological entanglements with both hydrogel networks.

Topological adhesion enables the design of adhesives for extreme pH environment. We demonstrated the strong adhesion between a hydrogel and a porcine stomach tissue in an extremely low pH (~ 1.5) with cellulose solution (Figure A5). The low pH resembles the physiological environment inside the stomach. We tested the bonding by lap shear test. The hydrogel used is much softer than the stomach tissue. The lap-shear test showed that the hydrogel remained firmly bonded to the tissue over a stretch of 11 times of its initial length (Movie A1).

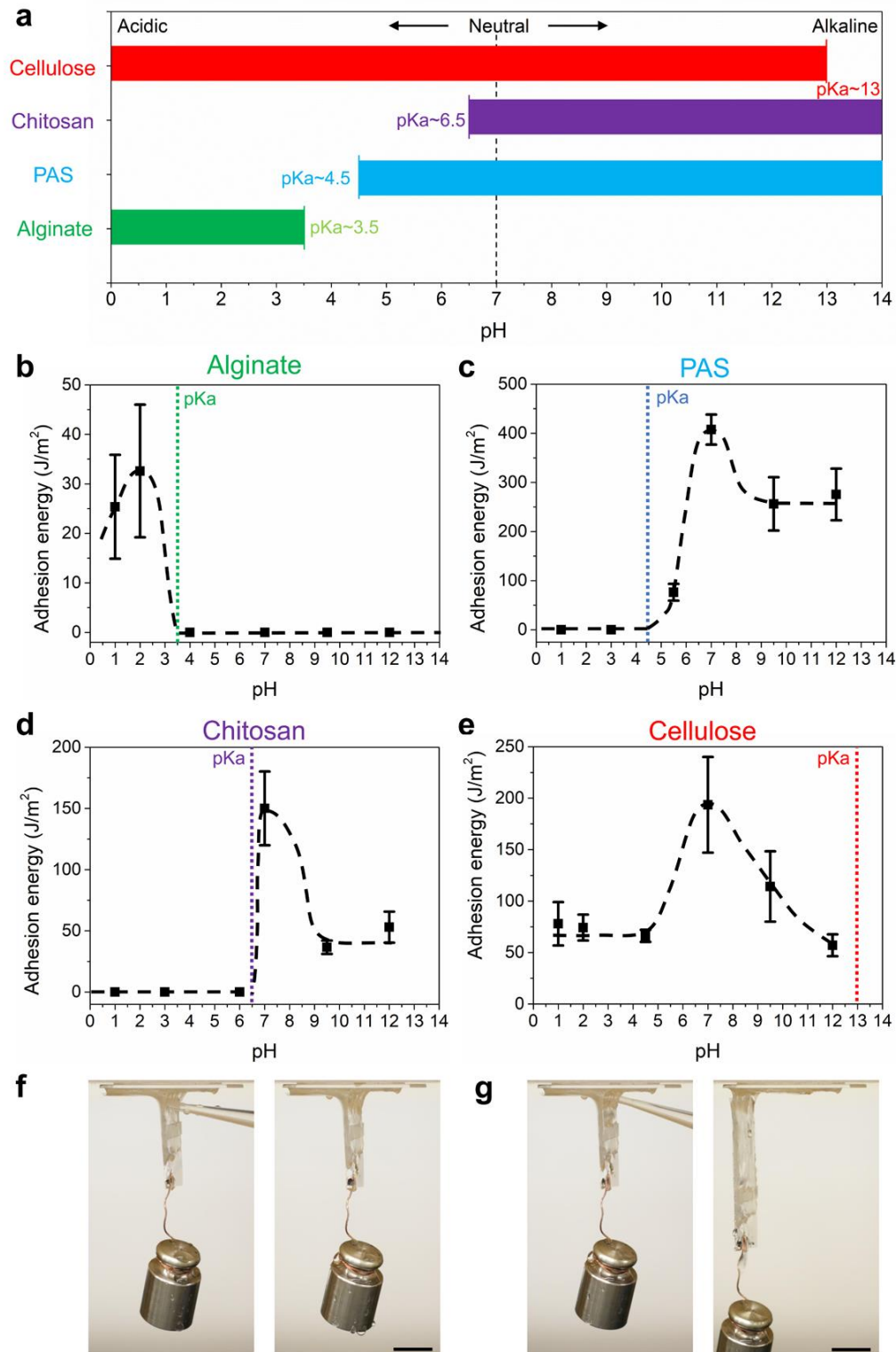


Figure 2.3 Adhesion in full range of pH. (a) The ranges in which four species of polymers form networks cover all pH levels. The adhesion energy depends on pH when two pieces of PAAM

(Continued) hydrogels are bonded with each species of polymers: (b) alginate, (c) PAS, (d) chitosan and (e) cellulose. All the data represents the mean and standard deviation of 4–6 experimental results. Two pieces of PAAM hydrogels were bonded with chitosan. The top hydrogel was attached to a rigid acrylic plate, and the bottom hydrogel was attached to a weight. (f) When water was dripped at the bonding front, the hydrogels remained bonded. (g) When an acid was dripped at the bonding front, the hydrogels debonded. The scale bar is 2 cm.

The molecular stitch is removable, on-demand, when the pH is changed back to the soluble range of the stitching polymers. We demonstrated this capability using chitosan-stitched PAAM hydrogels. We fixed the top hydrogel to a rigid acrylic plate and hung the bottom hydrogel with a weight. The weight itself did not cause debonding. We then dripped water at the bonding front for several times. No debonding was observed after 12 trails of dripping (Figure 2.3(f), Movie A2). In comparison, we dripped hydrochloride acid (1 M) at the same bonding front. The debonding progressively advanced at every single dripping, until two hydrogels completely detached (Figure 2.3(g), Movie A3). The capability of on-demand removal of the molecular stitch may motivate future design of smart adhesives or bandages.

Topological adhesion involves three polymer networks: the pre-existing networks of the two adherends, and the newly formed network of the stitching polymers. To disentangle, at least one of the three networks must break. The intrinsic energy to break a network is 10-100 Jm⁻² [110, 224-226]. This picture is fundamentally different from polymer chains physically entangled with the networks of two adherends without forming a network. The polymer chains can be disentangled and pulled out without breaking any network, requiring an energy of ~1 Jm⁻² [102, 104].

To confirm the formation of a strong and stable stitching polymer network, we measured the speed of crack as a function of energy release rate. When a crack extends at a certain speed, the measured energy release rate results from two processes: the disentanglement at the crack

front, and the hysteresis in the adherends. The latter effect reduces when the crack speed is low. We measured the energy release rate at crack speeds across many orders of magnitude (Figure 2.4). For chitosan-stitched PAAM hydrogels, the energy release rate arrives at a constant value of $\sim 60 \text{ Jm}^{-2}$ as the crack speed approaches zero. This relatively high value supports the hypothesis that the chitosan network and the PAAM network are topologically entangled: the debond breaks at least one of the networks.

To find whether the chitosan network or the PAAM network breaks, we also conducted the slow-crack test for a homogeneous PAAM hydrogel. The energy release rate of the homogeneous PAAM hydrogel is higher than that of the chitosan-stitched PAAM hydrogels at all crack speeds, and arrives at a constant value of $\sim 250 \text{ Jm}^{-2}$ as the crack speed approaches zero. This comparison indicates that the chitosan-stitched PAAM hydrogels disentangled by the breaking of the chitosan network, not the PAAM network. The slow-crack experiment by itself, however, is unable to differentiate whether the chitosan network broke by the scission of the chitosan chains, or by the unzipping of the hydrogen bonds between the chitosan chains.

Topological adhesion confirms a fundamental principle in fracture mechanics: adhesion is strong if debond elicits hysteresis in the adherends. We conducted the slow-crack experiment for chitosan-stitched hybrid alg-PAAM hydrogels. The stress-stretch curve of an alg-PAAM hydrogel exhibits pronounced hysteresis [224, 226, 227]. Our slow-crack data shows that the chitosan suture is strong enough to elicit the hysteresis in the alg-PAAM to achieve strong adhesion. However, the stress-strain curve of the alg-PAAM hydrogel is rate-dependent [228, 229]. The energy release rate is $\sim 3000 \text{ Jm}^{-2}$ at a crack speed of 10 mms^{-1} , but reduces to $\sim 400 \text{ Jm}^{-2}$ at $1 \text{ }\mu\text{ms}^{-1}$. By extrapolation, the energy release rate approaches 60 Jm^{-2} as the crack speed approaches zero. The hysteresis in the bulk greatly amplifies the energy release rate at high crack speed, but contributes negligibly to the energy release rate at low crack speed.

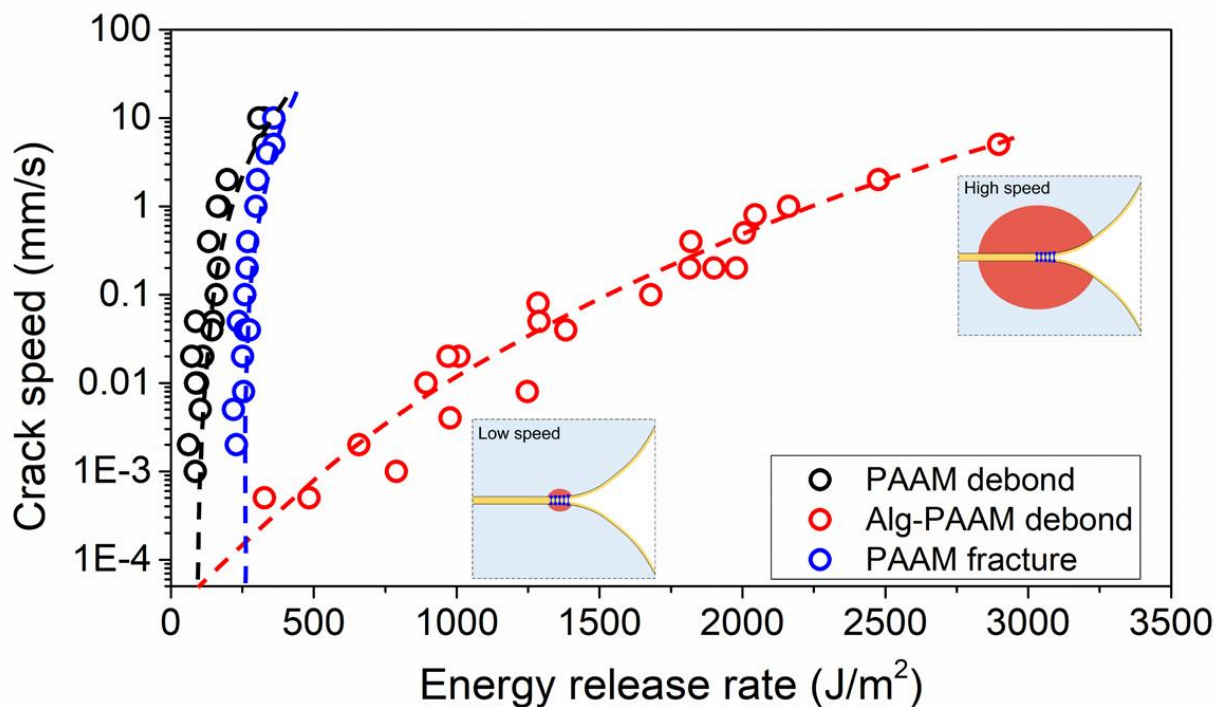


Figure 2.4 Crack speed as a function of energy release rate. Compare three systems: debond of chitosan-stitched PAAM hydrogels, debond of chitosan-stitched alg-PAAM hydrogels, and fracture of a homogeneous PAAM hydrogel. At any crack speed, the energy release rate of the homogeneous PAAM hydrogel is larger than that of the chitosan-stitched PAAM hydrogels. As the crack speed approaches zero, the energy release rate approaches 60 Jm^{-2} for debond, and 250 Jm^{-2} for fracture. For the chitosan-stitched alg-PAAM hydrogels, the energy release rate increases greatly with the crack speed, but approaches 60 Jm^{-2} at low crack speed. The insets indicate that the energy release rate results from the synergy of two processes: the breaking of the stitching polymer network and the hysteresis in the hydrogels. The hysteresis in the hydrogels greatly amplifies the energy release rate at high crack speed, but contributes negligibly to the energy release rate at low crack speed. Each data point represents a single test.

2.3 Conclusion

In summary, these experiments taken together support the hypothesis that suitable polymers form a network in topological entanglement with the networks of two wet materials,

and the topologically entangled networks lead to strong adhesion without requiring any functional groups from the wet materials. A given species of stitching polymers works for any wet materials upon triggering by an environmental stimulus, so long as the wet materials do not prevent the formation of the stitching polymer network. The topological adhesion can be applied to a large area, so long as the stitching polymers cover the entire bonding area. The stitching polymer network functions as a suture in the molecular scale, and this molecular suture can be designed to be permanent, transient, or removable on-demand. Topological adhesion is general, which is not limited to be triggered by pH but can be potentially triggered by other stimuli such as salt, temperature and light, along with their corresponding responsive polymers. For example, PNIPAM can be used as the thermo-responsive polymer, which forms a network when the temperature is above the lower critical solution temperature. As another example, when gold nanoparticles are mixed into the wet materials, they generate heat upon exposure to light [230], which trigger the topological adhesion using thermo-responsive polymers. It is hoped that the topological adhesion opens a field of development to achieve strong adhesion between wet materials, while retaining softness.

Chapter 3

Tough Adhesives for Diverse Wet Surfaces

Abstract: Adhesion to wet and dynamic surfaces, including biological tissues, is important in many fields, but has proven extremely challenging. Existing adhesives are either cytotoxic, adhere weakly to tissues, or cannot be utilized in wet environments. We report a bio-inspired design for adhesives consisting of two layers: an adhesive surface and a dissipative matrix. The former adheres to the substrate by electrostatic interactions, covalent bonds, and physical interpenetration. The latter amplifies energy dissipation through hysteresis. The two layers synergistically lead to higher adhesion energies on wet surfaces as compared with those of existing adhesives. Adhesion occurs within minutes, independent of blood exposure, and compatible with in vivo dynamic movements. This family of adhesives may be useful in many areas of application, including tissue adhesives, wound dressings, and tissue repair.

3.1 Introduction

Adhesives that can bond strongly to biological tissues would have broad applications ranging from tissue repair [44, 45] and drug delivery [13, 231], to wound dressings [42, 232] and biomedical devices [233, 234]. However, existing tissue adhesives are far from ideal. Cyanoacrylate (Super Glue) is the strongest class of tissue adhesive [211], but is cytotoxic; is incompatible with wet surfaces as it solidifies immediately upon exposure to water; and forms rigid plastics that cannot accommodate dynamic movements of tissues [174]. Nanoparticles [98] and mussel-inspired adhesives [162] adhere weakly to tissues, as their adhesion mainly relies on relatively weak physical interactions, typically leading to low adhesion energies of 1-10 Jm⁻². Commercial adhesives such as the fibrin glue TISSEEL (Baxter) [136] and polyethylene glycol-based adhesives [155] like COSEAL (Baxter) and DURASEAL (Confluent Surgical), can form covalent bonds with tissues. However, their matrix toughness and adhesion energies are on the

order of 10 Jm^{-2} [235]. Such brittle adhesives are vulnerable to debonding, because of cohesive failure in the adhesive matrix. For comparison, cartilage constitutes a matrix of high toughness (1000 Jm^{-2}) and bonds to bones with an adhesion energy of 800 Jm^{-2} [236].

3.2 Results and discussion

Achieving high adhesion energy requires the synergy of two effects. First, the adhesive should form strong bonds with the substrate. Second, materials inside either the adhesive or the substrate (or both) should dissipate energy by hysteresis. Tissue adhesives must also show compatibility with body fluids, as well as with cells and tissues. Here we report the design of a family of tough adhesives (TAs) for biological applications to meet those requirements. The design is inspired by a defensive mucus secreted by slugs (*Arion subfuscus*) that strongly adheres to wet surfaces [237]. This slug adhesive consists of a tough matrix with interpenetrating positively charged proteins [238]. Our TAs are made up of two layers: (i) an adhesive surface containing an interpenetrating positively charged polymer and (ii) a dissipative matrix (Figure 3.1(a)). The adhesive surface can bond to the substrate through electrostatic interactions, covalent bonds and physical interpenetration, while the matrix dissipates energy through hysteresis under deformation.

The TAs were designed based on two criteria: (i) the adhesive surface must wet negatively charged surfaces of tissues and cells, and form covalent bonds across the interface while being compliant to dynamic movements of tissues; (ii) the dissipative matrix must be tough and capable of dissipating energy effectively when the interface is stressed. To satisfy the first criterion, we employed a bridging polymer that bears positively charged primary amine groups under physiological conditions. The primary amines found in the slug adhesive are believed to play a major role in its mechanics and adhesion [239]. Such a polymer can be adsorbed to the tissue surface via electrostatic attraction, and provide primary amine groups to bind covalently with carboxylic acid groups from the hydrogel matrix and the tissue surface

(Figure 3.1(a)). If the target surface is permeable, the bridging polymer can also penetrate into the target surface, forming physical entanglements, and chemically anchor the adhesive. The second criterion is satisfied by using a hydrogel capable of dissipating energy as the dissipative matrix. For instance, alginate-polyacrylamide (Alg-PAAm) hydrogels effectively dissipate energy under deformation [108]. We hypothesize that by combining the interfacial bridging and background hysteresis, the TAs could form strong adhesion on wet surfaces.

With the use of these design principles, we fabricated a family of TAs that can adhere to wet surfaces. We chose porcine skin as the model tissue, as it closely resembles human skin and is robust, ensuring that ultimate adhesive failure occurs at the interface. To identify an appropriate bridging polymer, we tested five polymers including chitosan, polyallylamine (PAA), polyethylenimine (PEI), collagen and gelatin. The bridging polymer penetrated rapidly into the hydrogel matrix (Figure B1), forming a positively charged surface (Figure B2). Two coupling reagents, 1-ethyl-3-(3-dimethylaminopropyl) carbodiimide (EDC) and N-hydroxysulfosuccinimide (sulfo-NHS), were applied to facilitate covalent bond formation [176, 177]. Other coupling reagents or enzymes, such as transglutaminase, can also enable the formation of interface-bridging covalent bonds [240]. Our TAs were then applied on the epidermis of porcine skin with compression, and the resulting adhesion was quantified with adhesion energy (Figure B3). Among the tested polymers, polyallylamine and chitosan led to adhesion energy $>1000 \text{ Jm}^{-2}$ (Figure 3.1(b) and Figure B4), probably due to the high concentration of primary amines present on these polymers. In comparison, use of the coupling reagents or the bridging polymer alone led to 14 Jm^{-2} and 303 Jm^{-2} , respectively (Figure B5). Adhesion energy was sensitive to the concentration, but not the molecular weight of the bridging polymer (Figure B6).

We next examined the importance of the synergy between interfacial bridging and background hysteresis. Our TAs were compared with adhesives formed with either alginate (Alg) or polyacrylamide (PAAm) hydrogels, as these do not dissipate energy as effectively as the Alg-

PAAm hydrogels [108]. The coupling reagents and chitosan were again applied for interfacial bridging. The alginate hydrogel led to weak adhesion, as it is vulnerable to rupture and lacks effective energy-dissipating mechanisms to toughen the interface. The PAAm hydrogel resulted in higher adhesion, but not as high as the tough matrix of the Alg-PAAm hydrogel, which enables TAs to integrate high adhesion energy and high matrix toughness simultaneously (Figure 3.1(c) and Figure B4). This specific combination cannot be found among existing tissue adhesives (Figure 3.1(d) and Figure B7), including cyanoacrylate (CA), COSEAL, and a nanoparticle-based adhesive. Commercial adhesives are either formed with a brittle matrix such as COSEAL or lack strong interaction with tissues, as in the case of adhesive bandages. This finding is also echoed in many studies on adhesion between hard materials and rubbers [241, 242], and adhesion between hydrogels and inorganic oxidized surfaces [92].

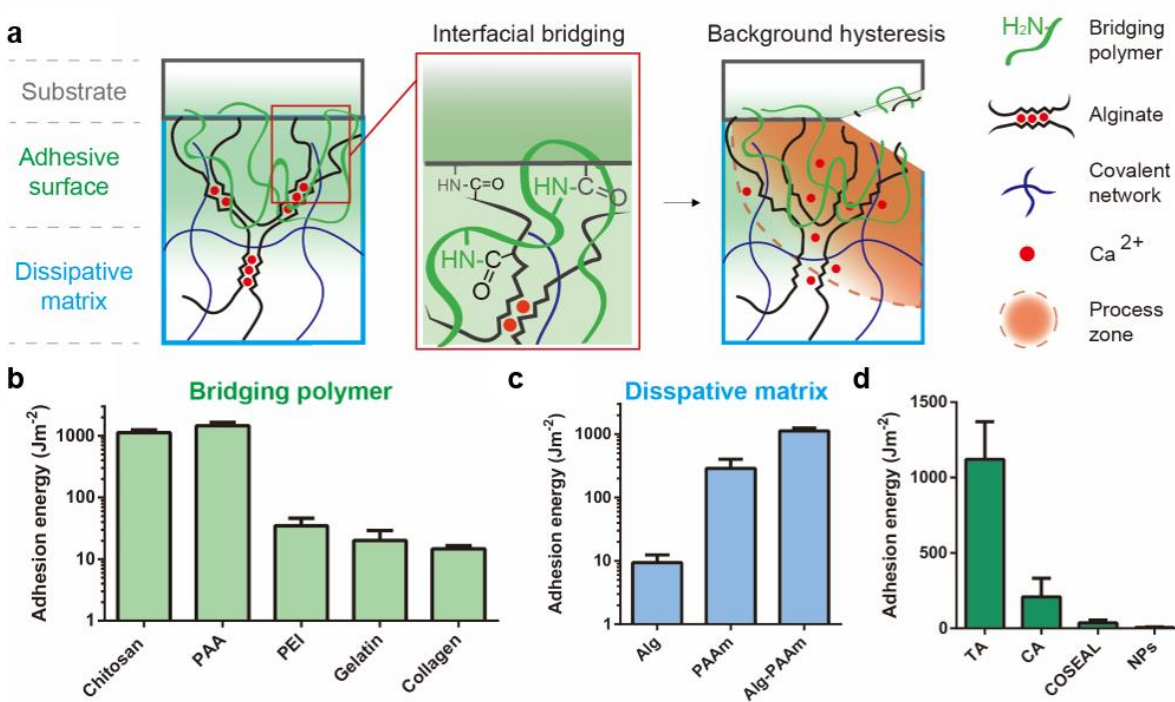


Figure 3.1 Design of tough adhesives (TAs). (a) TAs consist of a dissipative matrix (light blue square) made of a hydrogel containing both ionically crosslinked (calcium; red circles) and covalently crosslinked polymers (black and blue lines), and an adhesive surface that contains a

(Continued) bridging polymer with primary amines (green lines). The bridging polymer penetrates into TA and the substrate (light green region). When a crack approaches, a process zone (orange area) dissipates significant amounts of energy as ionic bonds between alginate chains and calcium ions break. (b) Adhesion energy on porcine skin was measured using different bridging polymers. PAA, polyallylamine; PEI, polyethylenimine. (c) Adhesion energy varies with the hydrogel matrix. Alg, alginate; PAAM, polyacrylamide. (d) Comparison between our TAs and other adhesives. CA, cyanoacrylate; NPs, nanoparticles. Error bars show standard deviation; sample size $n=4$.

Tough adhesives are applicable to a wide variety of wet surfaces, including tissues and hydrogels. Our TAs adhered strongly to porcine skin, cartilage, heart, artery, and liver (Figure 3.2(a)). Their adhesion energies on hydrogels are higher than those of nanoparticle-based solution ($1-10 \text{ Jm}^{-2}$) that were recently developed to glue hydrogels (Figure 3.2(b)). Unlike tissues, certain hydrogels, such as poly(hydroxyethyl methacrylate) lack the functional groups (amine or carboxylic acid) that we used to form interfacial covalent bonds, but these hydrogels still adhere well to TAs (Figures B8 and B9). Although the bridging polymer was found to interpenetrate into a variety of substrates, the penetration depth in a given time depended on the substrate permeability. Because hydrogels are more permeable than tissues, the penetration depth of fluorescein isothiocyanate–labeled chitosan (FITC-chitosan) in hydrogels was greater than that found in skin or muscle (Figure 3.2(c) and Figure B10) and likely underlies the strong adhesion of TAs to even chemically inert hydrogels.

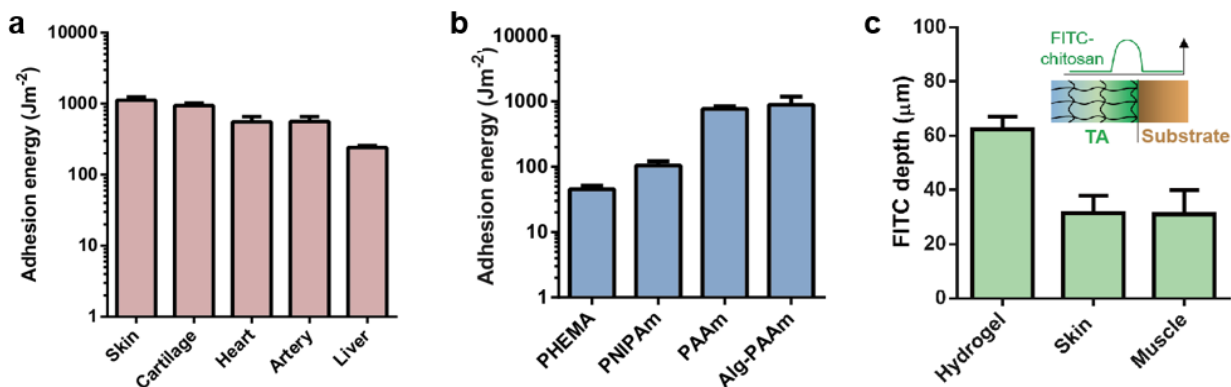


Figure 3.2 Adhesion on diverse wet surfaces. TAs adhere to a variety of (a) tissue surfaces and (b) hydrogels, including poly(hydroxyethyl methacrylate) (PHEMA), poly(N'-isopropylacrylamide) (PNIPAm) and polyacrylamide (PAAm) and alginate-polyacrylamide (Alg-PAAm) hydrogels. (c) Penetration depth of fluorescein isothiocyanate–labeled chitosan (FITC-chitosan) into PAAm hydrogels, skin and muscle. Error bars show standard deviation; sample size n=4.

We next evaluated the capacity of our TAs as tissue adhesives, particularly compared with that of the widely used CA. Our TAs exhibited a rapid increase in adhesion energy to porcine skin over time (Figure 3.3(a)). This rapid, but not immediate adhesion is likely to aid clinical translation and adoption of these tissue adhesives, as it allows the material to be applied in a facile manner. In contrast, CA solidifies upon contact with tissues, which makes handling and repositioning difficult [243]. The formation of tissue adhesion is often complicated under in vivo conditions because of exposure to blood and dynamic movements. To simulate this in vitro, the porcine skin was first covered with blood before the application of a TA (Figure B11 and Movie B2). The adhesion energy was found to be 1116 Jm⁻², which indicates strong adhesion even with blood exposure. In contrast, the adhesion provided by CA deteriorates significantly upon exposure to blood (Figure 3.3(b) and Figure B12). Our TAs were further tested on a beating porcine heart in vivo (Figure 3.3(c)). Freshly drawn blood was spread on the heart

surface at the site of application, followed by application of a TA and peeling tests (Movie B3). A strong adhesion was formed on the dynamic curved surface with a peak strength of 83 ± 31 kPa, which exceeds that of commercially available tissue adhesives (typically ~ 10 kPa) [46]. Our TAs were found to maintain strong adhesion (600 Jm^{-2}) after being implanted into rats for 2 weeks (Figure B13). They also exhibited excellent biocompatibility: In an in vitro cell study, human dermal fibroblasts were able to maintain full viability after 24-hour culture in a TA-conditioned medium, while the cells cultured in CA-conditioned medium were unable to spread and exhibited low viability (Figure 3.3(d) and Figure B14). The in vivo biocompatibility of our TAs was evaluated with subcutaneous implantation and myocardium attachment in rats. After performing a histological assessment, we concluded that the degree of inflammatory reaction produced by our TAs was lower than that produced by CA; additionally, our TAs were comparable to COSEAL in this category (Figure 3.3(e) and Figure B15).

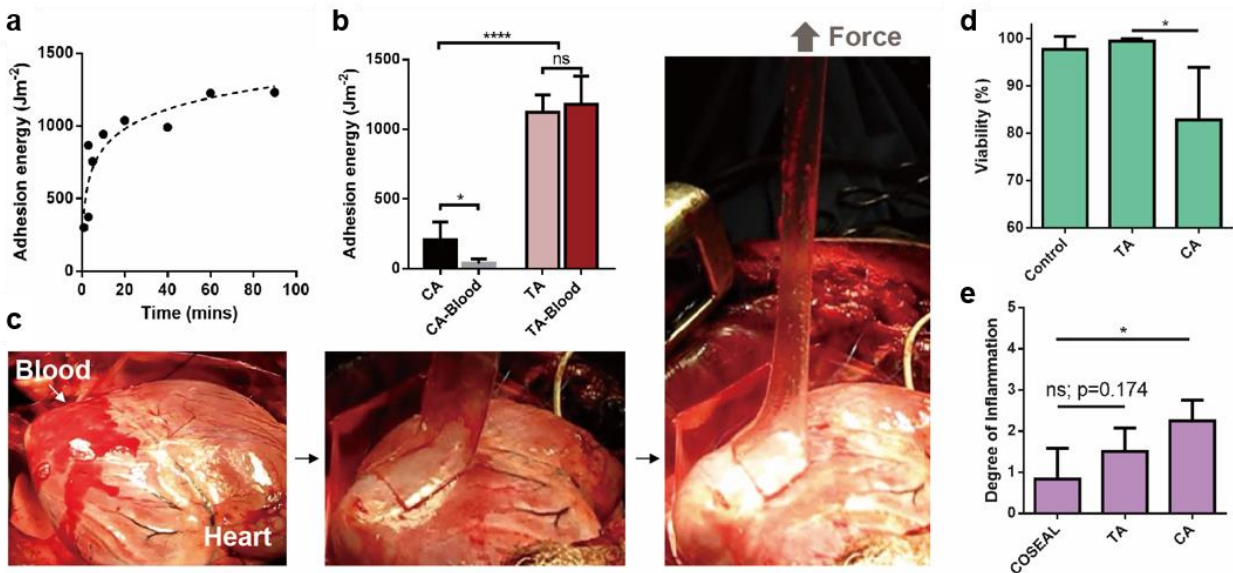


Figure 3.3 Adhesion performance and biocompatibility. (a) Adhesion kinetics of TAs to porcine skin. (b) Comparison of TA versus CA placed on porcine skin with and without exposure to blood. Sample size n=4-6. (c) In vivo test on a beating porcine heart with blood exposure. (d) In vitro cell compatibility was compared by quantifying the viability of human dermal fibroblasts. Sample size n=4. (e) In vivo biocompatibility was evaluated by using subcutaneous implantation

(Continued) in rats. The degree of inflammation was determined by a pathologist (0=normal, 1=very mild, 2=mild, 3=moderate, 4=severe, 5=very severe). Error bars show standard deviation; sample size n=4-6. P values were determined by the t-test; *, $p \leq 0.05$; ****, $p \leq 0.0001$; ns, not significant.

The design of TA can potentially enable many applications, including the gluing of tissues and attaching devices in vivo, tissue repair and attaining hemostasis. TAs can readily adhere to liver tissue (Figure 3.4(a)). Tensile testing demonstrated that a TA remained highly stretchable and sustained 14 times its initial length before debonding from the liver. The combination of strong adhesion and large deformability is vital when interfacing tissues and deformable devices, whereas existing adhesives hardly accommodate large deformation. For example, our TAs managed to anchor an actuator; recently developed to support heart function, onto myocardium surfaces (Figure B16). TAs are also potentially useful as a dressing for skin wounds. TAs adhered strongly to the epidermis of mice and readily accommodated dynamic movements of this tissue on the living animal (Figure B17 and Movie B4).

A TA can be used for tissue repair as either a preformed patch or an injectable solution. We first tested a TA as a sealant to close a big defect in a porcine heart (Figure 3.4(b)). Our TA was compliant and conformed closely to the geometry of the myocardium. While the heart was being inflated, the sealant expanded with the deformation, and no leakage was observed under strain up to 100%. The perfect seal was maintained after tens of thousands cycles of inflation-deflation (Figure B18 and Movie B5). The measured burst pressures of the TA sealant with and without a plastic backing were 206 mmHg and 367 mmHg, respectively (Figure 3.4(c)); these values exceed normal arterial blood pressure in humans (80-120 mmHg) and the performance of commercially available surgical sealants. Notably, the TA sealant malfunctioned due to cohesive failure, which is indicative of a strong adhesion interface (Figure B18 and Movie B6). We also developed an injectable TA based on an alginate-polyethylene glycol hydrogel. It can be

injected via syringe into a defect site and can form a tough matrix upon exposure to ultraviolet light (Figure B19). As a proof of concept, the injectable TA was used to repair a cylindrical defect in explanted cartilage discs, resulting in recovery of the compressive properties (Figure B20).

Tough adhesives can be used as a hemostatic dressing because of their compatibility with blood exposure, as shown in a hepatic hemorrhage model. A circular laceration was used to produce heavy bleeding on the left lobe of the liver in rats. Animals were treated immediately with the TA or with a commercial hemostat [SURGIFLO (Ethicon)] as a positive control or were left untreated as a negative control (Figure 3.4(d)). The blood loss was significantly reduced by the application of TA versus the negative control, and the TA's performance was comparable to that of SURGIFLO (Figure 3.4(e)). All animals survived for the experimental period of 2 weeks without secondary hemorrhage. However, substantial adhesions were found at the lesion site when untreated or treated with SURGIFLO; necrosis occurred in the livers of untreated animals (Figure B21). Neither of these were found in the animals treated with the TA.

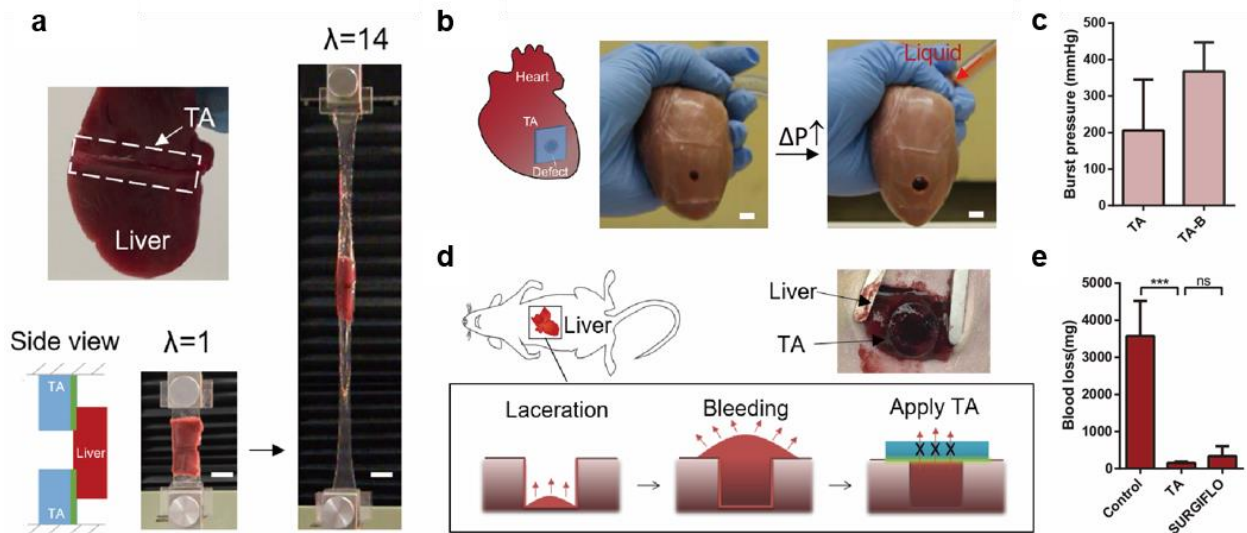


Figure 3.4 Application enabled by TAs. (a) TAs were used as tissue adhesives. A TA adhered to the liver and sustained 14 times its initial length before debonding. Scale bar, 20 mm. (b) TAs served as heart sealant. The TA sealant prevented liquid (red) leakage as the porcine heart was inflated. Scale bar, 10 mm. (c) Burst pressures of the TA sealant were measured without (TA)

(Continued) and with plastic backing (TA-B). (d) Use of a TA as a hemostatic dressing. A deep wound was created on rat liver and then sealed with a TA to stop the blood flow (labeled with red arrows). (e) Blood loss with the treatment of TA, SURGIFLO hemostat, and control (without treatment). Error bars show standard deviation; sample size $n=4$. P values were determined by the t-test; ***, $p \leq 0.001$; ns, not significant.

3.3 Conclusion

We report design principles of biocompatible TAs that combine chemical and physical processes at the interface and in the bulk of the adhesive to achieve high adhesion energy on various wet and dynamic surfaces. The mechanical performance and compatibility with cells and tissues allow these materials to meet key requirements for next-generation tissue adhesives.

Chapter 4

Topologies of Wet Adhesion

Abstract: Recent innovations have integrated hydrogels with various materials to enable tissue adhesives [9, 29, 100], implants [45, 49], interactive devices [40, 75], water matrix composites [76, 78, 80], chemical sensors [244], and ionotronics [30, 33, 91, 93]. Existing methods to adhere hydrogels to various materials invoke two aspects of adhesion: the chemistry of bonds [29, 94, 98, 244], and the mechanics of dissipation [29, 74, 91, 92]. Here we show that the ways to achieve strong hydrogel adhesion multiply considerably by examining another aspect of adhesion: the topology of connecting materials. We illustrate the potential by developing a specific topology, where a species of polymer chains bond to a material and form a network that stitches with the polymer network of a hydrogel. This bond-stitch topology enables diverse materials to form strong adhesion with hydrogels that have pre-formed polymer networks but have no functional groups amenable to chemical coupling. Furthermore, the topology readily enables on-demand loss of adhesion. We study the physics and chemistry of this topology, and describe its potential applications in medicine and engineering.

4.1 Introduction

The abundance of water in a hydrogel poses a particular challenge to its adhesion to various materials: the water molecules in the hydrogel behave like a liquid, readily change neighbors, and transmit little load [33]. Hydrogels adhere poorly to most materials, either hydrophobic or hydrophilic [99]. Indeed, most hydrogels adhere poorly with each other [98]. Rather, strong adhesion relies on the minority constitute of the hydrogel: the polymer network. A sparse polymer network of strong bonds in a hydrogel can (1) transmit significant load through the strong bonds, and (2) elicit dissipation in the bulk [74, 92, 107, 108]. Several approaches to adhere hydrogels to various materials have been reported recently, highlighting

two aspects of adhesion: the chemistry of bonds (e.g., covalent bonds, ionic bonds, and hydrogen bonds) [29, 94, 98, 244], and the mechanics of dissipation (e.g., plasticity, viscosity, and distributed damage) [29, 74, 91, 92].

The surface of a material and the polymer network of a hydrogel may form bonds by matching functional groups. This approach, however, limits the choices of materials and manufacturing processes. In seeking to adhere two hydrogels in which the polymer networks have no functional groups for chemical coupling, we noticed another aspect of adhesion: the topology of connecting materials [100]. We formed a thin layer of polymer network in topological entanglement with the polymer networks of the hydrogels (Figure 4.1(a)). That is, the new polymer network stitches the two existing polymer networks, acting as a molecular suture. Hydrogels in topological entanglement have strong adhesion, because separation requires at least one of the three polymer networks to rupture. By contrast, hydrogels in physical entanglement have weak adhesion, because separation only requires polymer chains to pull out against the low viscosity of water [117].

The abundance of water in a hydrogel also offers a particular opportunity to its adhesion to various materials: the fluidity and chemistry of water makes the hydrogel an ideal host for diverse topologies. By a topology of adhesion we mean a type of connectivity through bonds, chains, particles, networks, or their combinations. In hindsight, we classify existing approaches of hydrogel adhesion into several topologies: two polymer networks adhere by topological entanglement with a third polymer network [100] (Figure 4.1(a)), two polymer networks adhere directly by bonds [74, 94, 163, 191] (Figure 4.1(b)), a hydrogel and a nonporous solid adhere directly by bonds [92] (Figure 4.1(c)), two hydrogels adhere by particles [98] (Figure 4.1(d)), a hydrogel and a tissue adhere by polymer chains [29] (Figure 4.1(e)), and a hydrogel and a nonporous solid adhere by polymer chains [245, 246] (Figure 4.1(f)).

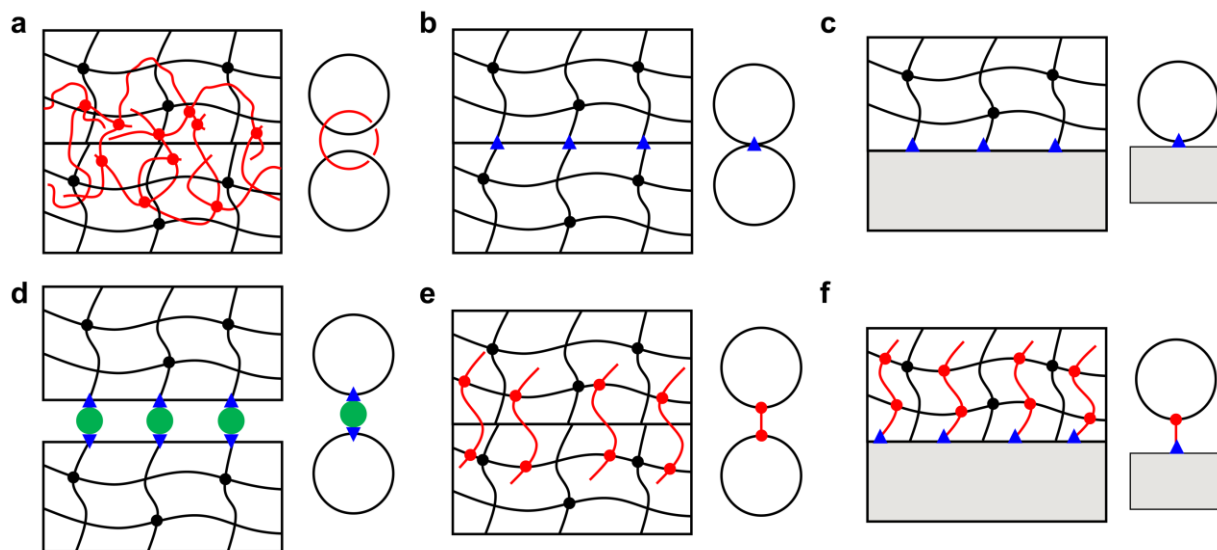


Figure 4.1 Several topologies of hydrogel adhesion. (a) Two polymer networks with no functional groups for chemical coupling adhere by a stitching network. (b) Two polymer networks with matching functional groups adhere by direct bonds. (c) A hydrogel and a nonporous solid adhere by direct bonds. (d) Polymer networks adhere through bonding with nanoparticles. (e) Polymer networks adhere through bonding with polymer chains. (f) A hydrogel and a nonporous solid adhere through bonding with polymer chains. In the conceptual pictures of topologies, a circle represents a polymer network, a block represents a nonporous solid, a segment represents a polymer chain, a green dot represents a nanoparticle, a red dot represents a bond inside polymer network, and a blue triangle represents a bond at interface.

4.2 Results and discussion

Many other topologies of hydrogel adhesion are possible, but have not been used (Figure C1). The synergy of the three aspects of adhesion—chemistry, mechanics, *and* topology—will enable strong adhesion between any hydrogels and any materials. To examine this synergy in some depth, here we delve into a particularly simple, hitherto unused, topology of hydrogel adhesion: a combination of bonds and stitches (Figure 4.2(a)). This bond-stitch topology aims to adhere a material (to be called an adherend) and a hydrogel of following attributes: the surface

of the adherend has functional groups amenable to chemical coupling, and the polymer network in the hydrogel is pre-formed and has no functional groups amenable to chemical coupling. We select a species of polymer chains bearing functional groups that (1) form bonds with the functional groups on the surface of the adherend, and (2) crosslink into a network in topological entanglement with the polymer network of the hydrogel.

We first illustrate this bond-stitch topology using a representative system, consisting of an acrylic elastomer (VHB 4905, 3M), a polyacrylamide (PAAM) hydrogel, and chitosan chains (Figure 4.2(b)). The Fourier-transform infrared spectroscopy (FTIR) shows that the surface of the VHB elastomer has carboxylic acid and ketone groups (Figure C2). The PAAM network in the hydrogel has amide groups, which are inert to chemical coupling. The chitosan chains carry amine and hydroxyl groups. The VHB elastomer and the PAAM hydrogel do not have matching functional groups, and adhere poorly [99]. We next demonstrate strong adhesion between the VHB elastomer and the PAAM hydrogel using the chitosan chains to form a bond-stitch topology.

When an aqueous solution of chitosan, pH = 5, on the surface of the VHB, some chitosan chains adsorb to the VHB surface by forming imine bonds [201, 247] (Figure C3), and other chitosan chains remain mobile (Figure 4.2(c)). (The amine groups and carboxylate groups can form ionic bonds, which are much weaker than the imine bonds.) When the PAAM hydrogel, pH = 7, is pressed onto the chitosan-coated VHB, the mobile chitosan chains diffuse into the hydrogel, and form a chitosan network through $\text{NH}_2\text{-OH}$ hydrogen bonds, in topological entanglement with the PAAM network (Figure 4.2(d), Figure C4, and Movies C1 and C2). The VHB-chitosan-PAAM system can sustain various types of mechanical loads without separation (Figure C5). We next study the chemistry and physics of this bond-stitch topology.

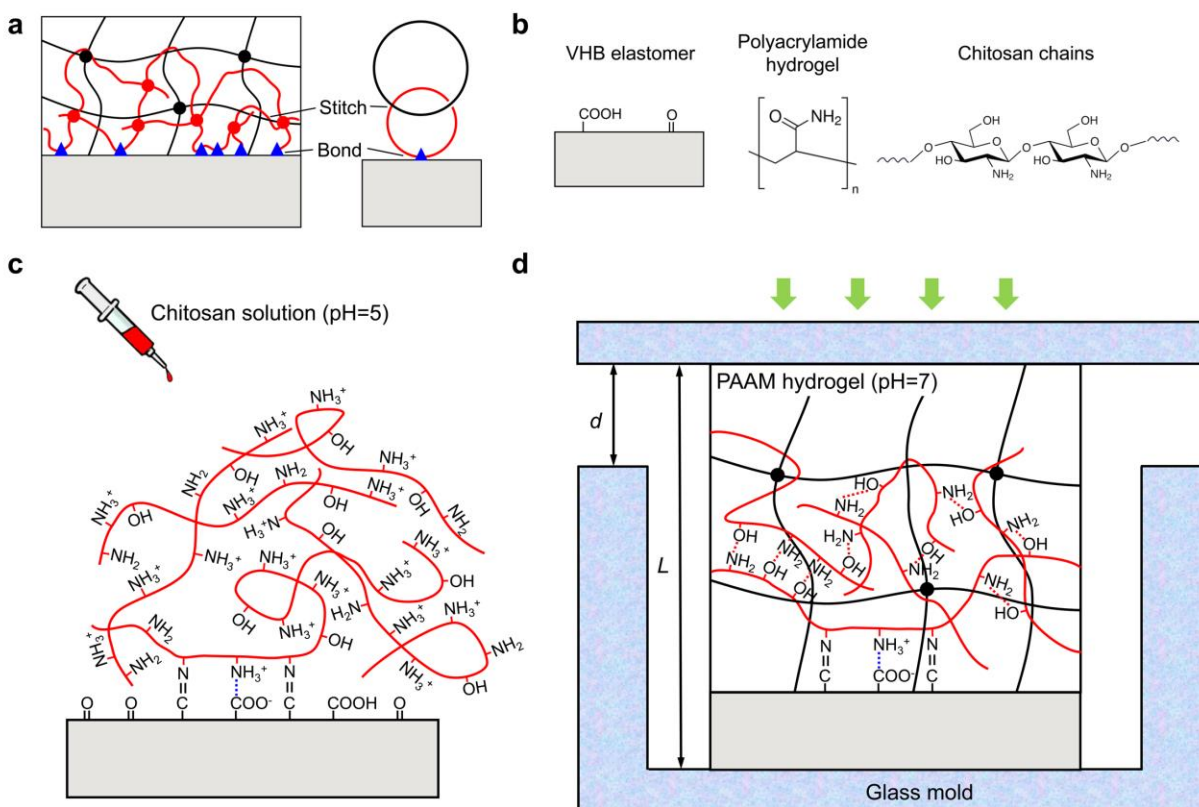


Figure 4.2 A bond-stitch topology. (a) The surface of a nonporous solid has functional groups amenable to chemical coupling, but the polymer network of a hydrogel has no functional groups amenable to chemical coupling. A species of polymer chains bond to the surface of the solid and stitch with the polymer network of the hydrogel. (b) An example of bond-stitch topology using the following materials: VHB elastomer, polyacrylamide hydrogel, and chitosan chains. (c) When an aqueous solution of chitosan ($\text{pH} = 5$) is spread on the surface of the VHB elastomer, some chitosan chains adsorb on the VHB surface through imine bonds and ionic bonds, and other chitosan chains remain mobile in the solution. (d) When a PAAM hydrogel ($\text{pH} = 7$) is pressed onto the chitosan-coated VHB with a strain $d/L = 7\text{-}15\%$, the mobile chitosan chains diffuse into the hydrogel, and crosslink into a chitosan network by $\text{NH}_2\text{-OH}$ hydrogen bonds, in topological entanglement with the PAAM network.

This bond-stitch topology builds up by three kinetic processes: the formation of imine

bonds between some chitosan chains and the VHB, the diffusion of the mobile chitosan chains into the hydrogel, and the formation of the chitosan network through the $\text{NH}_2\text{-OH}$ hydrogen bonds. We study the kinetics by measuring the adhesion energy as a function of time. We spread the chitosan solution on the VHB surface and immediately press the hydrogel on top, and then measure the adhesion energy as a function of time. The adhesion energy increases initially and reaches a plateau after 20 hours (Figure 4.3(a)). The data are consistent with the following requirements [100]: the formation of the chitosan network should be slow enough to let the mobile chitosan chains diffuse into the hydrogel and form a network entangled with the hydrogel, but not be too slow to let all the mobile chitosan chains diffuse away in the hydrogel without forming the network. The formation of the imine bonds between the chitosan chains and the VHB elastomer is much faster than the other two kinetic processes. To test this, we spread the chitosan solution on the VHB, wait for some time before pressing the hydrogel on top, and then measure the adhesion energy after the PAAM-VHB bilayer being pressed for 24 hours. The adhesion energy drops quickly when the chitosan solution on the VHB surface is present for less than 2 minutes, and maintains the same value with even longer wait time (Figure 4.3(b)).

The adhesion is sensitive to the pH in the hydrogel, and peaks at about $\text{pH} = 7$ (Figure 4.3(c)). When $\text{pH} \ll 7$, most NH_2 on chitosan are converted to NH_3^+ , and few $\text{NH}_2\text{-OH}$ hydrogen bonds are present to form the chitosan network. When $\text{pH} \gg 7$, the chitosan chains rapidly form a network and prohibit diffusing into the hydrogel. The adhesion is also sensitive to the concentration of salt in the hydrogel, because ionic screening disturbs the formation of imine bonds. The adhesion energy exceeds 150 J/m^2 when the concentration of salt is below 1 M, but reduces to zero as the concentration of salt is above 2 M (Figure 4.3(d)). The adhesion also depends on the concentration and length of the chitosan chains (Figure 4.3(e)-(f)).

We next confirm that this topology of adhesion indeed requires *both* bonds and stitches. We do so by using several species of polymer chains (Table C1). Similar to chitosan, poly(4-

aminostyrene) (PAS) chains can bond to the VHB elastomer and form a network to stitch with the PAAM hydrogel (Figure C8). The adhesion energy is measured above 300 J/m^2 (Figure 4.3(g)). In contrast, adhesion energy of 10 J/m^2 is measured using polyallylamine (PAA) and polyethylenimine (PEI), because they cannot form networks to stitch with the hydrogel network. We find that alginate chains lead to negligible adhesion energy, which is consistent with the previous time finding that alginate chains do not adhere well with the VHB elastomer [99], even though the alginate chains form a network that stitches with the PAAM hydrogel [100]. PAAM chains neither bond to the elastomer nor stitch to the hydrogel, and lead to negligible adhesion energy.

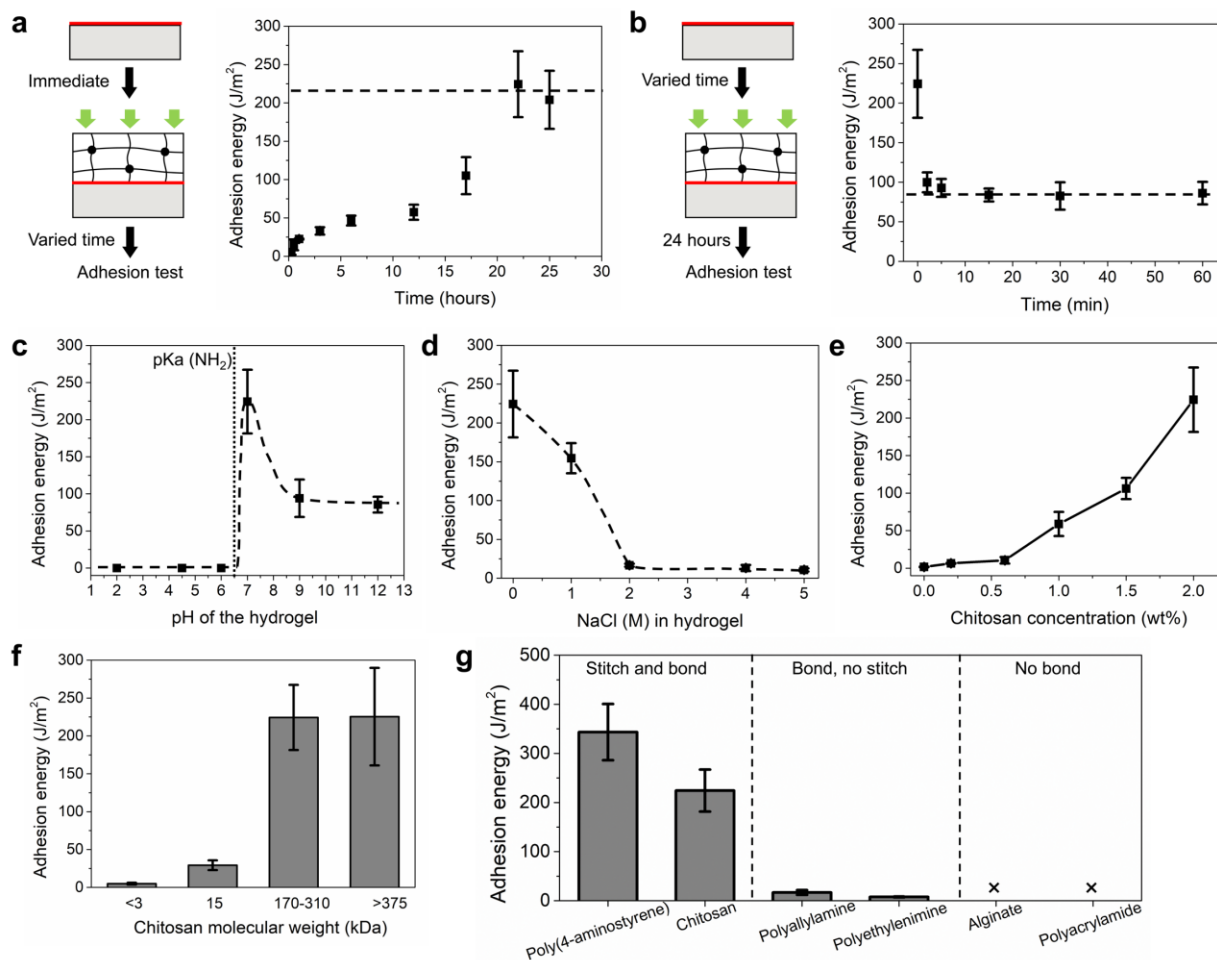


Figure 4.3 Adhesion energy as a function of several variables. (a) The time after compressing the PAAM hydrogel onto the chitosan-coated VHB. The PAAM hydrogel was compressed on top

immediately after the chitosan solution was spread on the VHB elastomer. (b) The time before compressing the PAAM hydrogel onto the chitosan-coated VHB. The adhesion energy was (Continued) measured after compressing for 24 hours. (c) The pH of the hydrogel. (d) Concentration of salt in the hydrogel. (e) Concentration of chitosan. (f) The molecular weight of chitosan. The concentration of chitosan was fixed at 2 wt%. (g) Polymers that both bond to the elastomer and stitch with the hydrogel provide strong adhesion. The lack of either bonds or stitches causes weak adhesion. The polymers used are listed in Table C1. All the data represent the mean and standard deviation of 3–5 experimental results.

Adhesion amplifies dramatically by the synergy of chemistry, mechanics, and topology (Figure 4.4(a)). As noted before, the VHB elastomer and the PAAM hydrogel by themselves adhere weakly. However, to separate the chitosan-bonded VHB and PAAM, one must break strong bonds. The chitosan and PAAM networks are topologically entangled. The networks of strong bonds transmit the intense stress at the front of the separation into the bulk of the VHB and PAAM, and cause inelastic deformation over a large volume of the materials. The topology elicits strong bonds, which in turn elicits bulk dissipation.

We illustrate this synergy by using hydrogels of various capabilities for dissipation (Table C2). The adhesion energies all approach the fracture energies of the hydrogels (Figure 4.4(b), and Figure C9). In particular, distributed damage in the alginate-PAAM hydrogel greatly raises the adhesion energy to 1,200 J/m². A similar amplification of adhesion is demonstrated using chitosan chains to form a bond-stitch topology with the VHB elastomer and an iron-polyacrylate-PAAM hydrogel (Figure C10). We further show that the PAS and chitosan chains adhere the PAAM hydrogel to various materials through several types of bonds (Figure 4.4(c), Table C3).

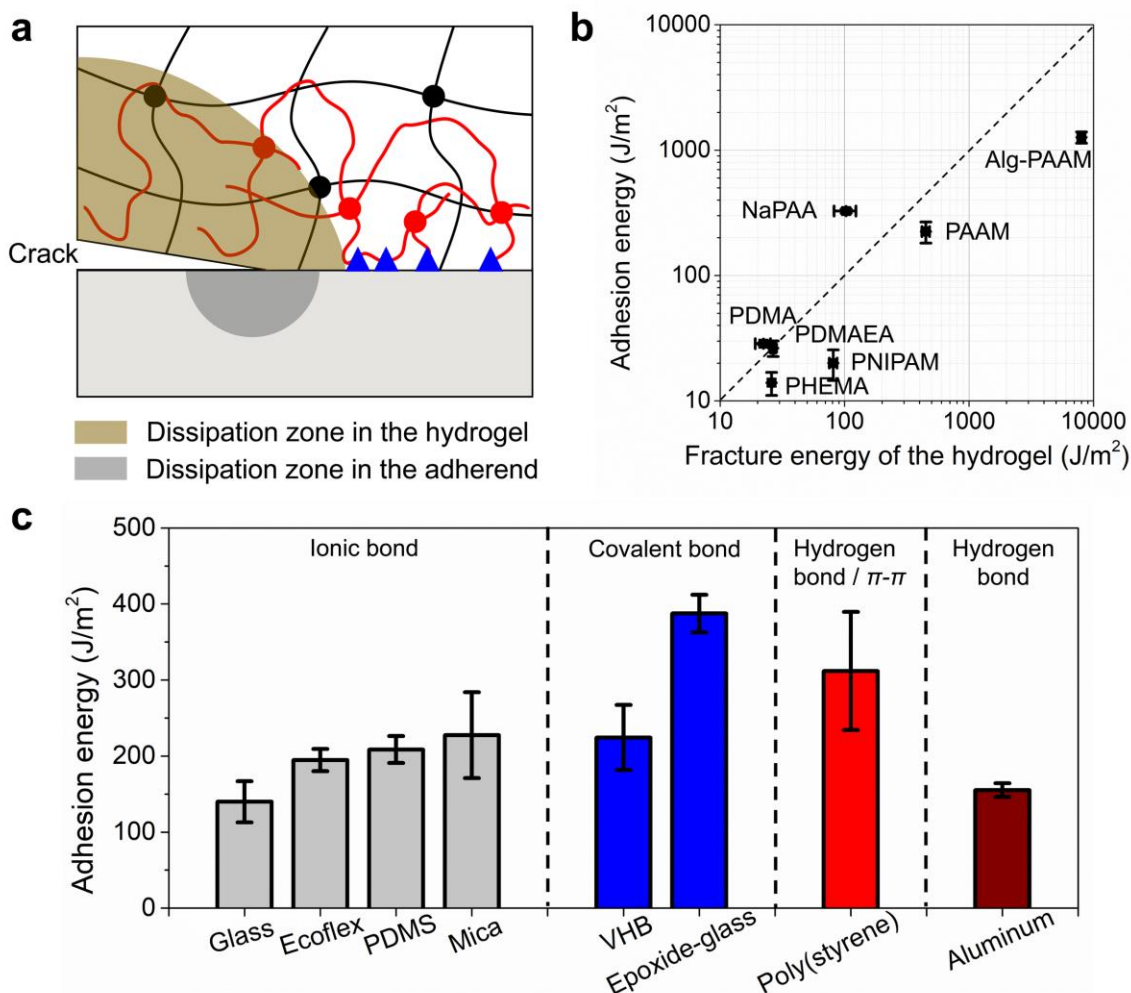


Figure 4.4 Strong adhesion through the synergy of chemistry, mechanics, and topology. (a) To separate a hydrogel and a material, an external force breaks the bonds, as well as causes inelastic dissipation in the bulk. (b) Adhesion energies approach fracture energies of hydrogels. (c) Adhesion energies measured for various adherends. Hydrogels, adherends and polymer chains are listed in Tables C2 and C3. All the data represent the mean and standard deviation of 3–5 experimental results.

The bond-stitch topology readily integrates various hydrogels and materials to create devices of potential applications in medicine and engineering. We make a wearable mechano-electrical transducer (Figure 4.5(a)). Two pieces of the PAAM hydrogel are glued on a VHB elastomer using the bond-stitch topology. The hydrogel is an ionic conductor, and the

elastomer is a dielectric. When the hydrogels contact each other, an electric current can flow, and the transducer is on. When the hydrogels separate under stretch, the electric current cannot flow, and the transducer is off. We mount the transducer on a knee to monitor the knee flexion during walking, as the gait speed directly relates to the muscle strength [248]. In one case, the gait speed is measured at ~ 10 s/cycle.

We also fabricate an elastomer-coated hydrogel patch (ECHP) for prolonged transdermal drug delivery, since the elastomer coating can limit the dehydration of hydrogel. We adhere the ECHP on a porcine skin, where the hydrogel and the elastomer adhere by the bond-stitch topology developed in this paper, and the hydrogel and the tissue adhere by the stitch-stitch topology developed previously [100] (Figure 4.5(b)). We measure the water loss of ECHP-skin assembly with time. The ambient temperature is 24 °C and the relative humidity is 20 %. The ECHP-skin assembly loses 25 % of weight and remains soft and transparent after 25 hours. Without the elastomer coating, hydrogel-skin assembly loses more than 50 % of weight and is completely dry (Figure C12). The ECHP is further tested on a rat *in vivo* (Movie C3). A pure hydrogel patch is included as a control. Both patches are firmly bonded on the skin of the rat initially, despite the dynamic movement of the rat. After 12 hours, the ECHP maintains transparency and strong bonded, but the hydrogel patch is completely dry and readily detached from the skin. The transparency of the ECHP can also benefit the real-time monitor of the wound-healing process.

The bond-stitch topology offers an opportunity to build functions into adhesion. For example, we can break the topology on demand, by changing the pH below 6.5. At low pH, the chitosan network dissociates, and the imines hydrolyze. We demonstrate the loss of adhesion using a 90-degree peeling apparatus. When hydrochloric acid (pH ~ 1) is dripped to the bonding front, the hydrogel spontaneously detaches from the VHB surface during peeling, and the exposed VHB surface is clean. When water of pH = 7 is dripped to the bonding front, the hydrogel ruptures during peeling, and a layer of ruptured hydrogel remains on the VHB surface

(Figure 4.5(c)). This example illustrates a principle: one can design the topology to enable both strong adhesion and easy detachment in response to cues.

The topology further offers possibilities to achieve strong adhesion in environment difficult to reach using existing methods. For example, we can adhere an elastomer and a hydrogel under water (Figure 4.5(d)). The chitosan solution is a shear-thinning fluid, and can be injected through a syringe and stay on a surface. We immerse a piece of VHB elastomer in the water, and inject the chitosan solution onto its surface through water, and then immediately press an alg-PAAM hydrogel on top. After one hour, the hydrogel-VHB bilayer can at least sustain a weight of 200 g, and does not separate even with intentional sway (Movie C4).

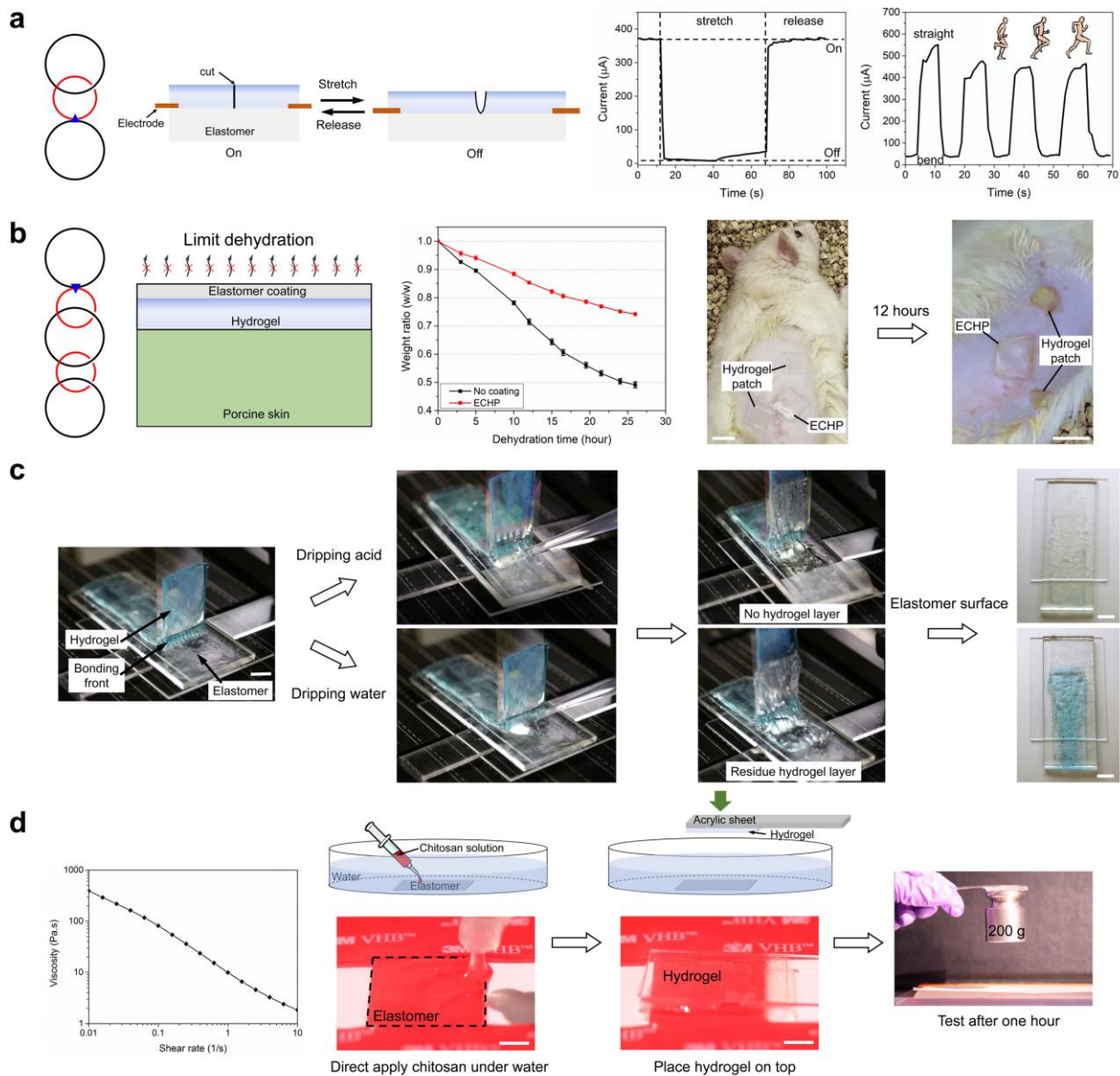


Figure 4.5 Applications enabled by topology. (a) Wearable mechano-electrical transducer. (b) Elastomer-coated hydrogel patch for transdermal drug delivery. (c) On-demand loss of adhesion. (d) Underwater adhesion. The scale bar in (b-d) is 1 cm.

4.3 Conclusion

In summary, we describe a design principle to achieve strong adhesion between any hydrogels and any materials. The principle invokes the synergy of chemistry, mechanics, and

topology: a topology elicits strong bonds, which in turn elicits bulk dissipation. We demonstrate a bond-stitch topology, study its fundamentals, and illustrate its potential uses in medicine and engineering. Bonds and stitches of numerous varieties are unexplored, and can be designed to accommodate different materials and manufacturing processes. The synergy can also enable functional adhesion, responsive to stimuli such as molecules, ions, temperature, and light. The field of innovation is wide open.

Chapter 5

Conclusion and Outlook

In recent years, we witness the rapid development of hydrogel hybrids of various kinds that has motivated many emerging technologies, from medical practices, wearable devices, to robots and cyborgs. In the course of exploring possible approaches to create strong hydrogel adhesion with diverse materials, we realize we should not limit to the chemistry, mechanics and topology to achieve strong adhesion, but also should concern the entire process of adhesion, that is, the process can accommodate different materials, various manufacturing processes, compatibility with adherends, and program functions into adhesion. The field is infantile, which brings opportunities for innovation, and also confronts challenges. In the following, we outlook the future direction of hydrogel adhesion in medicine, engineering and scientific research.

In medical practices, developing tissue adhesives that are strong, compatible, controllable yet applicable for various procedures is desirable. So far, traditional tissue adhesives use inject procedure, but the adhesion is weak; the recent developed tough adhesives use gluing procedure, but they require surgically exposed tissues, large adhesion area, and compression [29]. To mediate this challenge, injectable tough adhesives are desirable, which can spontaneously achieve strong adhesion without external energy input, while accommodate tissues of any geometry, tissues that are surgically difficult to access, provide minimal damages to other tissues and avoid compression. Moreover, hydrogels should be both biocompatible and mechanically compatible with tissues. The issue of biocompatibility has been addressed in tissue adhesives, but the issue of mechanical compatibility is not highlighted yet. The mechanical properties of different tissues vary greatly (the elastic modulus of liver is 1-10 MPa, while the elastic modulus of tendon is 100-1,000 MPa) [249]. To allow hydrogels to restore the mechanical functions of tissues, the mechanical properties of hydrogel should be designed to match those of tissues. For example, the hydrogel adhered on a beating heart should be soft and

not restrict the deformation of heart; the hydrogel which is used to repair a cartilage should be strong and tough enough to support load. Kinetics of adhesion is another important factor. Instant adhesion is useful in emergent hemostasis, while slow adhesion allows manipulation of the hydrogel in a facile manner, such as relocation of undesired adhesion sites. At last, the adhered hydrogels may be consistently intervened by ions, enzymes and certain chemicals present in the physiological fluids, and cause swelling, weakening, or degradation, which jeopardize the physical and mechanical properties of the hydrogel. These facts must be considered when hydrogels are designed to stay in the body for a long period of time.

The manufacture of next-level hydrogel hybrids should enable accurate control during assembly, miniaturization and rapid prototyping. Existing manufacture mainly rely on manual assembly. Manual assembly is laborious, time-consuming and contains errors. For example, it is extremely challenging to manually align and stack hundreds to thousands of fibers for making WMCs. Manual assembly prohibits miniaturization, because the resolution that human hands can operate is much larger than the desired size of a microchip ($\sim\mu\text{m}$). Similar to electronic chips that are widely used in modern technologies, soft hydrogel-based chips are anticipated to stimulate a ground-breaking innovations in the fields of medicine, wearable devices and robots. In addition, those hydrogel hybrids should be rapidly assembled to enable massive production. In the current technologies, 3D printing potentially provide ways to fabricate highly integrated structures in a rapid, controllable, scalable manner, and the resolution can be sub-millimeter level. Printed macroscopic-size hydrogel iontronics have already manifested functions as strain sensor [39], chemical sensor [40] and somatosensitive actuators [250]. The procedure in hydrogel printing is generally complicated, since it involves fine-tuning the rheology of hydrogel precursors, chemical reactions, external energy sources (i.e., ultraviolet irradiation and heat), surface wettability control, humidity control and oxygen-free environment.

The hydrogel adhesion offers a unique platform to study the relation between chemistry and mechanics. For example, using the slow crack test to measure the energy release rate as a

function of the crack speed (G - v curve), one can identify the failure mechanism [100], determine the relation between the adhesion energy and the dissipation [100, 251], and the relation between the intrinsic value of adhesion energy and the strength of bonds [100, 117, 252]. By using fatigue tests, one can determine how weak bonds in a hydrogel retards the crack extension [119]. In turn, one can use chemistry to design mechanics. One example is the addition of sacrificial bonds or networks into the original polymer network of hydrogel to introduce hysteresis to improve fracture energy and adhesion energy [29, 74, 92, 100]. Another example is the addition of hygroscopic salt and hydrophobic coating to hydrogel to limit the dehydration in an open air [64].

Developing fatigue-resistance adhesion is essential in many practical applications. The fatigue of a material can be cyclic and static. Cyclic fatigue is the failure of a material under prolonged cyclic loads. Even though such load is small and does not cause failure of adhesion during the first few cycles, but in the long-term, the adhesion is susceptible to fail. The study of cyclic fatigue in hydrogels initiates fair recent [3, 119, 226, 253, 254], and the fatigue of hydrogel adhesion has not yet been explored. The mechanism how chemistry relates to the cyclic fatigue is not well understood, but is important to design fatigue-resistant hydrogel. Static fatigue is the failure of a material under prolonged static loads. The study of static fatigue in the hydrogel adhesion is also new [100, 251, 252]. One fundamental principle from these studies is that the hysteresis in the hydrogel greatly improve adhesion energy at high crack speed, and contributes negligibly to adhesion energy at low crack speed. Another form of static fatigue is stress corrosion. Stress corrosion is a failure of material in the combined stress and corrosive environment such as water, chloride and ammonia. A classic example is the moisture-assisted cracking of glass, where the water molecules in the environment attack the Si-O-Si bonds in a glass, and fracture the glass by forming two surfaces covered with monolayers of H-O-Si [255-257]. Since hydrogels contain abundant water, if the adhesion is created through silane coupling method, or the adherend is silicone elastomer, Si-O-Si bonds are involved in the adhesion,

which is highly risky for stress corrosion.

Many other challenges and opportunities are beyond listing, and will keep emerging with new materials, new functions, and new applications. The ancient science is rejuvenated in the context of those new ingredients. With the evolving hydrogel adhesion, we should gain broad knowledge across multiple disciplines, and also be creative.

Appendix A. Supporting information for Chapter 2

Materials

All chemicals were purchased and used without further purification. Monomers for hydrogels included acrylamide (AAM; Sigma-Aldrich, A8887), 2-Hydroxyethyl methacrylate (HEMA; Sigma-Aldrich, 128635), N-isopropylacrylamide (NIPAM; Sigma-Aldrich, 415324), N,N-Dimethylacrylamide (DMA; Sigma-Aldrich, 274135), acrylic acid (AAc; Sigma-Aldrich, 147230) and [2-(Acryloyloxy)ethyl]trimethylammonium chloride solution (DMAEA; Sigma-Aldrich, 496146). To prepare alg-polyacrylamide tough hydrogels, ionically crosslinkable alginate biopolymer (FMC Biopolymer, Manugel GMB) was used and crosslinked with calcium sulfate slurry (calcium sulfate dihydrate; Sigma-Aldrich, c3771). N,N'-methylenebisacrylamide (MBAA; Sigma-Aldrich, M7279) was used as the covalent crosslinker. Ammonium persulfate (APS; Sigma-Aldrich, A9164), sodium persulfate (NaPS, Sigma-Aldrich, 216232) and α -Ketoglutaric acid (Sigma-Aldrich, 75890) were used as initiators for polymerization in different pH. N,N,N',N'-tetramethylethylenediamine (TEMED; Sigma-Aldrich, T7024) was used as crosslinking accelerator for APS and NaPS.

The stitching polymers employed in the study include chitosan chains of four different molecular weights: $M_w > 375,000$ Da (Sigma-Aldrich, 419419), $M_w \sim 190,000-310,000$ Da (Sigma-Aldrich, 448877), $M_w \sim 15,000$ Da (Polysciences, 21161-50) and $M_w \leq 3,000$ Da (Carbosynth, OC28900), alginic acid sodium salt ($M_w \sim 120,000-190,000$ Da, Sigma-Aldrich, 180947), poly(4-aminostyrene) (PAS, $M_w > 150,000$ Da; Polysciences, 02823-1) and cellulose ($M_w \sim 500,000$ Da; Sigma-Aldrich, 435236).

Methods

Preparation of hydrogels

Polyacrylamide hydrogel: 40.56 g acrylamide powder was first dissolved in 300 ml deionized water, and MBAA was added as covalent crosslinker (MBAA to acrylamide weight ratio is 0.0006:1). To prepare PAAM hydrogel of $\text{pH} < 7$, α -Ketoglutaric acid was used as UV initiator (α -Ketoglutaric acid to acrylamide weight ratio is 0.002:1). The pH of precursor solution was tuned by dripping HCl solution. The precursor solution was subsequently poured into a glass mold and covered with a 3-mm-thick glass plate, and exposed under UV irradiation (30W, 365nm curing UV light, McMaster-Carr) for one hour and set for hours to complete polymerization. To prepare PAAM hydrogel of $\text{pH} \geq 7$, APS or NaPS was used as initiator (APS to acrylamide weight ratio is 0.01:1; NaPS to acrylamide weight ratio is 0.007:1), in coupling with TEMED as crosslinking accelerator (TEMED to acrylamide weight ratio is 0.0028:1). We dripped NaOH to achieve a desired pH. The precursor solution was then poured into a glass mold and covered with a 3-mm-thick glass plate to complete polymerization.

PHEMA hydrogel: 46 ml HEMA was dissolved in 200 ml DI water. We sequentially added MBAA (MBAA to HEMA weight ratio is 0.00033:1), TEMED (TEMED to HEMA weight ratio is 0.002:1) and APS (APS to HEMA weight ratio is 0.0054:1) into the HEMA solution and mixed. The precursor solution was then poured into a glass mold and covered with a 3-mm-thick glass plate to complete polymerization.

PNIPAAm hydrogel: 21.52 g NIPAM powder was dissolved in 100 ml DI water. We sequentially added MBAA (MBAA to NIPAM weight ratio is 0.000377:1), TEMED (TEMED to NIPAM weight ratio is 0.0023:1) and APS (APS to NIPAM weight ratio is 0.006:1) into the NIPAM solution and mixed. The precursor solution was then poured into a glass mold and covered with a 3-mm-thick glass plate to complete polymerization.

PDMA hydrogel: 4.12 ml DMA was diluted in 20 ml DI water. We sequentially added 0.0031 g MBAA (MBAA to DMA weight ratio is 0.00078:1), TEMED (TEMED to DMA weight ratio is

0.003:1) and APS (APS to DMA weight ratio is 0.0067:1). The precursor solution was mixed and poured into a glass mold and covered with a 3-mm-thick glass plate to complete polymerization.

NaPAA hydrogel: 8.22 ml acrylic acid (AAc) was dissolved in 21.78 ml DI water. We sequentially added 0.004864 g MBAA (MBAA to AAc weight ratio is 0.00056:1) and 0.009 g α -Ketoglutaric acid (α -Ketoglutaric acid to AAc weight ratio is 0.001:1). We added NaOH to tune the pH of the solution to be neutral. The precursor solution was mixed and poured into a glass mold and covered with a 3-mm-thick glass plate, exposed under UV irradiation for one hour and set for hours to complete polymerization.

PDMAEA-Q hydrogel: 16 ml DMAEA was dissolved in 14ml DI water. We added NaOH to tune the pH of the solution to be neutral. We sequentially added MBAA (MBAA to DMAEA weight ratio is 0.0017:1) and APS (APS to DMAEA weight ratio is 0.0027:1). The precursor solution was then poured into a glass mold and covered with a 3-mm-thick glass plate to complete polymerization.

Alg-PAAM tough hydrogel: 40.56 g acrylamide powder and 6.78 g alginate powder were dissolved together in 300 ml deionized water. We then sequentially added MBAA (MBAA to acrylamide weight ratio is 0.0006:1) and TEMED (TEMED to acrylamide weight ratio is 0.0028:1). The solution was mixed and degassed. Next, we added APS (APS to acrylamide weight ratio is 0.01:1) as initiator and calcium sulfate slurry as ionic crosslinker (CaSO_4 to acrylamide weight ratio is 0.022:1) into the solution. To prevent fast gelation of alginate, the precursor solution was quickly mixed and immediately poured into a glass mold and covered with a 3-mm-thick glass plate to complete polymerization.

Preparation of stitching polymer solutions

Chitosan solution: 4-Morpholineethanesulfonic acid (MES hydrate; Sigma-Aldrich, M8250) was used to prepare an acidic buffer solution. We first prepared the MES buffer solution by dissolving 0.976 g MES hydrate powder into 50 ml DI water and adjusted the pH to 4.5 by

dripping NaOH with a pH meter (Mettler Toledo SevenEasy™ Series Meters). We then added 1 g chitosan powder (Mw~190,000-310,000 Da) into the buffer solution and sufficiently stirred with a magnetic stirring bar until chitosan powder was completely dissolved. The final pH of solution was about 5.

PAS solution: We prepared the MES buffer solution as described above and adjusted the pH to 1 by dripping HCl with a pH meter. We then added 1 wt% PAS into the buffer solution and sonicated in an ultrasonic bath (Branson Ultrasonics) with a constant temperature of 48 °C overnight. After PAS was completely dissolved, the solution was clear with a deep yellow color. We re-adjusted the pH of solution back to 4.

Alginate solution: 2 wt% alginic acid sodium salt was dissolved in DI water. The solution was vigorously mixed and sonicated in an ultrasonic bath with a constant temperature of 48 °C for an hour.

Cellulose solution: The cellulose solution was prepared following the recipe.[258] Briefly, 7 wt% NaOH pellets (Macron) and 12 wt% urea powders (Sigma-Aldrich, U5128) were directly dissolved in DI water. The alkaline solution was pre-cooled at -20 °C before use. Next, we added 2 wt% cellulose powders into the alkaline solution and vigorously mixed until transparent solution was yielded.

Experimental procedure of bonding

The prepared chitosan solution was directly spread on the surface of one piece of hydrogel with thickness of ~500 μm. Another piece of hydrogel was placed on top, and compress the two pieces of hydrogels with 5.5 % strain with customized glass molds. The whole structure was then sealed in a plastic bag to prevent dehydration. The weight of bilayer was measured after 24 hours and showed only 0.2 wt% difference, indicating negligible water loss during the procedure.

Confocal microscopy

We used FITC labeled chitosan (Chitosan-Fluorescein; Akina, Inc., KITO-9) to track the diffusion of chitosan chains in hydrogels. PAAM hydrogels were prepared with pH of 5, 7 and 12. We prepared a 2 wt% chitosan solution, with FITC-chitosan and chitosan ($M_w \sim 190,000$ - $310,000$ Da) in a weight ratio of 1:9. The solution was covered from light. We bonded two pieces of polyacrylamide hydrogels with the FITC-chitosan solution. The entire sample was imaged with a confocal fluorescence microscopy (Leica tcs-sp5), with an excitation wavelength of 490 nm and emission wavelength of 525 nm for FITC. A series of confocal images were taken by scanning the sample along its thickness at different time after bonding. The images were reconstructed in 3D using ImageJ to visualize the diffusion kinetics and the adhesion layer.

T-peeling tests for measuring the adhesion energy

All tests except the low-peeling-rate tests were conducted in an open air and at room temperature. For tests with low peeling rate (<0.04 mms^{-1}), the samples were tested in a humidity chamber to prevent dehydration of hydrogel. The humidity chamber was home-made with acrylic sheets and equipped with a household cool mist humidifier and a humidity control system (Zoo med, HygroTherm Humidity and Temperature Controller). The relative humidity in the chamber was maintained about 92 %. The hydrogel sample was 50 mm in length, 20 mm in width and 1.5 mm in thickness (Figure A2). The back sides of the hydrogels were glued with stiff polyester films of thickness 100 μm (clear polyester film, McMaster-Carr) with Krazy glue (cyanoacrylate). For hydrogels with pH near neutral, we directly used the Krazy glue to bond the polyester film and the hydrogel. However, for hydrogels with pH too low or too high, the Krazy glue failed to bond the polyester film and hydrogel. The low pH inhibited the polymerization of cyanoacrylate, and the high pH made the polymerization too fast. Both led to unsatisfactory bonding quality.[170] To overcome this issue, we dripped few drops of NaOH (1 M) or HCl (1 M) solution on the back surface of the hydrogel to adjust the local pH close to neutral.

Consequently, the Krazy glue can be successfully applied to bond the polyester film and the hydrogel. The volume of the few drops applied was much smaller than that of the hydrogel. The T-peeling test was conducted immediately following the dripping. The time was only several minutes, insufficient for the OH^- or H^+ ions to diffuse across the whole hydrogel to neutralize it. As a result, the pH was only changed locally on the back surface of the hydrogel, but did not affect the pH in the bulk hydrogel, especially close to the interface between the two pieces of hydrogels, where topological adhesion was performed. The polyester films restrict deformation of hydrogels during the T-peeling test. The free ends of the hydrogels were fixed to an Instron testing machine with 10 N or 500 N load cells. The peeling rate was fixed at 0.4 mms^{-1} . For slow crack tests, the peeling rate was varied by orders of magnitude. The peeling force as a function of displacement was recorded. The adhesion energy was calculated as twice the value of the peeling force at plateau divided by the width of the sample [259].

Pure shear tests for measuring bulk toughness of hydrogels

We used pure shear tests to measure the fracture energy of the hydrogels. For each test, two samples of the same hydrogel with dimension $50 \times 10 \times 1.5 \text{ mm}$ ($90 \times 10 \times 1.5 \text{ mm}$ for PAAM hydrogels) were made: one with a pre-crack of 20 mm cut by razor blade, and the other without. All the samples were tested individually on an Instron testing machine with a 500 N load cell. The loading rate was fixed at 0.2 mms^{-1} . The unnotched samples were used to measure the stress-stretch curve. In the reference state when the sample is not deformed, the height of the sample is H ; after loading, the height becomes λH . The area beneath the stress-stretch curve gives the strain energy density stored in the hydrogel, $W(\lambda)$. The notched samples were used to measure the critical stretch λ_c , where the notch turns into a running crack. The fracture energy is calculated as $\Gamma = W(\lambda_c) H$ [108, 259].

Bonding a hydrogel and a stomach tissue

A fresh porcine stomach was obtained from a local grocery store. A piece of stomach tissue was carefully cut with a size of 3.7 cm×4.4 cm, and subsequently soaked in a simulated gastric acid (Ricca Chemical, 7108-32, simulated Gastric Fluid (without Pepsin), 0.2 % (w/v) sodium chloride in 0.7 % (v/v) hydrochloric Acid, pH~1.5) for one hour. We then spread cellulose solution on the tissue surface and immediately attached a piece of PAAM hydrogel under gentle pressure. The PAAM hydrogel is much softer than the stomach tissue. The elastic modulus of the PAAM hydrogel is about 1 kPa, while the elastic modulus of the stomach tissue is about 1 MPa [249]. We tested the bonding by the lap shear test after several hours (Movie A1).

On-demand detachment

Chitosan solution was used to bond two pieces of PAAM hydrogels. The top hydrogel was attached to a rigid acrylic plate, and the bottom hydrogel was attached to a weight of 100 g (equivalent to an energy release rate of 50 Jm⁻²). The weight itself does not cause debonding. Next, we dripped water directly at the bonding front, and observed no debonding after 12 trials (Movie A2). We then dripped hydrochloride solution (1 M) directly at the same bonding front, and observed progressive debonding after every single dripping, until the two pieces of hydrogels completely detached (Movie A3).

Figures

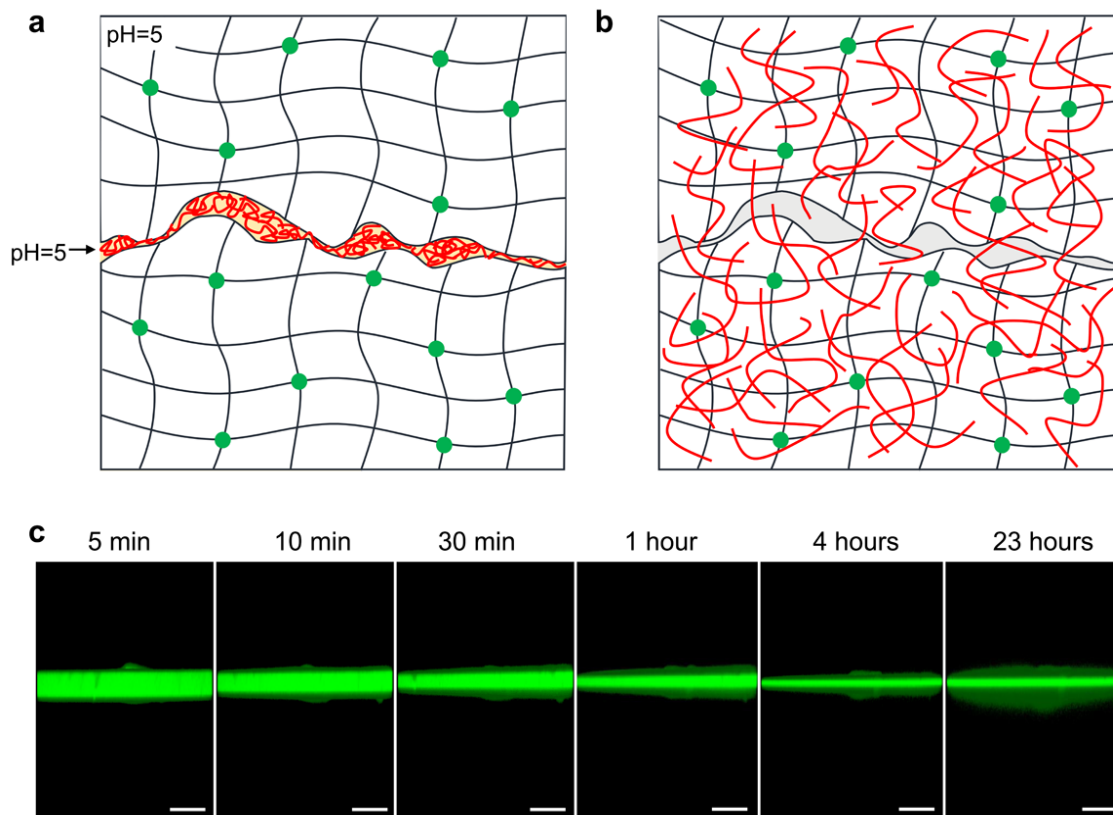


Figure A1 Chitosan chains do not form a network when the pH of hydrogel is lower than the pKa of chitosan. (a) Chitosan solution of pH = 5 is spread at the interface of two hydrogels of pH = 5. (b) Chitosan chains diffuse into both hydrogels. Because chitosan is soluble at pH = 5, the chitosan chains diffuse across the entire hydrogels and do not form a network. (c) A sequence of confocal images show chitosan chains diffuse away from the interface. The chitosan chains keep diffusing away even after 23 hours. The scale bar is 300 μm .

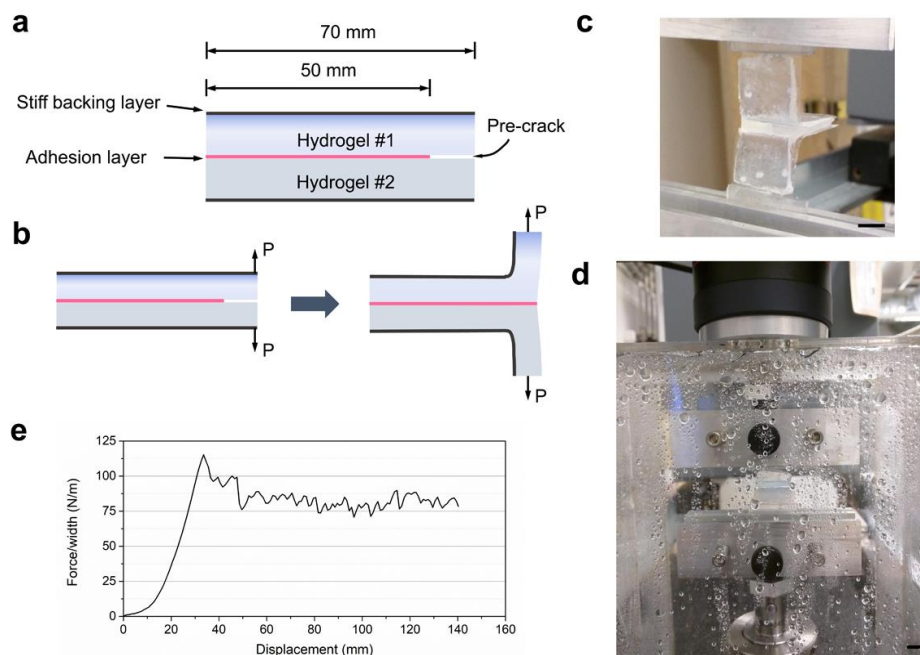


Figure A2 The T-peeling test. (a) Schematics of a hydrogel bilayer. (b) Schematics of the T-peeling test. (c) Photo of the T-peeling test. (d) Photo of the T-peeling test conducted in a humidity chamber. (e) Representative force-displacement curve of the T-peeling test. The adhesion energy is calculated as two times the steady-state force at the plateau divided by the width of the bilayer. The scale bar in (c) and (d) is 1 cm.

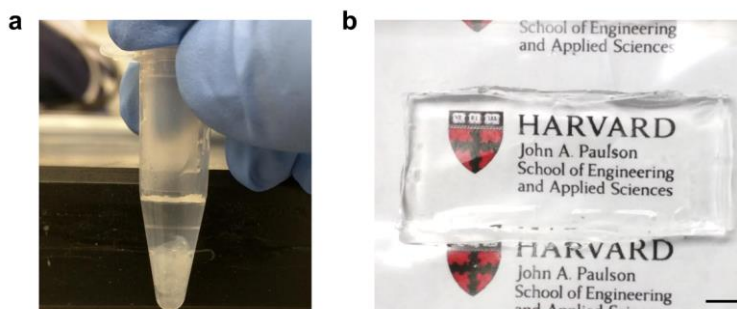


Figure A3 Visual comparison of chitosan precipitation. (a) When a chitosan solution (pH = 5) is dripped with NaOH (1 M), chitosan chains precipitate out and the solution becomes turbid. (b) When chitosan chains bond two pieces of PAAM hydrogels with pH > 7, the interface remains optically transparent. The scale bar is 5 mm.

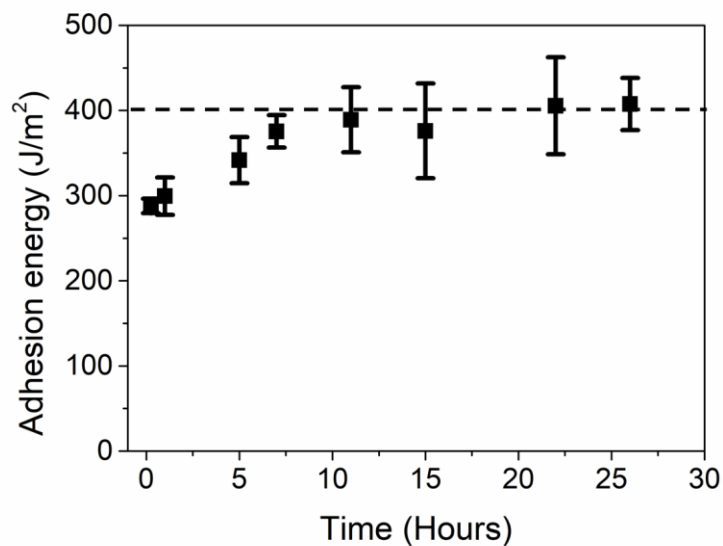


Figure A4 Adhesion kinetics for PAAM hydrogels bonded with PAS. The adhesion energy builds up to $\sim 300 \text{ Jm}^{-2}$ within 15 min after bonding, and reaches an equilibrium value of $\sim 400 \text{ Jm}^{-2}$ about 10 hours.

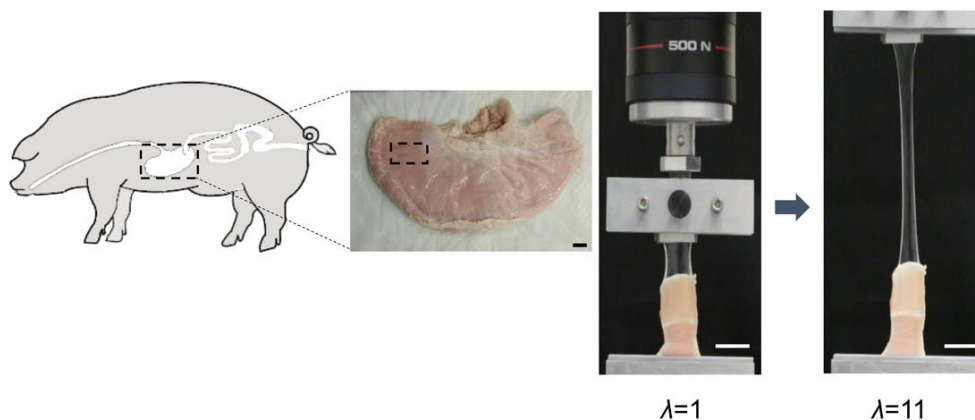


Figure A5 Demonstration of tissue adhesives used in extremely acidic environment. A piece of gastric acid-treated porcine stomach tissue (pH ~ 1.5) was bonded with a PAAM hydrogel using cellulose. Under uniaxial tension, the hydrogel was stretched as large as 11 times its initial length without debonding. The scale bar is 3 cm.

Tables

Table A1. Hydrogels used in the tests

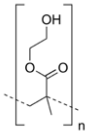
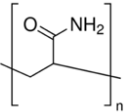
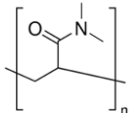
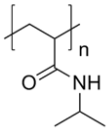
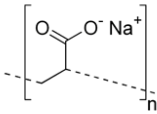
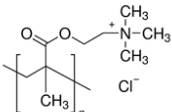
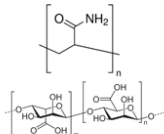
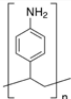
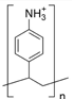
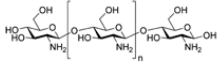
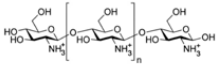
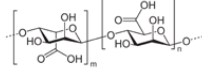
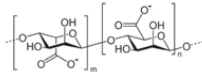
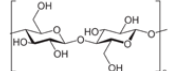
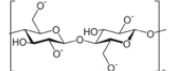
Polymer chain of hydrogel	Molecular structure	Charges on polymer chains	Interaction with Chitosan
Poly(hydroxyethylmethacrylate) (PHEMA)		Neutral	Weak hydrogen bond
Poly(acrylamide) (PAAM)		Neutral	Weak hydrogen bond
Poly(dimethylacrylamide) (PDMA)		Neutral	Weak hydrogen bond
Poly(N-isopropylacrylamide) (PNIPAM)		Neutral	Weak hydrogen bond
Sodium polyacrylate (NaPAA)		Negatively charged	Weak hydrogen bond and ionic bond
[2-(Acryloyloxyethyl) trimethylammonium chloride] (PDMAEA)		Positively charged	Weak hydrogen bond and positive charge repulsion
Polyacrylamide/alginate		Neutral/Negatively charged	Weak hydrogen bond and ionic bond

Table A2. Stitching polymers used in the tests

Stitching polymers	Molecular structure	pKa	Soluble pH	Soluble state	Bonding pH	Crosslinks in networks
Poly(4-aminestyrene)		4.6	<4.6		>4.6	<ul style="list-style-type: none"> • NH₂--NH₂ H-bond • π-π stacking
chitosan		6.5	<6.5		>6.5	<ul style="list-style-type: none"> • NH₂--OH H-bond
Alginate		3.5	>3.5		<3.5	<ul style="list-style-type: none"> • COOH--COOH H-bond
Cellulose		13	>13		<13	<ul style="list-style-type: none"> • OH--OH H-bond

Movies

Movie A1 Cellulose is used to achieve strong adhesion between a PAAM hydrogel and a porcine stomach tissue treated with gastric acid (pH = 1.5).

Movie A2 Hydrogels remain bonded when water is dripped at the bonding front.

Movie A3 On-demand detachment when hydrochloride acid solution is dripped at the bonding front.

Appendix B. Supporting information for Chapter 3

Materials

High molecular weight sodium alginate ($M_w = 265\text{kDa}$) with high guluronate content (PROTANAL LF20/40; FMC Technologies) was used for in vitro experiments. Low molecular weight sodium alginate was prepared by irradiating the high molecular weight sodium alginate (PROTANAL LF20/40; FMC Technologies) under γ -rays at a dose of 5Mrad following the previous protocol [260]. Ultrapure sodium alginate with low endotoxin levels (MVG and VLVG; ProNova Biomedical AS) was used for in vivo studies. Chitosan of low-, medium- and high-molecular weight was purchased from Sigma and used for in vitro experiments, and ultrapure chitosan (CL 214, FMC Corporation) with low endotoxin levels was used for in vivo experiments. The bridging polymers including polyallylamine, gelatin, and polyethyleneimine were purchased from Sigma, and type I collagen was purchased from Advanced BioMatrix. The coupling reagents 1-ethyl-3-(3-dimethylaminopropyl) carbodiimide hydrochloride (EDC) and N-hydroxysulfosuccinimide (sulfo-NHS) were purchased from Thermo Fisher Scientific. Medical grade cyanoacrylate (Loctite 4541 Prism) was purchased from Henkel Corporation. Monomers including acrylamide (AAM), *N,N'*-methylenebis(acrylamide) (MBAA), polyhydroxyethyl methacrylate (HEMA), free-radical initiator ammonium persulfate (APS), photoinitiator IRGACURE 2959 (I2959) and polymerization accelerator tetramethyl-ethylenediamine (TEMED) were purchased from Sigma. Polyethylene glycol diacrylate (PEGDA) was synthesized following a modified protocol [261]. Fluorescein isothiocyanate-labeled chitosan (FITC-chitosan) was synthesized according to the previously reported protocol [262]. Fluorescent microspheres of 500nm diameter with surface carboxylate groups were purchased from Thermo Fisher Scientific. COSEAL surgical sealant and SURGIFLO hemostatic matrix were purchased from Baxter and Ethicon, respectively. Porcine skin, liver, heart, lung and cartilage were purchased from a local grocery store.

Methods

Tough Adhesive Synthesis. To prepare a tough adhesive in form of preformed patch, a hydrogel was preformed as the dissipative matrix, and then its surface was treated with the bridging polymer and coupling agents for carbodiimide coupling reaction. Alginate-polyacrylamide hydrogels were synthesized following a modified protocol based on a previously reported protocol [263]. In brief, sodium alginate and acrylamide were first dissolved in HBSS at 2% and 12% respectively, and stirred overnight till a clean solution was obtained. This solution of 10mL was then mixed with 36 μ L of 2% covalent cross-linker MBAA, 8 μ L of accelerator TEMED, 226 μ L of 0.27M initiator APS, and 191 μ L of 0.75M ionic cross-linker CaSO₄ slurries. The mixture gelled inside a closed glass mold at room temperature overnight.

To make an injectable tough adhesive, alginate-polyethylene glycol diacrylate (alginate-PEGDA) hydrogel was chosen as the dissipative matrix. The ultrapure alginate (MVG and VLVG at 1:1 ratio) and PEGDA (20kDa) were dissolved in distilled water at 5% and 60%, separately. The two solutions were then syringe-mixed at 1 to 1 volume ratio, and mixed with calcium sulfate slurries and I2959. The final concentrations of I2959 and calcium sulfate were 0.1% and 20mM. The adhesive was cured with UV light of wavelength 365nm (DYMAX 2000 Flood) for 10 minutes.

The bridging polymers polyallylamine, chitosan, gelatin, and polyethyleneimine were dissolved into MES buffer at 2.0% and the pH was adjusted to 6. The collagen was used as a stock solution (1.0%). 1-ethyl-3-(3-dimethylaminopropyl) carbodiimide (EDC), sulfated or unsulfated N-hydroxysuccinimide (NHS) were used as the coupling reagents. The final concentrations of EDC and sulfated NHS in the solution of the bridging polymer were both 12mg/mL. The mixture of the bridging polymer and coupling reagents (~250 μ L) was applied to the surface of the dissipative matrix (15x70 mm²) prior to application. Compression was applied before mechanical testing, typically for 5-30 minutes unless stated otherwise. For the injectable tough adhesive, the mixture of bridging polymer and coupling reagents was casted onto the

surface of the substrate, before injecting and curing the alginate-PEGDA matrix.

Matrix Toughness Measurement. Pure shear tests were carried out to measure the matrix toughness. In brief, rectangular specimens ($50 \times 5 \times 1.5 \text{ mm}^3$) were stretched by an Instron machine (model 3342 with load cell of maximum 1000N). For notched samples, an edge crack of length 20mm was cut using a razor blade in the middle of the gauge section of the specimen. The stretch rate was fixed at 2 min^{-1} . From the stress-stretch curves of the unnotched and notched specimens, the matrix toughness was calculated following the method reported previously [263].

Adhesion Energy Measurements. The adhesive performance was quantified as adhesion energy, namely the amount of energy required to increase a unit area of interfacial crack. The adhesion energy was determined with either peeling adhesion tests, or bilayer adhesion tests when the substrate had low bulk toughness.

Peeling Adhesion Test. The adhesion energy was measured with 180 degree peeling tests. A ribbon of the tough adhesive ($15 \times 1.5 \times 80 \text{ mm}^3$) was adhered to a substrate with one end open, forming a bilayer with an edge crack. The back of the tough adhesive was also bonded to a rigid polyethylene terephthalate (PET) film with Crazy Glue, in order to limit deformation to the crack tip, and thus all the work done by the machine would be equal to the energy dissipated at the crack tip. The free ends of the tough adhesive and the substrate were attached to plastic sheets, to which the machine grips were attached. An Instron machine was used to apply unidirectional tension, while recording the force and the extension. The loading rate was kept constant at 100 mm/min. The adhesion energy was two times the plateau value of the ratio of the force and width [259].

Bilayer Adhesion Test. When hydrogels of low bulk toughness were tested, a bilayer adhesion test was used to measure adhesion energy. The hydrogels tested with this method

include polyacrylamide, poly(hydroxyethyl methacrylate) and poly(N'-isopropylacrylamide) hydrogels. The bilayer specimens were prepared by compressing a tough adhesive of 45x20x1.5 mm³ on a hydrogel of 30x20x1.5 mm³. A notch was introduced at length 5mm. A rigid polyethylene terephthalate (PET) film with thickness 120 μm (Transparency Copy Film, PP2500, 3M) was glued to the testing hydrogel as a backing layer with Krazy glue. The specimen was stretched by an Instron machine with a constant loading rate of 0.5 mm/s, while the force-stretch curves were recorded. The adhesion energy G can be calculated by $G = P(\lambda - 1) - U_s(\lambda)$, where P and λ are the critical force per unit width (the force in the current state divided by the width of the sample in the un-deformed state) and the critical stretch when debonding occurs [99]. U_s is the strain energy stored in the substrate divided by the area of the substrate in the undeformed state when debonding occurs, which is the area under the recorded force-stretch curve of the substrate with stretch from 1 to λ . In the case that both arms were glued to the PET film, the adhesion energy $G = P(\lambda - 1)$.

Dependence of Adhesion on Concentration and Molecular Weight of Chitosan. This study investigated how the adhesion depended on the concentration and molecular weight of the bridging polymer. The chitosan concentration was varied from 0.3 to 1.5 wt% in preparing the tough adhesives. The molecular weight of the chitosan was varied by using low, medium and high molecular-weight chitosan purchased from Sigma. The resulting adhesives were applied onto an alginate-polyacrylamide hydrogel as a model substrate, and the adhesion energy was measured with peeling adhesion tests.

Physical Interpenetration of Bridging Polymer. Interpenetration of the bridging polymer into the dissipative matrix of the TAs was imaged using FITC labeled chitosan and confocal microscopy. The FITC-chitosan was dissolved into MES buffer to 2 wt% with pH adjusted to 6,

and then the mixture of 20 μL was distributed on the surface of a hydrogel disk of diameter 6 mm with or without EDC/NHS. The incubation time was varied from 2 to 30 minutes, before aspirating the excess FITC-chitosan solution. Fluorescent microspheres of 20 μL volume were added onto the same hydrogel surface, followed by extensive rinsing with DI water for 30 seconds. The fluorescent microspheres carry carboxylate groups on their surface that can bind with the primary amines on the FITC-chitosan, forming amide bonds via carbodiimide chemistry. A confocal fluorescence microscopy (Zeiss LSM710) was used to image the gel surface, with the excitation wavelengths set to 490 nm for FITC and 588 nm for the fluorescent microspheres.

Confocal Imaging of Adhesion Interface. Tough adhesives were prepared using FITC-chitosan as the bridging polymer, and adhered to porcine skin, or polyacrylamide hydrogels. Adhesion was performed in the dark, and allowed to develop for one hour. The samples were cryoprotected in 20% sucrose/PBS at room temperature and embedded in OCT before being frozen on dry ice. Transverse cryosections (50 μm) were cut using a cryostat (Leica CM1950) and imaged by confocal fluorescence microscopy (Zeiss LSM710). The excitation wavelength of FITC was set to be 490 nm, and bright field images were also collected.

Sterile Processing. Endotoxin-free alginate (MVG and VLVG) and chitosan (CL 214) were used in the in vitro cell culture and in vivo animal studies. The alginate and chitosan were first dissolved in distilled water at 0.5% (w/v). The solutions were then sterile filtered (Corning Filter System 0.22 μm membrane pores; low protein binding), frozen at -20°C , and then placed onto a lyophilizer (SP Scientific) for a week. After lyophilization, the sterile alginate and chitosan were stored at -20°C before usage. The other chemicals including AAM, MBAA, APS, TEMED, EDC and sulfo-NHS were sterilized by filtering right before usage. The sterile alginate-polyacrylamide hydrogels were synthesized following the same protocol above in the TC hood. After the

reaction, the hydrogels were soaked in HBSS for 30 minutes, and then rinsed three times before usage. The sterile chitosan (CL 214, FMC Corporation) was reconstituted with distilled water at 4%. The aqueous solution of EDC and sulfo-NHS at 24mg/mL was sterile filtered before mixing with the 4% sterile chitosan solution at 1:1 ratio. The mixture was used to modify the surface of the sterile alginate-polyacrylamide hydrogel immediately before application.

In Vivo Adhesion Test. Female Yorkshire swine with a bodyweight of 60-75 kg were used. All animals received humane care in accordance with the 1996 Guide for the Care and Use of Laboratory Animals recommended by the US National Institute of Health. The experimental protocol was approved by the Boston Children's Hospital Institutional Animal Care and Use Committee. The pigs were anesthetized by intramuscular injection of tiletamine/zolazepam (7 mg/kg) and xylazine (4 mg/kg), intubated with a cuffed endotracheal tube and ventilated with a volume control ventilator (Hallowell EMC Model 2000, Hallowell EMC, Pittsfield, MA) at a rate of 10-20 breaths per minute. Anesthesia was maintained with isoflurane (1-2%). Fentanyl and Buprenorphine were used for analgesia, and a maintenance IV infusion of 150-300 ml per/hour was administered. The chest cavity was accessed via midline sternotomy and the pericardium was opened to expose the heart surface. The tough adhesives were applied to the beating heart surface of the left ventricle and held in place to 3 minutes using a custom-made applicator. This application did not affect heart function. We attempted to peel the tough adhesives off of the surface of the heart while continuously recording the force used to lift it off. Videos were also recorded. In some of the experiments we added freshly drawn arterial blood to the surface of the heart prior to applying the tough adhesive in order to assess the effect of the presence of blood.

In vitro Cell Compatibility Study. Tough adhesive (TA) and cyanoacrylate (CA) were incubated separately in 1 mL DMEM containing 10% FBS at 37 °C for 24 hours, and the masses in use were fixed at 22mg. To further assess the cell compatibility of the ingredients used to

make TA, conditioned medium was also prepared by incubating the alginate-polyacrylamide hydrogel of 20mg or 2 μ L solution of chitosan and EDC/Sulfated NHS in which the chitosan concentration was at 2wt% and the final concentrations of EDC and Sulfated NHS in the solution of bridging polymer were both 12 mg/mL in medium as well. Human dermal fibroblasts were plated in 96-well plates (1.2x10⁴ cells per well, n=5 per condition). Cells were treated with each conditioned media (200 μ L per well) and incubated for 24 hours at 37°C and 5% CO₂. Cell viability was determined with a LIVE/DEAD Viability/Cytotoxicity kit for mammalian cells (Thermo Fisher Scientific); An Olympus IX81 inverted microscope was used to image live cells with excitation/emission at 495nm/515nm, and dead cells at 495nm/635nm separately.

In vivo Biocompatibility and Stability Test. Endotoxin-free alginate and chitosan were used for the in vivo studies. The experiments were carried out in accordance with the Harvard University Standing Committee on the Use of Animals in Research and Teaching.

Subcutaneous Implantation. Two dorsal skin incisions were conducted, and two subcutaneous pockets were created by blunt preparation per animal (175-200g). Tough adhesives (TA), cyanoacrylate (CA) and COSEAL (from Baxter) were implanted into the dorsal subcutaneous pockets (n=4 for TA and CA; n=6 for COSEAL). The implanted materials were 200-400 mg. The skin incisions were closed with wound staples, and the animals were returned to their cages after recovery from anesthesia. At 2 weeks, the animals were euthanized by CO₂ inhalation, and the implants as well as the surrounding tissue were explanted and further processed for histological analysis. The diameters of the explants were measured with a caliper to evaluate the swelling in vivo. The samples were fixed with 4% paraformaldehyde (PFA) at 4°C overnight, followed by rinsing with PBS for 3 times, and then processed for histology and hematoxylin and eosin (H&E) staining at the Rodent Pathology Core at Harvard Medical School. The histological sections were imaged with a Nikon E800 upright microscope. The degree of inflammation was assessed by a blinded histopathology expert.

Myocardium Attachment. This study was carried out with Female Sprague Dawley rats (225-275g). In brief, the epicardial surface was exposed and the heart was manipulated as previously described [264]. Tough adhesives or cyanoacrylate plus alginate-polyacrylamide hydrogels were compressed against the epicardial surface using a custom made applicator to allow the adhesive to set. The incisions in the animals were closed with sutures, and animals were returned to their cages after recovery from anesthesia. Two weeks later, hearts were explanted, fixed in 4% paraformaldehyde (PFA) at 4°C overnight, followed by rinsing with PBS for 3 times, and then processed for histology and hematoxylin and eosin (H&E) staining. The histological sections were imaged with a Nikon E800 upright microscope, from which the thickness of inflammatory region was determined. The degree of inflammation was subsequently assessed by a blinded histopathology expert.

In vivo Stability Test. The stability of tough adhesives and their adhesive performance were evaluated by measuring the adhesion energy of TA-hydrogel interfaces after subcutaneous implantation. A lap-shear specimen was formed by compressing a rectangular stripe of tough adhesive (15x50x1 mm³) onto a piece of alginate-PAAm hydrogel of the same dimension. The bonding area was around 15x20 mm². Specimens were implanted into large dorsal subcutaneous pockets in rats following the same protocol of subcutaneous implantation above. At 2 weeks, the specimens were explanted. The adhesion energy was measured with bilayer adhesion tests described above.

Long-Term Cyclic Tests of Heart Sealant. A fresh porcine heart was obtained from a local grocery store. A circular defect of 4mm diameter was created with biopsy punch on the atrium wall of the heart. The defect was then sealed with a 8mm-diameter disc of the tough adhesive. The heart with the attached sealant was submersed in a large reservoir of PBS. The inflation-deflation movement of the heart was mimicked by pumping air in and out for 18 hours (22,000 cycles in total). Photos and videos were recorded to examine any leakage at the sealant site.

Burst Pressure Measurements. This study was carried out by following the ASTM F2392 standard protocol for measuring burst strength of surgical sealants. Myocardium tissues of 3-5mm thickness were isolated from fresh porcine hearts purchased from a local grocery store. A 3mm-diameter hole was punched at the center of the myocardium tissue. A 15mm-diameter tough adhesive with and without gluing its back to a rigid PET film was adhered onto the myocardium tissue. The pressure was applied by pumping PBS using a syringe pump (Harvard Apparatus PHD 2000 Dual Syringe Pump) at a rate of 2 mL/min from the bottom of the specimen. During the measurement, the pressure was recorded as a function of time and the burst pressure was identified when a burst occurred.

Attachment of Soft Actuators on Myocardium. A soft actuator was fabricated following a protocol reported previously, which was used to support heart function [233]. To attach the actuator onto a myocardium surface, it was first sandwiched with two sheets of TAs that bonded together to fully encapsulate the device, and then compressed onto a myocardium surface of a porcine heart. The device was actuated with a pneumatic scheme following the previous protocol [233]. The interface between the TA and the heart was examined for debonding or rupture during actuation.

Hepatic Hemorrhage Model. This study, involving Female Sprague Dawley rats (175-200g), was carried out in accordance with the Institute for Animal Care and Use Committee, Harvard University. Liver laceration was performed to create an uncontrolled hemorrhage condition in rats, as per previous reports in the literature [265, 266]. In brief, the animals were anesthetized via isoflurane by inhalation (4%), and then by ventilation (2%). A ventral midline laparotomy incision was performed, and the left lobe of the liver was exposed. A nearly full-thickness wound was created with a biopsy punch of 6mm, followed by laceration with a scissor. Immediately

after injury, the tough adhesive (TA) or the hemostatic matrix SURGIFLO (from Ethicon; as a positive control) was applied on the lesion site (n=4). Untreated animals were included for negative control (n=4). During the surgery, the blood was carefully collected with filter papers at time points of 2, 5 and 10 minutes. The total amount of the blood loss at each time point was determined by weighing the papers and recorded. The abdomen was closed 15 minutes after the wound creation and treatment. The animals were allowed to recover from anesthesia before returning to the cage. The animals were monitored to check secondary hemorrhage. At 2 weeks, the animals were euthanized by CO₂ inhalation, and the livers were explanted and further processed for histological analysis. The samples were fixed with 4% paraformaldehyde (PFA) at 4°C for 2 days, followed by rinsing with PBS for 3 times, and then processed for histology and hematoxylin and eosin (H&E) staining at the Rodent Pathology Core at Harvard Medical School. The histological sections were imaged with a Nikon E800 upright microscope.

Attachment of Tough Adhesive to Skin. All work was done with C57BL/6J mice (female, aged 6-8 weeks; Jackson Laboratories) and was carried out in accordance with the Institute for Animal Care and Use Committee, Harvard University, and National Institutes of Health and institutional guidelines. Mice were anesthetized with isoflurane, and a region of the dorsum was shaved. Anesthesia was maintained with isoflurane (1-2%). Two pieces of tough adhesive of 6mm diameter were applied with a custom designed applicator for 2 minutes. For the use of skin wound dressing (n=4), a skin wound was created with a biopsy punch of 4 mm on the dorsum. The tough adhesive of 10mm diameter was applied with compression for 2 minutes. Tegaderm film (from 3M) was attached to minimize water loss and fixed onto the dorsum using suture or wound staples. The mice were returned to their cages after recovery from anesthesia. Videos were taken to assess the adhesion under the movement of mice. The attachment of the tough adhesives was monitored on day 1 and 7.

Effect of Interfacial Bridging on Adhesion. The importance of building strong chemical bonds for interfacial bridging was next examined, by comparing TA with adhesives that were modified with either the coupling reagents or the bridging polymer alone (Figure B5). EDC was applied at very low concentration ($\sim 0.1\%$ by weight of TA), which undergoes fast hydrolysis (half-life time ~ 10 minutes) in aqueous solutions [177]. Use of the coupling reagents EDC/Sulfo-NHS alone led to very low adhesion energy (14 Jm^{-2}); without the bridging polymer, the dissipative matrix is likely to be repelled electrostatically by the negatively charged tissue surfaces. The bridging polymer without the coupling reagents led to moderate adhesion energy (303 Jm^{-2}). The purely electrostatic attraction in this situation is not as strong as covalent bonds bridging the two surfaces. In contrast, the tough adhesive consisting of both the bridging polymer and the coupling reagents led to high adhesion energy (1121 Jm^{-2}).

Comparison between TA and Existing Adhesives. Figure B7 summarizes the adhesion energy and matrix toughness of a variety of adhesives that are used in the clinic or under development, as well as cartilage. Many commercially available adhesives such as fibrin glues and COSEAL have low adhesion energy and low matrix toughness. Because they often comprise a brittle matrix [92, 98, 136], which often causes debonding due to cohesive failure of the adhesive matrix, thus the low matrix toughness sets the upper bound for the adhesion energy. Adhesive bandages, despite of tough elastomer matrix, rely on very weak interaction with tissues, leading to high matrix toughens and low adhesion energy. Our design enables TA to combine high adhesion energy and high matrix toughness simultaneously, which rivals that of cartilage.

Adhesion of TA to Hydrogels. The toughness of the substrates to which TA adheres sets an upper bound for the adhesion energy. Indeed, when a tough hydrogel like alginate-polyacrylamide hydrogel was used as the substrate, the adhesive achieved adhesion energy on

the order of 1000 Jm^{-2} . Alternatively, the adhesion energy was similar to the bulk toughness of the substrate, if the substrate toughness was lower than 1000 Jm^{-2} (for example, adhesion to PAAm) (Figure B8 and B9).

Injectable Adhesives for Cartilage Repair. The design of tough adhesives can be extended to injectable hydrogels. We chose alginate-polyethylene glycol diacrylate hydrogels as the dissipative matrix for injectable tough adhesives. The pregel solution can be injected via syringe into a defect site, and formed a tough matrix upon exposure to UV light. The injectable TA sustained a large compressive stress (6.6MPa) without rupture (Figure B19). Due to the compressive property, the injectable TA was used to repair a cylindrical defect in explanted cartilage discs. The defect surface was first casted with the mixture of the bridging polymer and the coupling reagents for interfacial bridging, followed by injection and UV-curing of the injectable TA. Strong adhesion formed between the adhesive and surrounding tissues (Figure B20). The results showed that no debonding or rupture of the TA was observed after compression testing, indicative of strong adhesion and tough matrix; the compressive property of the repaired cartilage was restored as compared to untreated tissues.

Figures

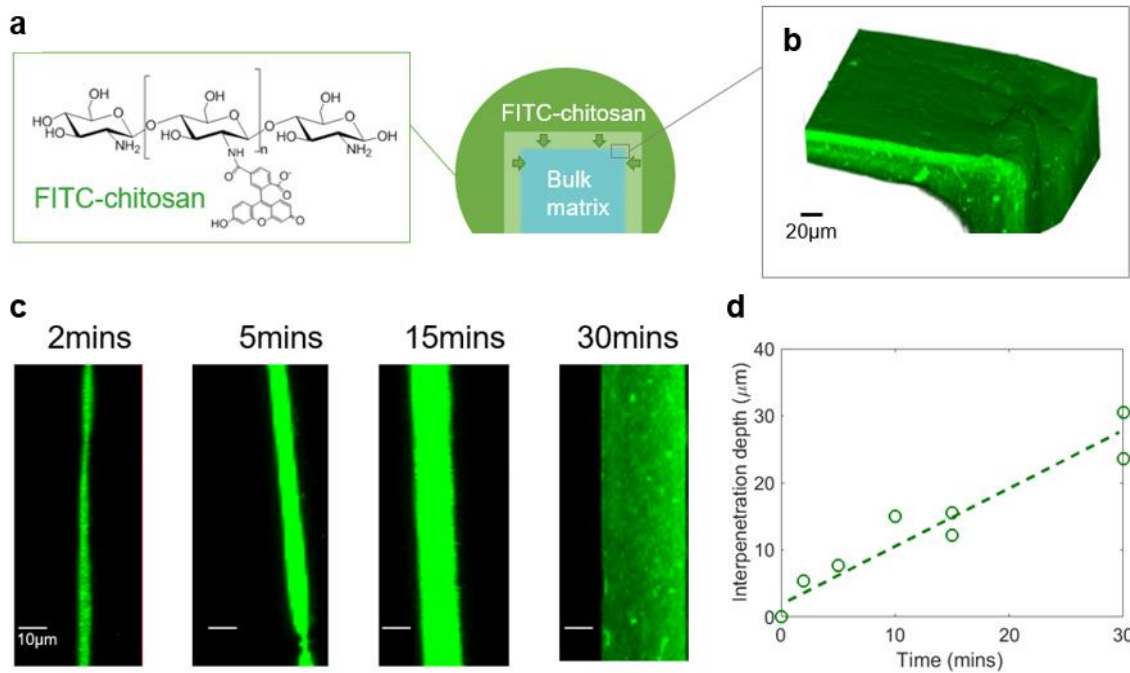


Figure B1 Physical interpenetration of bridging polymer into bulk matrix. (a) FITC-chitosan was applied to the alginate/polyacrylamide hydrogel comprising the dissipative matrix, and allowed to diffuse into the gel. (b) The diffusion of FITC-chitosan over time was imaged by confocal fluorescence microscopy. Scale bar, 20 μm . (c) Images of the adhesive surface containing FITC-chitosan at different incubation times. Scale bar, 10 μm . (d) The depth of chitosan interpenetration increased with the incubation time.

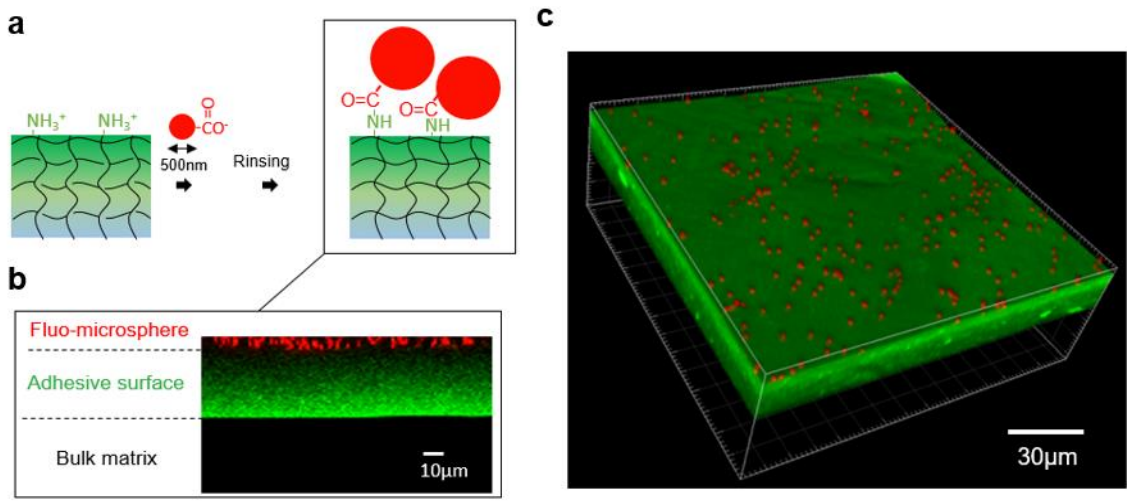


Figure B2 Retention of fluorescent microspheres on adhesive surface of TA. (a) Schematic showing that fluorescent microspheres of 500nm diameter (red) are spread on a tough adhesive consisting of FITC-chitosan interpenetrating adhesive surface (green), and after rinsing with PBS repeatedly, the microspheres remain on the tough adhesive via electrostatic attraction and formation of amide bonds. (b) 2D cross-section image of the sandwich structure: fluorescent microspheres (red), FITC-chitosan interpenetrating adhesive surface (green) and bulk matrix of the tough adhesive (from top to bottom). As the microsphere size is larger than the mesh size of the tough adhesive (on the order of 10 nm), the microspheres remain on the outer surface. (c) 3D construct of fluorescent microspheres adherent to a tough adhesive.

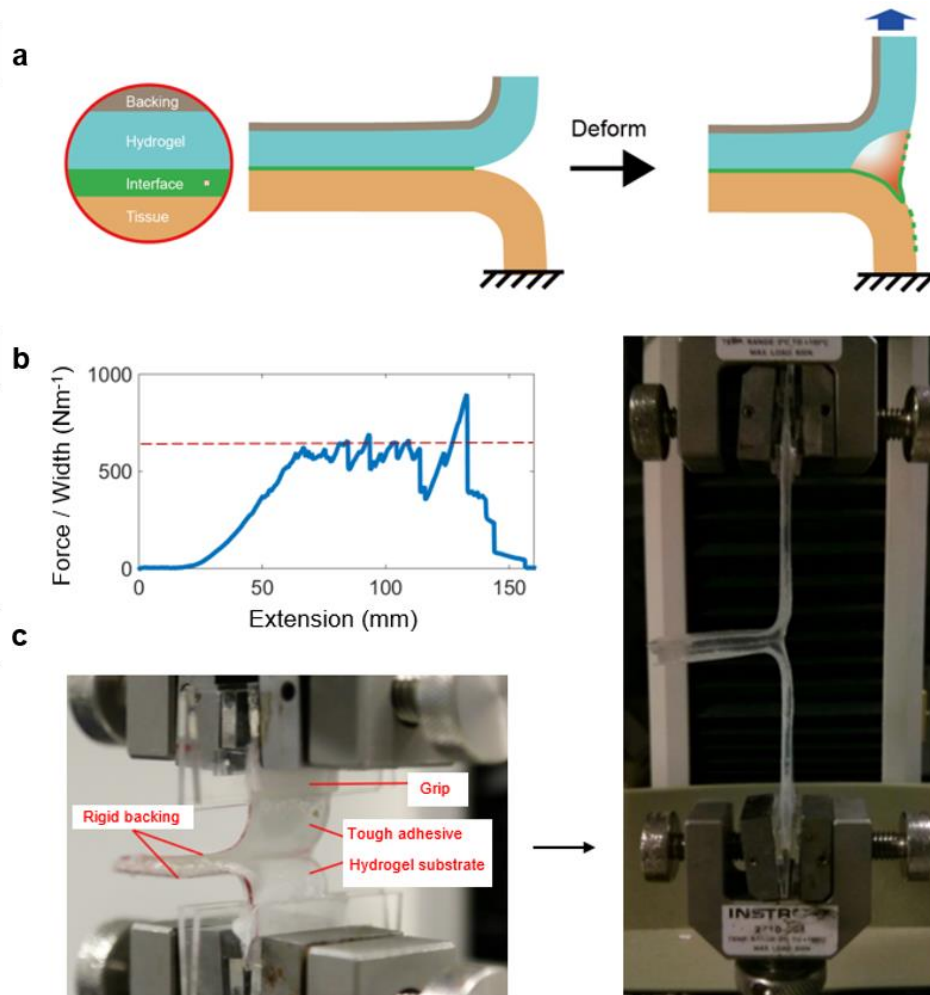


Figure B3 Peeling adhesion test. (a) Schematics of the composition of the TA-tissue specimen for adhesion measurements, and the TA-skin bilayer specimen being deformed using a 180-degree peeling test. One side of the TA was glued to a rigid plastic film as a backing layer, to eliminate energy dissipation in regions away from the crack tip. (b) The adhesion energy was determined by applying strain to the two arms of the sandwich specimen, and is defined as two times the plateau value of the force per width required for extension when the crack propagates under steady state (red dashed line). (c) Digital photos showing the TA-hydrogel specimen under peeling test.

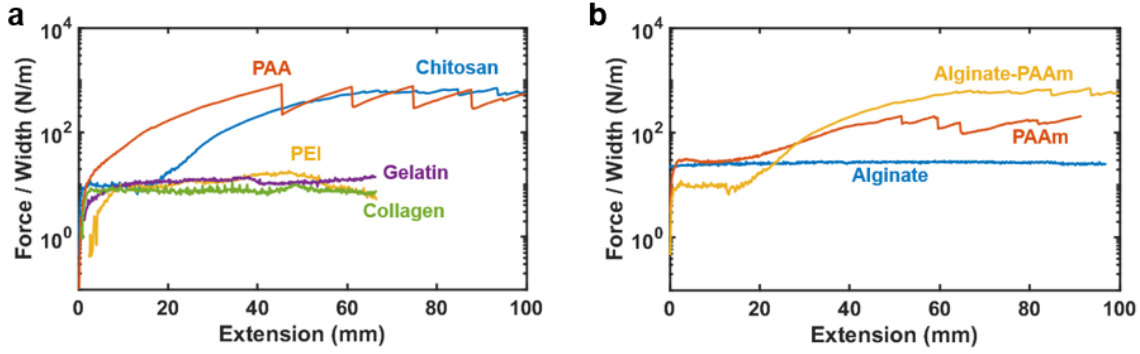


Figure B4 Force-extension curves of peeling tests. The adhesion energy was calculated based on the average value of force/width at the plateau. (a) Various polymers were used as bridging polymers in the design of tough adhesives, including chitosan, polyallylamine (PAA), polyethylenimine (PEI), gelatin and collagen. (b) Different hydrogels were tested as the dissipative matrix of tough adhesives, including alginate, polyacrylamide (PAAm) and alginate-PAAm hydrogels. Sample size $n=4$.

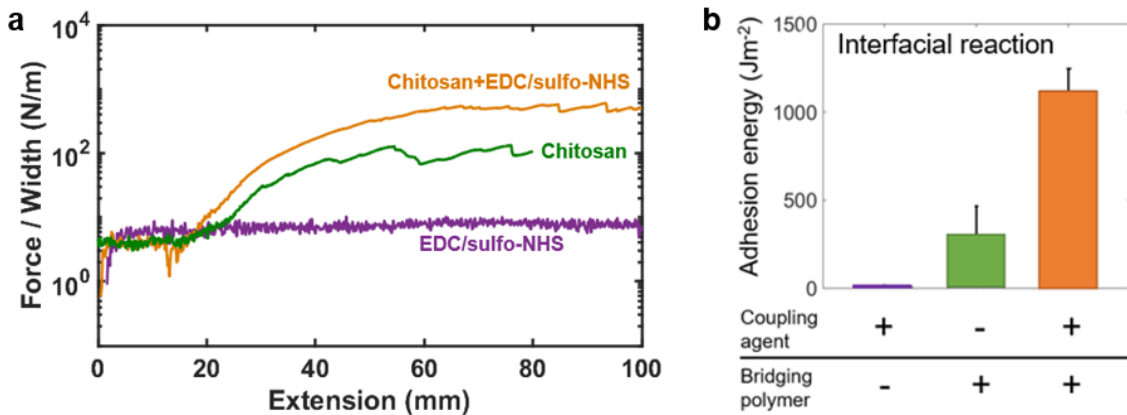


Figure B5 Effects of interfacial reaction on adhesion energy to porcine skin. The alginate-polyacrylamide hydrogel served as the dissipative matrix. Chitosan and EDC/sulfo-NHS were used as the bridging polymer and coupling reagents, respectively. The adhesion energy was calculated based on the average value of force/width at the plateau. (a) Force-extension curves of peeling tests. (b) Measured adhesion energy to porcine skin. Error bars show standard deviation; sample size $n=4$.

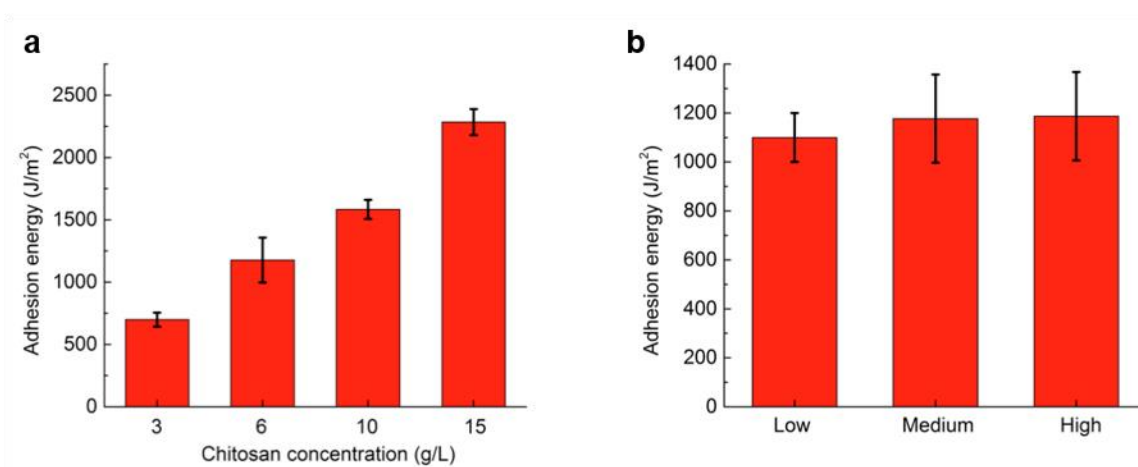


Figure B6 Effects of concentration and molecular weight of the bridging polymer on adhesion energy. An alginate-polyacrylamide hydrogel was used as a model substrate. The concentration (a) and molecular weight (b) of chitosan were varied in making the tough adhesives. Error bars show standard deviation; sample size n=4.

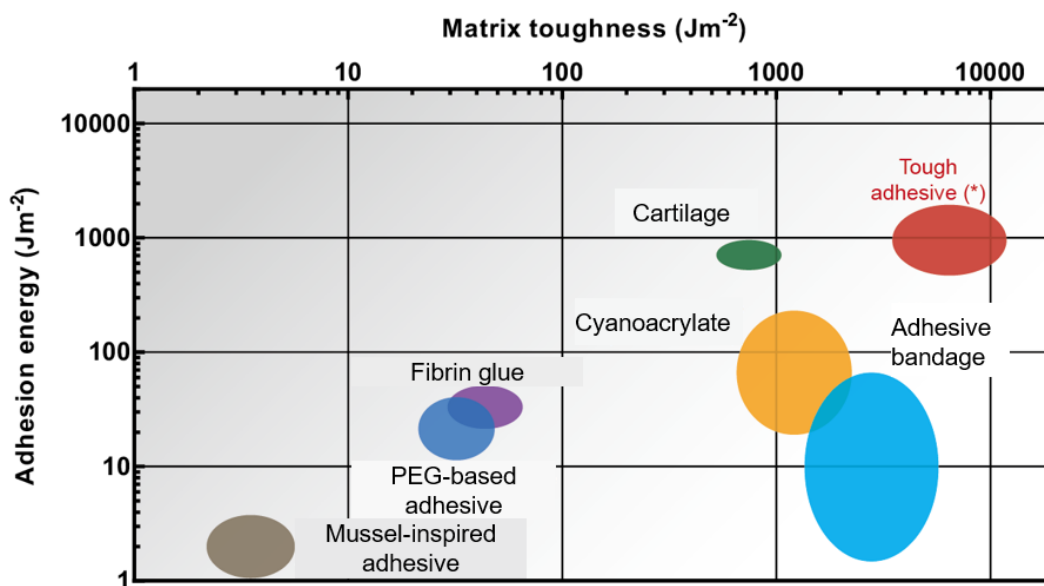


Figure B7 Comparison of adhesion energy and matrix toughness of various adhesives and cartilage. The data that was obtained with our measurements is labeled with asterisks, in which the matrix toughness was measured with pure shear tests and the adhesion energy was measured with peeling adhesion tests.

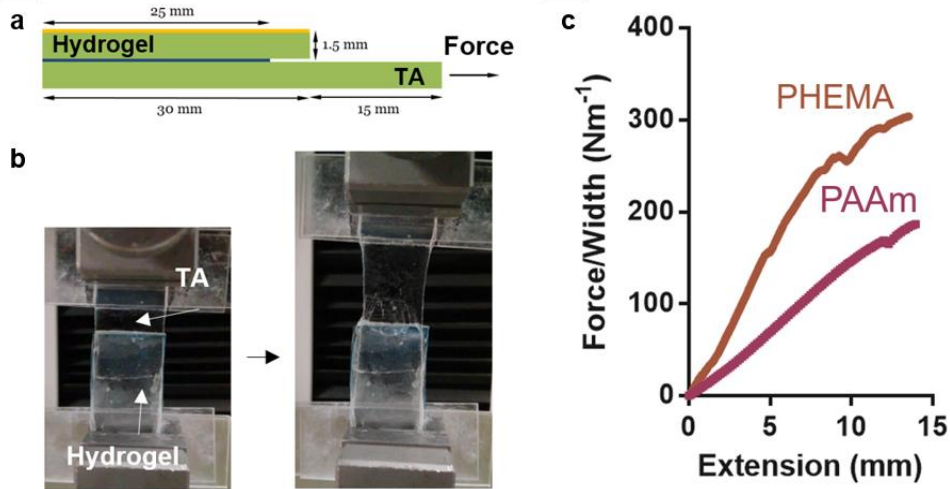


Figure B8 Bilayer adhesion test. (a) Schematic of a bilayer specimen comprising a tough adhesive and a hydrogel with one side bonded to a polyethylene terephthalate film (labelled in yellow). Polyacrylamide hydrogel (PAAm) and poly(hydroxyethyl methacrylate) hydrogel (PHEMA) were tested. The free arm of TA was stretched by an Instron machine. (b) Photos of a bilayer adhesion specimen before and after debonding. (c) Force-extension curves of the TA-PAAm and TA-PHEMA specimens, which end when a pre-existing crack started to propagate.

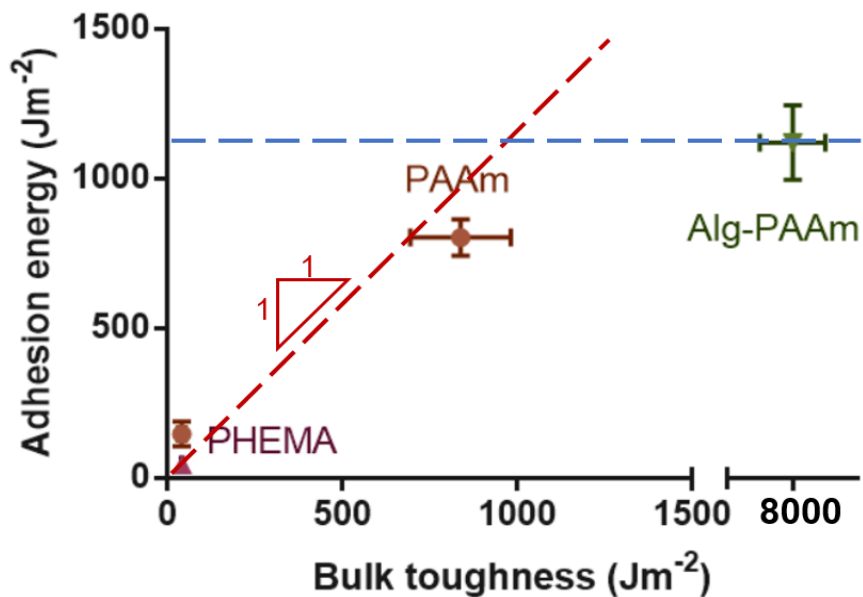


Figure B9 Correlation between adhesion energy and bulk toughness of the hydrogel to which

(Continued) the tough adhesive adheres. Polyhydroxyethyl methacrylate hydrogels (PHEMA), alginate-PAAm hydrogels (Alg-PAAm) and polyacrylamide hydrogels (PAAm) were tested. The PAAm hydrogels were prepared with 2 levels of bulk toughness. The red dashed line indicates that the adhesion energy equals to the bulk toughness, and the blue dashed line indicates the maximum adhesion energy obtained with the TA. Error bars show standard deviation; sample size $n=4$.

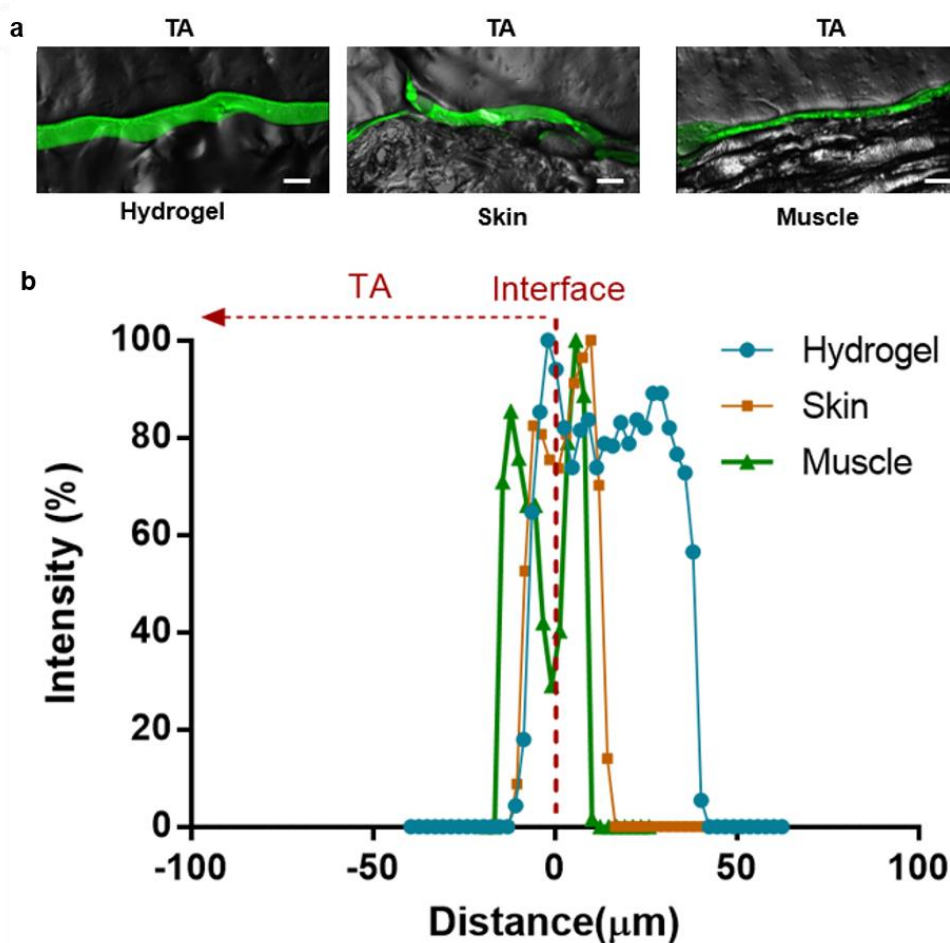


Figure B10 Bridging polymer at the interface. (a) Confocal images of cryosections of the tough adhesive (TA)-polyacrylamide hydrogel, TA-skin and TA-muscle interfaces. The images include bright field signals and green fluorescence from FITC-chitosan. (b) Fluorescent intensity profile across the interfaces, where the location of interface is marked with a red dashed line and the TA is positioned on the left side.

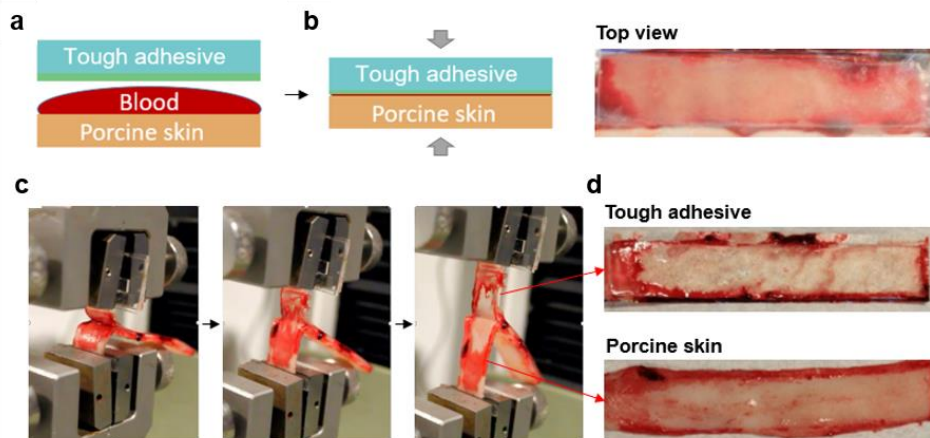


Figure B11 Adhesion formation with exposure to blood. (a) Effect of blood exposure was evaluated by covering the whole surface of porcine skin with whole blood, before the TA was applied. (b) The TA was compressed onto the skin to form adhesion. (c) The specimen was stretched with an Instron machine at a constant rate of 100 mm/min, while the side of the tough adhesive was glued to a rigid plastic film to concentrate energy dissipation at the interfacial crack. During the stretching, fibrillar structures were observed at the crack tip, indicative of large deformation and effective energy dissipation. (d) After debonding, the surfaces of the TA and skin was examined for debris of adhesive particles and blood residues.

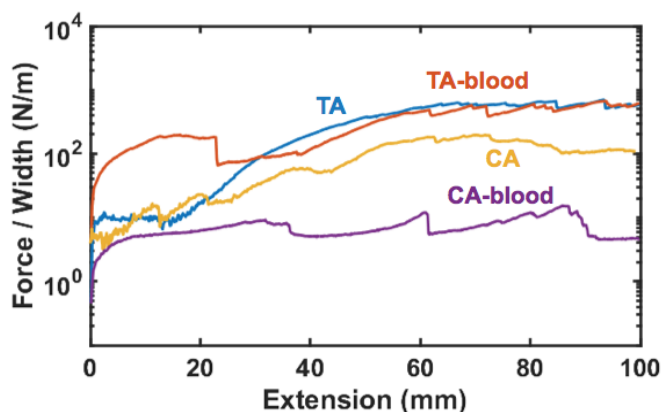


Figure B12 Force-extension curves of peeling tests. The adhesion energy was calculated based on the average value of force/width at the plateau region. The tough adhesive (TA) and cyanoacrylate (CA) were applied onto the porcine skin with and without initial exposure to blood on porcine skin surface.

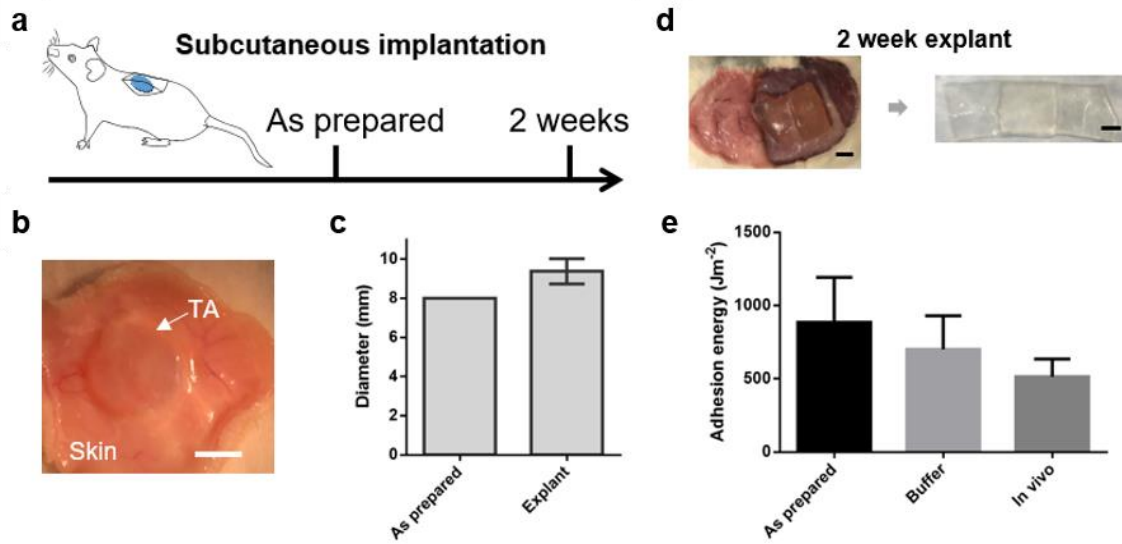


Figure B13 Adhesion was maintained over time in vivo. (a) Schematic and timeline for subcutaneous implantation in rats. (b) Digital photo of the implanted TA with surrounding tissues. Scale bar, 5mm. (c) Diameters of the implants before and after implantation. (d) Digital photos of a bilayer adhesion specimen that was implanted in vivo for 2 weeks. The specimen was formed with the adhesion between the TA and alginate-polyacrylamide hydrogel. Scale bar, 10mm. (e) Adhesion energy of the as-prepared specimens and those after being soaked in DMEM buffer or implanted in vivo for 2 weeks. Error bars show standard deviation; sample size $n=4$.

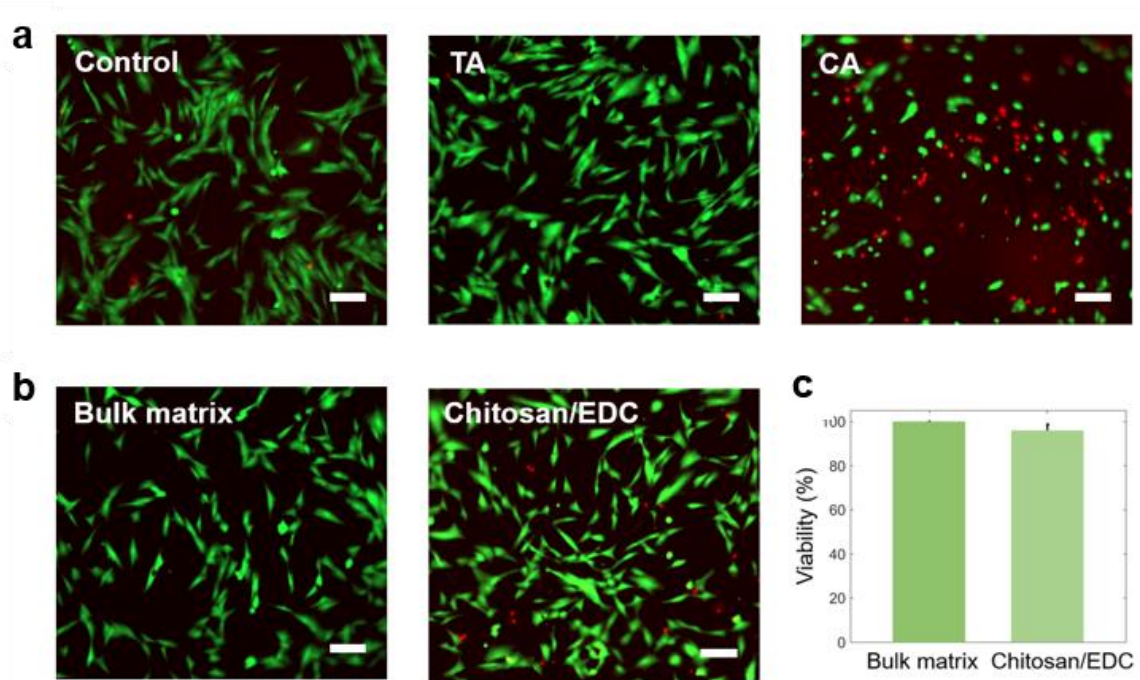


Figure B14 In vitro cell compatibility. (a) Fluorescent images of human dermal fibroblasts after 24-hour culture in conditioned mediums of DMEM control, TA, CA. (b) Fluorescent images of cells in conditioned mediums of bulk matrix, or the mixture of the bridging polymer chitosan and the coupling reagents EDC/NHS. Scale bar, 100 μ m. (c) Cell viability was compared between the conditions by quantifying the percentage of live cells (viability). Error bars show standard deviation; sample size n=5.

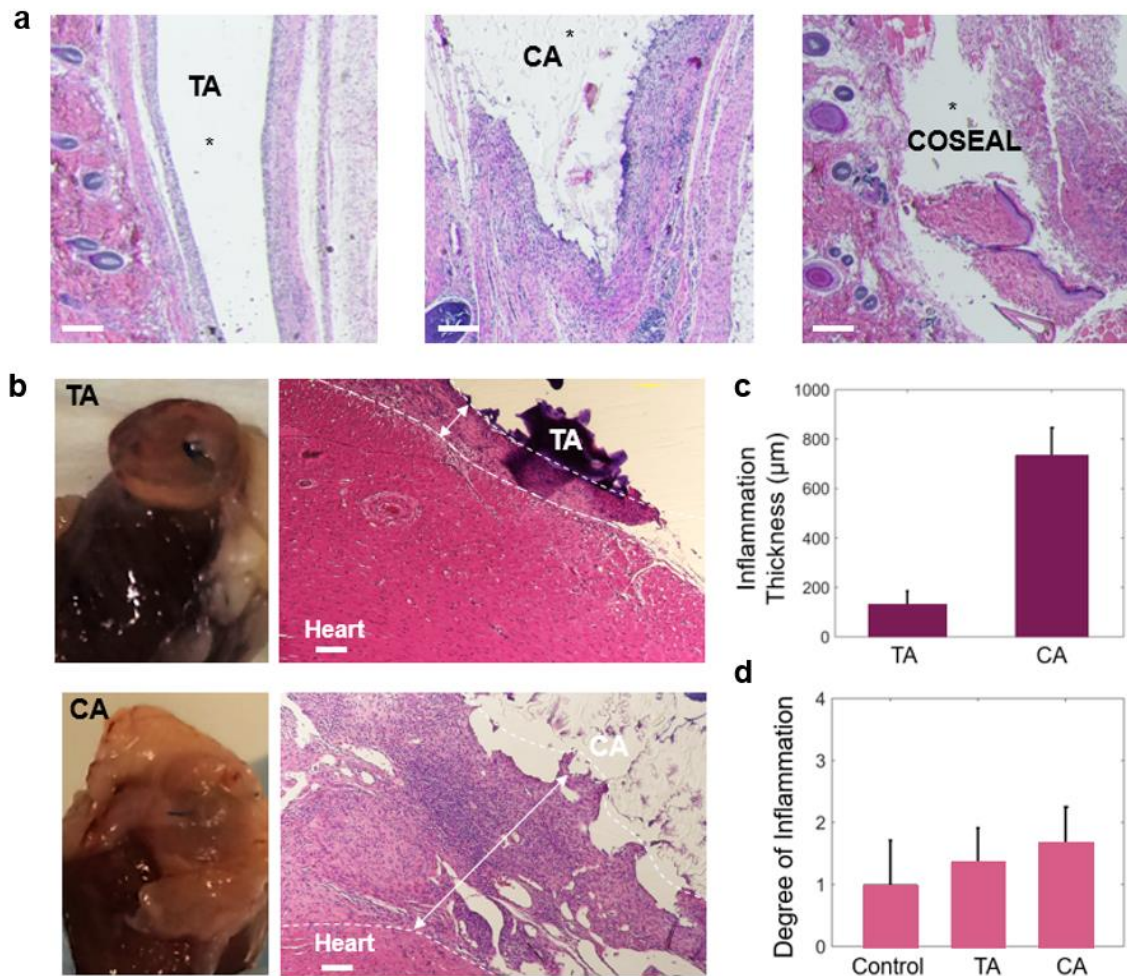


Figure B15 In vivo biocompatibility. (a) Histological sections of implants (labeled with asterisks) and surrounding tissues. TA, CA and COSEAL from Baxter were implanted into rats subcutaneously for 2 weeks. Scale bar, 200µm. (b) Images and histological sections of TA and CA attached onto the rat myocardium for 2 weeks. CA elicits more fibrosis than TA. Scale bar, 100µm. (c) Thickness of inflammatory region measured from histological sections. Error bars show standard deviation; sample size n=5. (d) Degree of inflammation was determined by a pathologist (blinded analysis) for all three conditions (0=normal, 1=very mild, 2=mild, 3=moderate, 4=severe, 5=very severe).

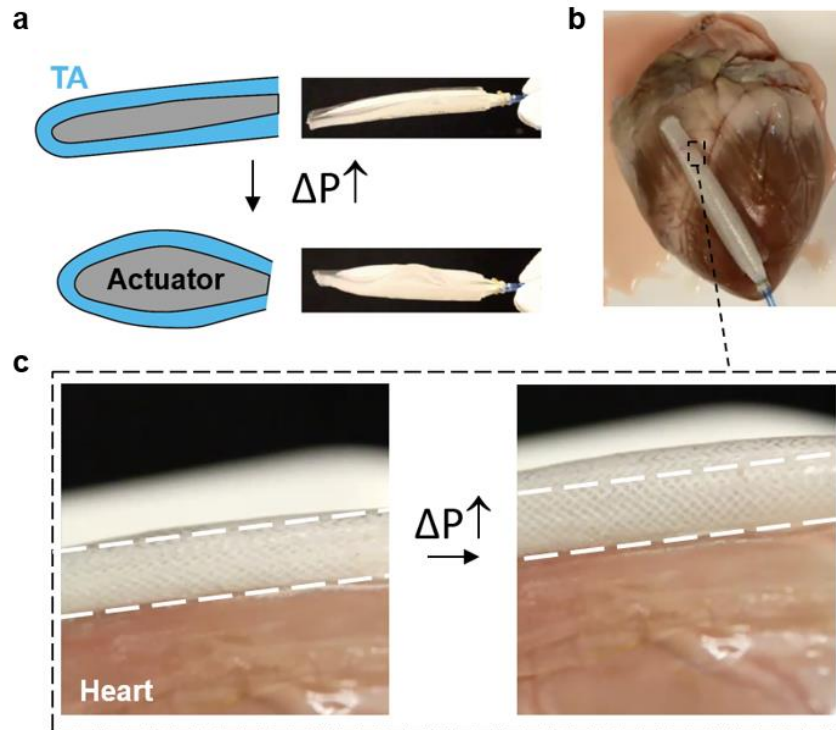


Figure B16 Encapsulation and attachment of soft actuators with TA onto myocardium surface. (a) An actuator was encapsulated with TA and functioned properly. (b) TA anchored the actuator onto a porcine heart. (c) TA accommodated the deformation of the attached actuators without debonding or rupture during actuation.

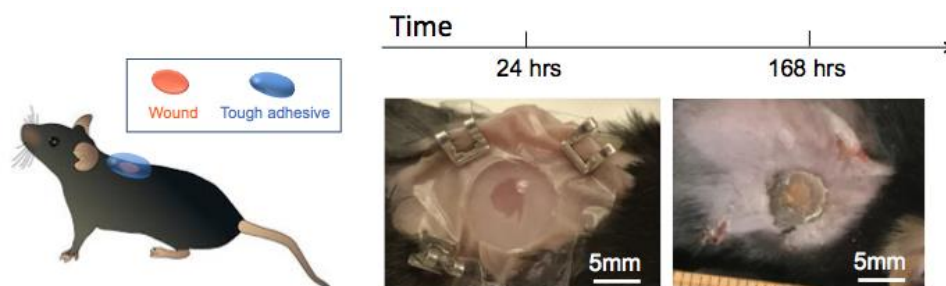


Figure B17 Skin wound dressing of tough adhesive. A 10mm disc of tough adhesive was attached on the dorsum of mice, where a skin wound of 4mm diameter was created with biopsy punch. The attachment of the tough adhesive dressing was monitored in 24 and 168 hours. Although the adhesive dried by 168 hours, the TA remained strongly adherent to the skin. Scale bar, 5mm.

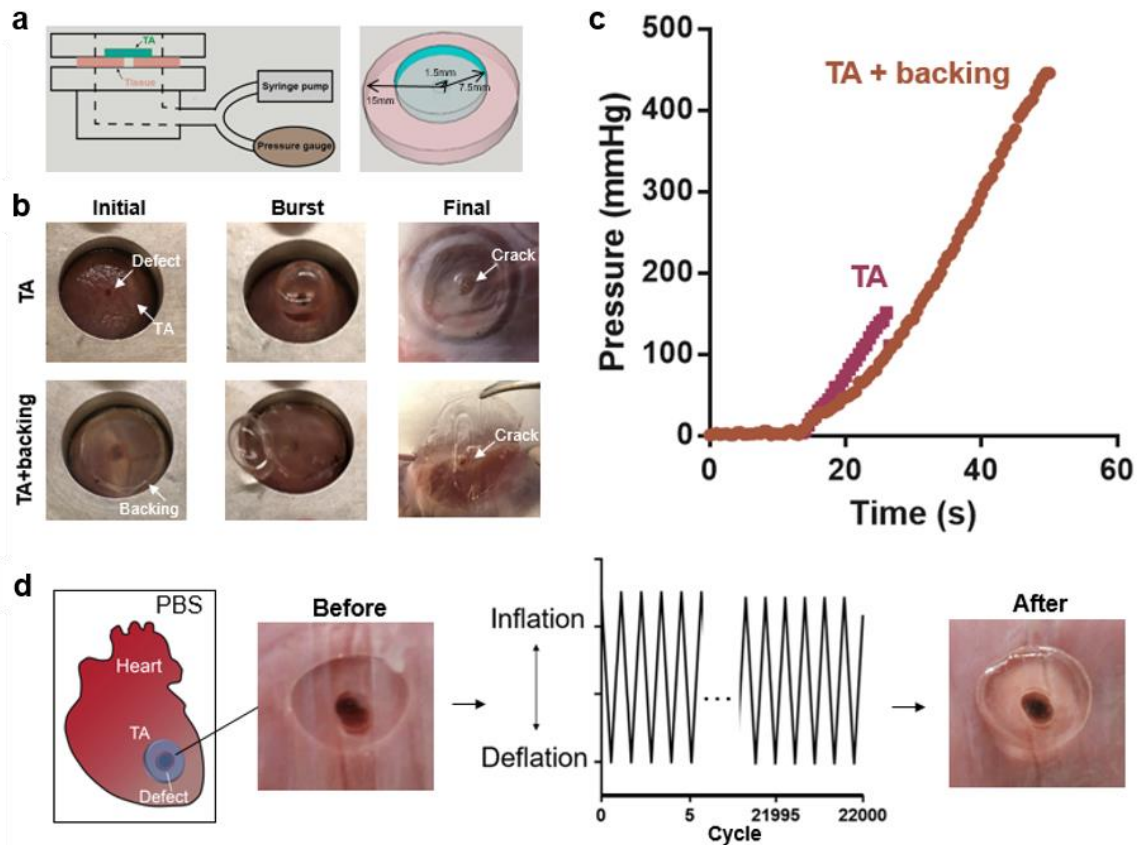


Figure B18 Performance of tough adhesive sealants. (a) Experimental setup for the burst pressure measurement. PBS was pumped into the specimen chamber under a constant flow rate of 2 mL/min, while the pressure was recorded with a pressure gauge. The dimensions of the TA sealant, defect hole and tissue specimen. (b) Images of the TA-myocardium specimen before and after burst. A rigid PET film was attached to the back of TA sealant. The pathway of crack propagation after burst indicated cohesive failure of the sealant without debonding. (c) Pressure-time curves of the TA sealant with and without backing, which end at the time point when a burst occurs. (d) Schematic and photos of the TA sealant before and after a long-term reliability tests. The repaired heart was inflated/deflated with pressurized air for 22,000 cycles while being immersed in PBS for 18 hours.

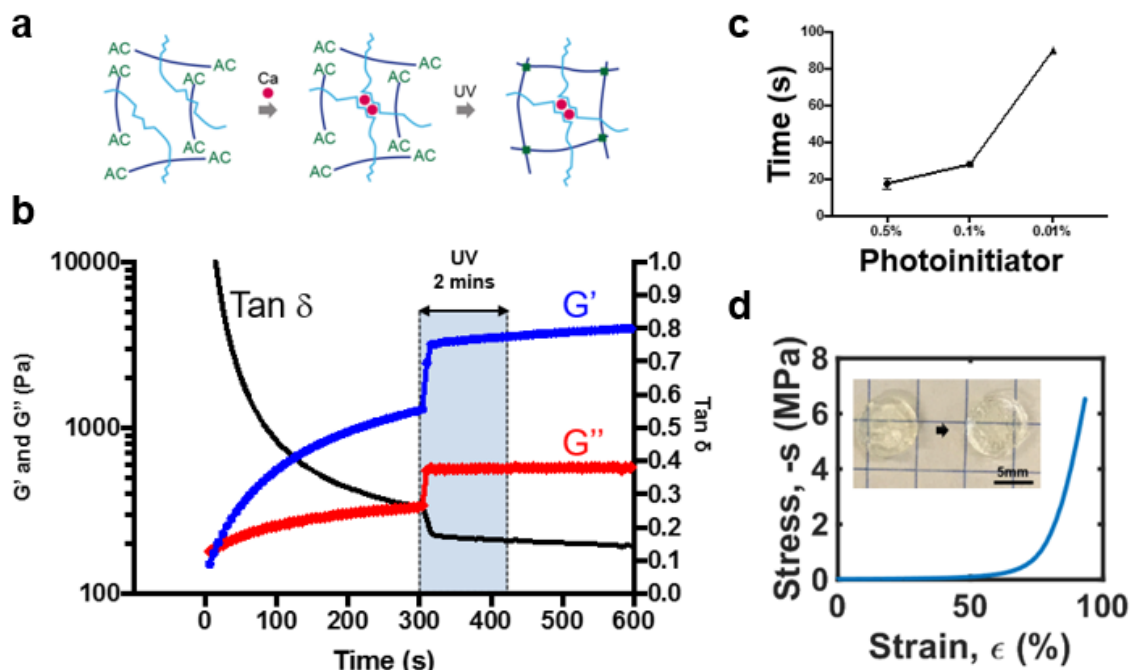


Figure B19 Gelation and compressive properties of injectable tough adhesives. UV-curable polyethylene glycol (PEG)-alginate hydrogels serve as the dissipative matrix for the injectable TAs. (a) Schematic of two-step gelation process of the injectable TA, in which the alginate (light blue lines) is cross-linked with calcium ions (red circles) and the PEG network (dark blue lines) is formed when the UV light triggers the cross-linking reaction between acrylate (AC) functional groups on PEG chains. (b) Kinetics of shear modulus (storage modulus G' and loss modulus G'') and loss angle ($\tan \delta$) versus time. (c) Effects of the photoinitiator concentration on the gelation time of the PEG network. (d) Compressive stress-strain curves of the injectable TA. The inset shows the photos of the materials before and after the compression test where the maximum compressive stress was 6.6 MPa. Sample size $n=3$.

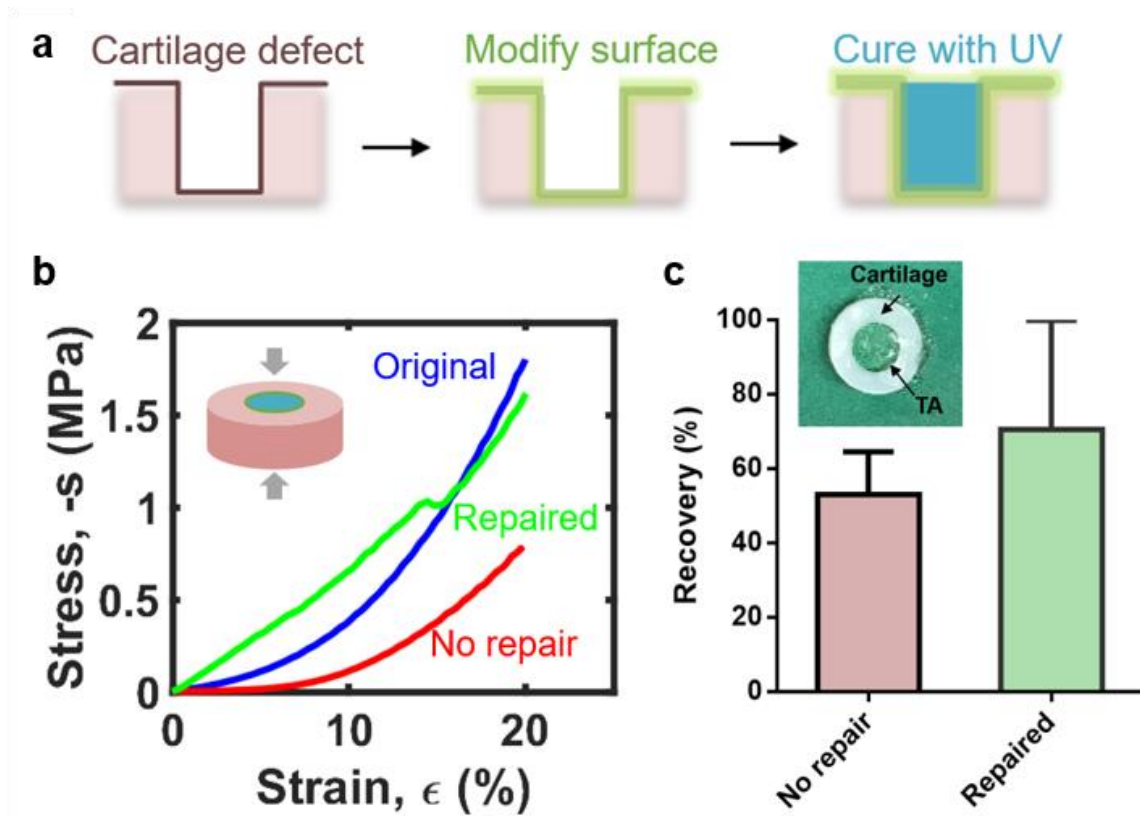


Figure B20 In vitro demonstration using an injectable TA to repair a defect in articular cartilage. (a) The site of application is treated with chitosan and EDC/sulfo-NHS for interfacial bridging, filled with pregel solutions and exposed immediately to UV for rapid gelation. (b) Compressive stress-strain curves of the cartilage explant before and after repair. (c) The recovery was evaluated by the ratio of stress levels at 20% strains. The inset is a photo of cartilage disc repaired with TA.

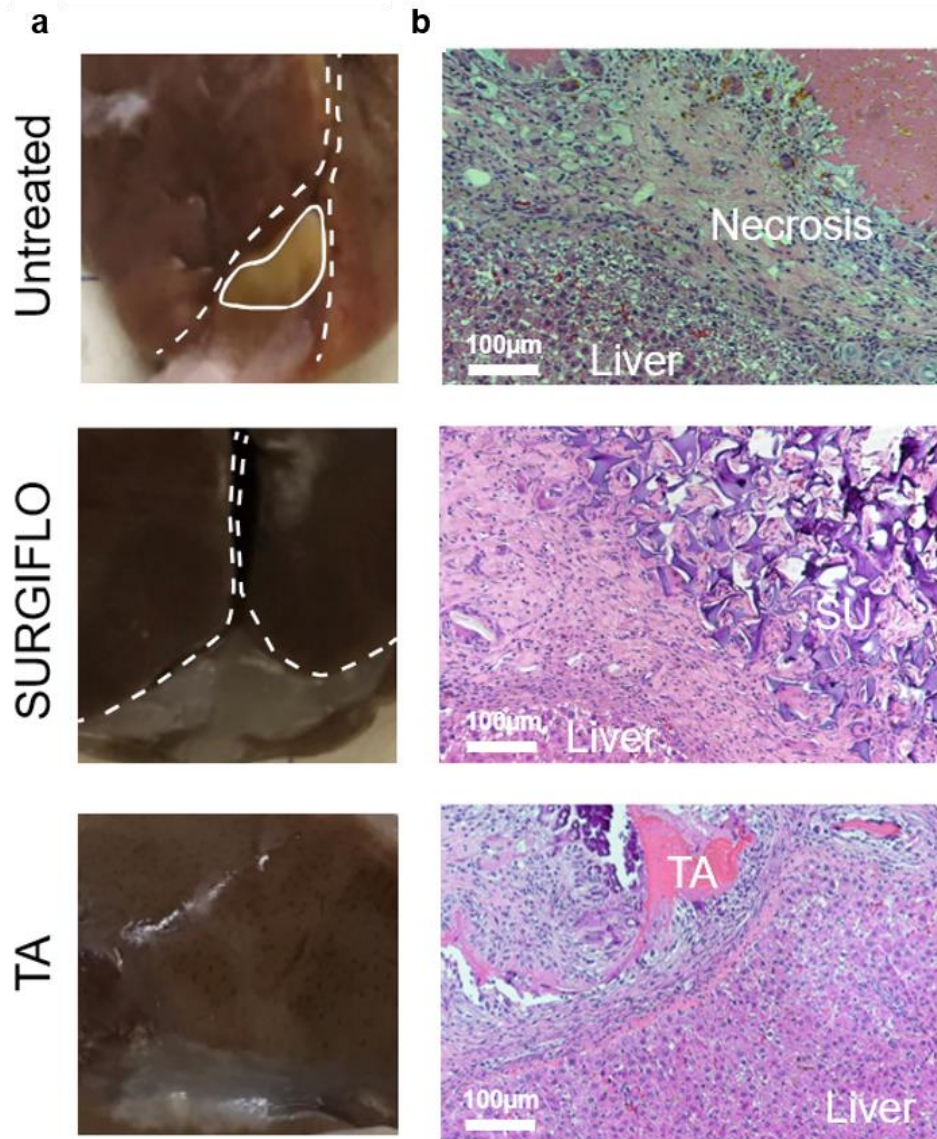


Figure B21 Digital photos of explanted livers and corresponding histological sections. (a) Digital photos of the livers explanted from the rats that were untreated, or treated with a commercial hemostat SURGIFLO and with tough adhesives (TA). The boundaries of multiple lobes of the livers that adhered to the lesion sites are marked with white dashed lines. The area of necrosis is marked with white solid lines. (b) Histological sections of the explanted livers and implants at the lesion sites.

Movies

Movie B1 3D construct of a tough adhesive. The tough adhesive consists of an adhesive surface containing FITC-chitosan in which fluorescent microspheres of 500nm diameter were immobilized.

Movie B2 Peeling adhesion test of a tough adhesive on porcine skin with blood exposure. The tough adhesive was applied on a piece of porcine skin that was first covered with blood, followed by peeling test.

Movie B3 In vivo adhesion test of tough adhesive. A ribbon of tough adhesive was applied to a beating porcine heart, followed by a peeling test in vivo.

Movie B4 Attachment of tough adhesive on skin. Two pieces of tough adhesives were applied to the epidermis of mice, and the adhesion was analyzed as the animal moved.

Movie B5 Burst pressure test of tough adhesive sealant. Tough adhesives with and without a plastic backing film were attached onto myocardium tissues and subject to pressurized saline till a burst occurred.

Movie B6 Tough adhesive as sealant under static and cyclic deformation. A piece of tough adhesive was used to seal a defect on a porcine heart, and prevented leakage during thousands cycles of heart inflation-deflation.

Appendix C. Supporting information for Chapter 4

Materials

All chemicals were purchased and used without further purification. Monomers for hydrogels included acrylamide (AAM; Sigma-Aldrich, A8887), 2-Hydroxyethyl methacrylate (HEMA; Sigma-Aldrich, 128635), N-isopropylacrylamide (NIPAM; Sigma-Aldrich, 415324), N,N-Dimethylacrylamide (DMA; Sigma-Aldrich, 274135), acrylic acid (AAc; Sigma-Aldrich, 147230) and [2-(Acryloyloxy)ethyl]trimethylammonium chloride solution (DMAEA; Sigma-Aldrich, 496146). To prepare alg-polyacrylamide tough hydrogels, ionically crosslinkable alginate biopolymer (FMC Biopolymer, Manugel GMB) was used and crosslinked with calcium sulfate slurry (calcium sulfate dihydrate; Sigma-Aldrich, c3771). N,N'-methylenebisacrylamide (MBAA; Sigma-Aldrich, M7279) was used as the covalent crosslinker. Ammonium persulfate (APS; Sigma-Aldrich, A9164), sodium persulfate (NaPS, Sigma-Aldrich, 216232) and α -Ketoglutaric acid (Sigma-Aldrich, 75890) were used as initiators for polymerization in neutral, alkaline, and acidic environments. N,N,N',N'-tetramethylethylenediamine (TEMED; Sigma-Aldrich, T7024) was used as crosslinking accelerator for APS and NaPS.

The polymers employed in the study include chitosan chains of four different molecular weights: $M_w > 375,000$ Da (Sigma-Aldrich, 419419), $M_w \sim 190,000$ - $310,000$ Da (Sigma-Aldrich, 448877), $M_w \sim 15,000$ Da (Polysciences, 21161-50) and $M_w \leq 3,000$ Da (Carbosynth, OC28900), poly(4-aminostyrene) (PAS, $M_w > 150,000$ Da; Polysciences, 02823-1), polyallylamine (PAA, $M_w \sim 58,000$ Da; Sigma-Aldrich, 283223), polyethylenimine, branched (PEI, $M_w \sim 25,000$ Da; Sigma-Aldrich, 408727), alginic acid sodium salt ($M_w \sim 120,000$ - $190,000$ Da, Sigma-Aldrich, 180947), and polyacrylamide (PAAM, $M_n \sim 150,000$; Sigma-Aldrich, 767379).

Methods

Preparation of hydrogels

Polyacrylamide hydrogels: 40.56 g acrylamide powder was first dissolved in 300 ml deionized water, and MBAA was added as covalent crosslinker (MBAA to acrylamide weight ratio is 0.0006:1). To prepare PAAM hydrogels of pH < 7, α -Ketoglutaric acid was used as UV initiator (α -Ketoglutaric acid to acrylamide weight ratio is 0.002:1). The pH of precursor solution was tuned by dripping HCl solution. The precursor solution was subsequently poured into a glass mold and covered with a 3-mm-thick glass plate, and exposed under UV irradiation (30W, 365nm curing UV light, McMaster-Carr) for one hour and set for hours to complete polymerization. To prepare PAAM hydrogels of pH \geq 7, APS or NaPS was used as initiator (APS to acrylamide weight ratio is 0.01:1; NaPS to acrylamide weight ratio is 0.007:1), in coupling with TEMED as crosslinking accelerator (TEMED to acrylamide weight ratio is 0.0028:1). We dripped NaOH to achieve a desired pH. The precursor solution was then poured into a glass mold and covered with a 3-mm-thick glass plate to complete polymerization.

PHEMA hydrogels: 46 ml HEMA was dissolved in 200 ml DI water. We sequentially added MBAA (MBAA to HEMA weight ratio is 0.00033:1), TEMED (TEMED to HEMA weight ratio is 0.002:1) and APS (APS to HEMA weight ratio is 0.0054:1) into the HEMA solution and mixed. The precursor solution was then poured into a glass mold and covered with a 3-mm-thick glass plate to complete polymerization.

PNIPAAm hydrogels: 21.52 g NIPAM powder was dissolved in 100 ml DI water. We sequentially added MBAA (MBAA to NIPAM weight ratio is 0.000377:1), TEMED (TEMED to NIPAM weight ratio is 0.0023:1) and APS (APS to NIPAM weight ratio is 0.006:1) into the NIPAM solution and mixed. The precursor solution was then poured into a glass mold and covered with a 3-mm-thick glass plate to complete polymerization.

PDMA hydrogels: 4.12 ml DMA was diluted in 20 ml DI water. We sequentially added 0.0031

g MBAA (MBAA to DMA weight ratio is 0.00078:1), TEMED (TEMED to DMA weight ratio is 0.003:1) and APS (APS to DMA weight ratio is 0.0067:1). The precursor solution was mixed and poured into a glass mold and covered with a 3-mm-thick glass plate to complete polymerization.

NaPAA hydrogels: 8.22 ml acrylic acid (AAc) was dissolved in 21.78 ml DI water. We sequentially added 0.004864 g MBAA (MBAA to AAc weight ratio is 0.00056:1) and 0.009 g α -Ketoglutaric acid (α -Ketoglutaric acid to AAc weight ratio is 0.001:1). We added NaOH to tune the pH of the solution to be neutral. The precursor solution was mixed, poured into a glass mold, and covered with a 3-mm-thick glass plate, exposed under UV irradiation for one hour and set for hours to complete polymerization.

PDMAEA-Q hydrogels: 16 ml DMAEA was dissolved in 14 ml DI water. We added NaOH to tune the pH of the solution to be neutral. We sequentially added MBAA (MBAA to DMAEA weight ratio is 0.0017:1) and APS (APS to DMAEA weight ratio is 0.0027:1). The precursor solution was then poured into a glass mold and covered with a 3-mm-thick glass plate to complete polymerization.

Alg-PAAM tough hydrogels: 40.56 g acrylamide powder and 6.78 g alginate powder were dissolved together in 300 ml deionized water. We then sequentially added MBAA (MBAA to acrylamide weight ratio is 0.0006:1) and TEMED (TEMED to acrylamide weight ratio is 0.0028:1). The solution was mixed and degassed. Next, we added APS (APS to acrylamide weight ratio is 0.01:1) as initiator and calcium sulfate slurry as ionic crosslinker (CaSO_4 to acrylamide weight ratio is 0.022:1) into the solution. To prevent fast gelation of alginate, the precursor solution was quickly mixed and immediately poured into a glass mold and covered with a 3-mm-thick glass plate to complete polymerization.

Preparation of stitching polymer solutions

Chitosan solution: 4-Morpholineethanesulfonic acid (MES hydrate; Sigma-Aldrich, M8250) was used to prepare the acidic buffer solution. We first prepared MES buffer solution by

dissolving 0.976 g MES hydrate powder in the 50 ml DI water, and adjusted the pH to 4.5 by dripping NaOH with a pH meter (Mettler Toledo SevenEasy™ Series Meters). We then added 1 g chitosan powder (Mw ~ 190,000-310,000 Da) into the buffer solution, and sufficiently stirred with a magnetic stirring bar until the chitosan was completely dissolved. The final pH of solution was about 5.

PAS solution: We prepared the MES buffer solution as described above and adjusted the pH to 1 by dripping HCl with the pH meter. We then added 1 wt% PAS into the buffer solution and vigorously mixed. Subsequently, we sonicated the PAS solution in an ultrasonic bath (Branson Ultrasonics) with constant temperature of 48 °C overnight. After the PAS was completely dissolved, the solution was clear with a deep yellow color. We re-adjusted the pH of solution back to 4.

All other polymer solutions (PAA, PEI, alginate and PAAM) were prepared with 2 wt% polymer concentration in either MES buffer solution or water.

Experimental procedure of bonding. The prepared polymer solution was directly spread on the surface of an adherend with a thickness of ~500 μm, calculated by dividing the prescribed volume with the area of the surface. A piece of hydrogel was immediately placed on top. The bilayer was compressed with strain d/L of 7-15 % by customized glass molds. The whole sample was then sealed in a plastic bag to prevent dehydration. The weight of bilayer was measured after 24 hours and showed only 0.2 wt% difference, indicating negligible water loss during the procedure.

Surface modification of silicone elastomers. The surfaces of silicone elastomers (PDMS, Sylgard 184, and Ecoflex, Smooth-on) were thoroughly cleaned with ethanol and deionized water and dried at room temperature. Following the protocol from ref. [74] (Figure C11), the silicone elastomer was soaked in the benzophenone solution (Sigma-Aldrich, B9300) (10 wt% in

ethanol) for 10 min to allow benzophenone to adsorb on the surface. The surface was then dried again through an air gun. Next, we placed the elastomer in a mold of the same size, poured an acrylic acid solution (2 M) onto the elastomer, and covered it with a 3-mm-thick glass plate. We subsequently polymerized the acrylic acid under UV irradiation (30 W 365 nm curing UV light, McMaster-Carr) for one hour. The surface adsorbed benzophenone was excited and would abstract a hydrogen from the surrounding unreactive C-H bonds on the surface of the elastomer, resulting in surface-initiated radicals. The acrylic acid monomers were initiated from the surface, and propagated to grow polymer chains, giving rise to carboxylic acid-modified surface.

Oxygen plasma treatment. Glass and aluminum were oxygen plasma treated before use. Briefly, glass and aluminum sheets were thoroughly cleaned sequentially with acetone, deionized water, ethanol and isopropyl alcohol, and completely dried thereafter. The cleaned samples were subsequently treated by oxygen plasma (SPI Supplies, Plasma Prep II) at an O₂ pressure of 18 psi, vacuum pressure of 275 mTorr, and radio frequency (RF) power of 80 W for 120 s. The adhesion was performed immediately after the treatment.

Mechanical tests

Bilayer adhesion tests. All tests were conducted in open air and at room temperature. The preparation and procedure are illustrated in the Figure C5. A VHB liner made of polyethylene (PE) was directly used as the stiff backing layer to restrict the deformation of the VHB and the hydrogel beneath it. The bilayer tests were performed on an Instron machine (Instron 3342) with 50 N load cell. The hydrogel was fixed on one grip, and the hydrogel-elastomer bilayer was fixed on the other grip. The loading rate was fixed at 0.2 mm/s. During the tests, the force-stretch curves were recorded, and the critical force and stretch of debonding were identified through a digital camera. The adhesion energy was calculated using formula $G = P(\lambda-1)-U_s(\lambda)$ [99], where P and λ are the critical force per unit width (the force divided by the width of the

sample in the undeformed state) and critical stretch for debonding, $U_s(\lambda)$ is the strain energy stored in the hydrogel divided by the area of the hydrogel in the undeformed state, i.e. the area under the recorded force-stretch curve with stretch from 1 to λ . The typical force-displacement curves are shown in the Figure C5(d).

90-degree peeling adhesion tests. All tests were conducted in open air and at room temperature. The preparation and procedure are illustrated in the Figure C6. 90-degree peeling tests were conducted on an Instron machine (Instron 5966) with a 500 N load cell and a 90-degree peeling apparatus. All adherends were fixed on a moving platform, while the hydrogel was glued with a stiff polyester film of thickness 100 μm (clear polyester film, McMaster-Carr) with Krazy glue, and fixed to an upper grip. For fixing the VHB elastomer, the VHB elastomer was directly attached on a rigid acrylic plate and mounted on the moving platform. For fixing a mica, the mica was glued on a rigid acrylic plate with Krazy glue and mounted on the moving platform. For fixing a silicone elastomer, we first glued the silicone elastomer on a SBR rubber (Economical Abrasion-Resistant SBR Rubber, McMaster) with a commercially available silicone glue (Sil-Poxy, silicone adhesive, Smooth-on), and then glued the SBR rubber on a rigid acrylic plate with Krazy glue. The entire three layers were mounted on the moving platform. For other adherends, we directly mounted them on the moving platform. The peeling rate was fixed at 0.2 mm/s. We recorded the peeling force as a function of displacement. The adhesion energy was calculated as the average force at plateau divided by the width of the sample.

Pure shear tests for measuring the fracture energy of hydrogels. All samples were tested individually on an Instron testing machine (Instron 5966) with a 500 N load cell. The loading rate was fixed at 0.2 mm/s. For each test, two samples of the same hydrogel with dimensions $50 \times 10 \times 1.5 \text{ mm}^3$ ($90 \times 10 \times 1.5 \text{ mm}^3$ for PAAM hydrogels) were made: one was precut by a crack of 20 mm, and the other was uncut. The uncut sample was used to measure the

stress-stretch curve. In the undeformed state, the height of the sample was H ; after stretch, the height became λH . We plotted the nominal stress (the force divided by the cross-sectional area of the sample in the undeformed state) as a function of the stretch λ . The area beneath the stress-stretch curve gave the strain energy density stored in the hydrogel, $W(\lambda)$. The pre-cut sample was used to measure the critical stretch λ_c , where the initial crack turned into a running crack. The fracture energy was calculated as $\Gamma = W(\lambda_c)H$, ref.[108, 259].

Fabrication of iron-polyacrylate-PAAM hydrogel. The procedure is illustrated in the Figure C10. Briefly, a PAAM hydrogel was first bonded on a VHB elastomer using chitosan solution. The sample was immersed in a precursor composed of 2 M AAm, 0.4 M or 0.3 M AAc, and 0.004 M α -ketoglutaric acid in a petri dish for one day, so that the precursor had sufficient time to diffuse into the PAAM hydrogel. The petri dish with the immersed sample was covered with a polyethylene film and polymerized under UV irradiation for 2 hours. The polyethylene film prevented the oxygen inhibition of the polymerization. After polymerization, the precursor became PAAM-co-PAAc copolymers, which interpenetrated with the PAAM network. We then took the sample out and immersed in a 0.06 M FeCl_3 reservoir for two days. The Fe^{3+} ions diffused into the PAAM hydrogel and crosslinked the PAAM-co-PAAc copolymers by forming coordination complex with the carboxyl groups of the acrylic acid. The hydrogel turned dark brown after the crosslinking process. The sample was subsequently immersed in DI water for three days to remove the excess Fe^{3+} ions from the hydrogel.

Fabrication and test of wearable mechano-electrical transducer. A PAAM hydrogel containing 1 M sodium chloride was bonded on the surface of an VHB elastomer with chitosan solution (concentration was 2 wt%). We subsequently used a razor blade to cut the bonded hydrogel into two strips. The two stripes of hydrogel were attached initially. The structure, called *transducer* here, was connected in a circuit by placing two pieces of aluminum foils in contact

with the hydrogels at two ends. We applied an alternating voltage of amplitude 1 V and frequency 1 kHz through a signal generator (KEYSIGHT, 33500B), and recorded the electric current via a multi-meter (Fluke 8846A). As a voltage was applied, the electric current was measured about 375 μA . When we mechanically stretched the transducer to about double the initial length, the two hydrogels instantly separated but remained firmly bonded on the VHB substrate, and the electric current suddenly dropped to 25 μA . After about 20 seconds, we released the transducer to its original length, the two hydrogels attached again, and the electric current restored to 375 μA .

Transdermal patch bonded in vivo on a rat. This study, involving Female Sprague Dawley rats (200-275 g) was carried out in accordance with the Institute for Animal Care and Use Committee, Harvard University. In brief, the rat was anesthetized by inhalation of isoflurane (3-4 %), and the dorsum was shaved and disinfected using 70 % ethanol. An elastomer coated hydrogel patch (EHP) was fabricated by bonding a VHB elastomer with thickness of 0.5 mm on a piece of PAAM hydrogel using chitosan solution. The EHP of dimensions 1 cm \times 1 cm \times 2 mm was bonded in vivo on the skin of the rat using chitosan solution, and gently pressed for 2 minutes. A pure hydrogel patch was also included as a control. The rat was then allowed to fully recover from anesthesia on a heating pad. Before returning to the cage, both patches on the skin were inspected and confirmed firmly adhered despite dynamic movement of the rat. After 12 hours, we examined both patches in terms of the softness, remaining water, and adhesion.

Measurement of the viscosity of chitosan solution. We measured the viscosity of chitosan solution of 2 wt% concentration using a rheometer (TA Instruments Discovery HR-3 Hybrid Rheometer) with a cone and plate geometry at temperature of 25 $^{\circ}\text{C}$. Flow sweep was used with shear rates ranging from 0.01 to 100 s^{-1} .

Underwater adhesion. We first attached a VHB elastomer sheet on an acrylic sheet, and then glued an alg-PAAM hydrogel on the VHB sheet using chitosan solution. Another VHB elastomer sheet was attached at the bottom of a petri dish and immersed in the water. We used a syringe to directly inject a chitosan solution of 2 wt% concentration through the water onto the VHB surface. We immediately covered the alg-PAAM hydrogel on the VHB surface under the water and applied gentle pressure. After one hour, we took the hydrogel-VHB bilayer out. The VHB liner was peeled off so that the VHB elastomer can adhere with various weights made of stainless steel.

Study chitosan diffusion using confocal microscopy

Fluorescein isothiocyanate (FITC) was purchased from ThermoFisher Scientific, and the fluorescein isothiocyanate-labeled chitosan (FITC-chitosan) was synthesized according to the previously reported protocol [262]. The FITC-chitosan was dissolved in the 4-Morpholineethanesulfonic acid (MES) buffer solution (0.1 wt%) with pH adjusted to 5. The solution was covered from light. The polyacrylamide hydrogel and the VHB elastomer were subsequently soaked in the FITC-chitosan solution for one day. The samples were imaged with a confocal fluorescence microscopy (Zeiss LSM710), with the excitation wavelength set to 490 nm and emission wavelength 525 nm. The confocal images were recorded, and three-dimensional constructions were built for analysis. The results showed that the FITC-chitosan chains can diffuse into the hydrogel and form a homogeneous phase, but not into the VHB elastomer (Figure C4).

Chemistry of bonding and stitching

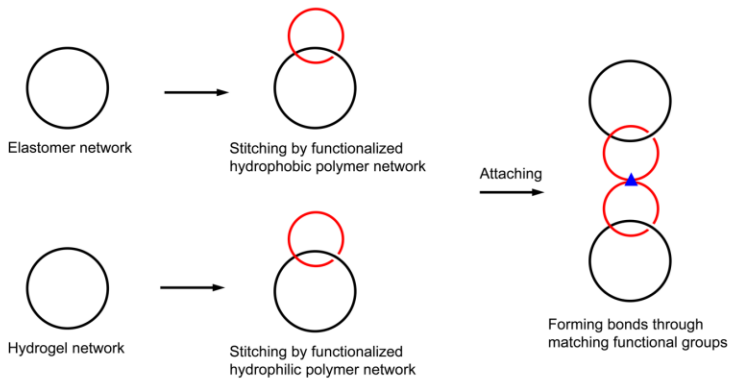
Chitosan chains bear amine groups of $pK_a \sim 6.5$. The dissociation of charged amine groups, $[NH_3^+] \rightleftharpoons [NH_2] + [H^+]$, has an equilibrium constant $K_a = [NH_2][H^+]/[NH_3^+]$. By definition, $pK_a = -\log[K_a]$, and $pH = -\log[H^+]$. The ratio between NH_2 and the charged NH_3^+ , is

therefore $[\text{NH}_2]/[\text{NH}_3^+] = \exp(\text{pH}-\text{pKa})$. When $\text{pH} < \text{pKa} = 6.5$, $[\text{NH}_2] < [\text{NH}_3^+]$, and the chitosan chains dissolve in water as a polyelectrolyte. When $\text{pH} > 6.5$, $[\text{NH}_2] > [\text{NH}_3^+]$, and the $\text{NH}_2\text{-OH}$ hydrogen bonds promote the chitosan chains to form a network [100]. VHB elastomers have carboxylic acid groups of $\text{pKa} \sim 4.5$ (ref.[267]) on the surface (Figure C2). The dissociation of charged carboxylic groups, $[\text{COOH}] \rightleftharpoons [\text{COO}^-] + [\text{H}^+]$, has an equilibrium constant $K_a = [\text{COO}^-][\text{H}^+]/[\text{COOH}]$. By the same definition, the ratio between the dissociated COO^- and COOH is $[\text{COO}^-]/[\text{COOH}] = \exp(\text{pH}-\text{pKa})$. When $\text{pH} < 4.5$, $[\text{COO}^-] < [\text{COOH}]$, the surface is more neutral. When $\text{pH} > 4.5$, $[\text{COO}^-] > [\text{COOH}]$, the surface is more negatively charged. To form imine bonds, the optimal pH is around 4 (ref.[247]). To form chitosan network, the pH should be above 6.5. We prepare chitosan solution of $\text{pH} = 5$.

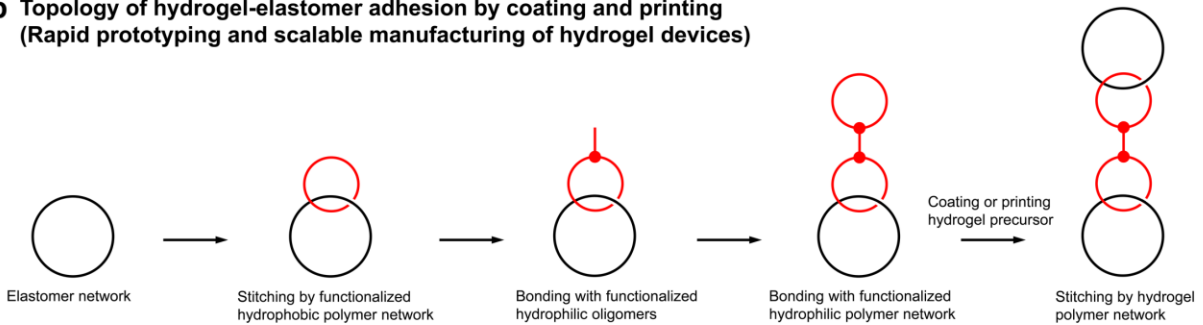
When the chitosan solution ($\text{pH} = 5$) is spread on the surface of the VHB elastomer, some chitosan chains form imine bonds and ionic bonds with VHB, and other chitosan chains remain mobile. When the PAAM hydrogel ($\text{pH} = 7$) is pressed onto the chitosan-coated VHB, the mobile chitosan chains diffuse into the PAAM hydrogel and, in response to the pH in the hydrogel, form a chitosan network that stitches with the PAAM network. After reaching thermodynamic equilibrium, the final pH at the interface is close to 7. The amount of ionic bonds is greatly reduced due to the neutralization of amines on chitosan chains, but the imines remain stable. In addition, also note that the bond energy of one ionic pair in water is $\sim kT$ at room temperature [125, 268], much weaker than that of an imine bond ($\sim 210 kT$) [201] (kT is the temperature in the unit of energy). Therefore, the interfacial bonds are dominantly contributed by imine bonds. The chemistry of bonds and stitches using poly(4-aminostyrene) is similar (Figure C8).

Figures

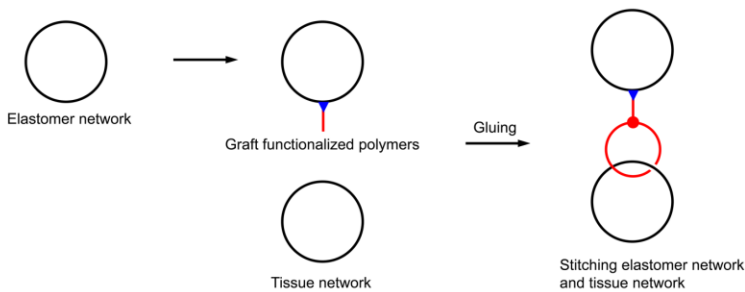
a Topology of hydrogel-elastomer adhesion by attaching (Facile fabrication of hydrogel devices)



b Topology of hydrogel-elastomer adhesion by coating and printing (Rapid prototyping and scalable manufacturing of hydrogel devices)



c Topology of tissue-elastomer adhesion by gluing (Medical implants)



d Topology of metal-hydrogel-tissue adhesion by gluing (Wearable electronics)

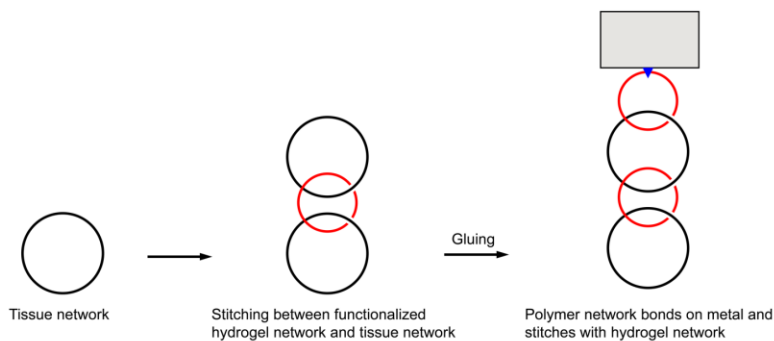


Figure C1 Some other topologies proposed for potential applications. (a) A topology of

(Continued) hydrogel-elastomer adhesion by attaching. (b) A topology of hydrogel-elastomer adhesion by coating and printing. (c) A topology of tissue-elastomer adhesion by gluing. (d) A topology of metal-hydrogel-tissue adhesion by gluing.

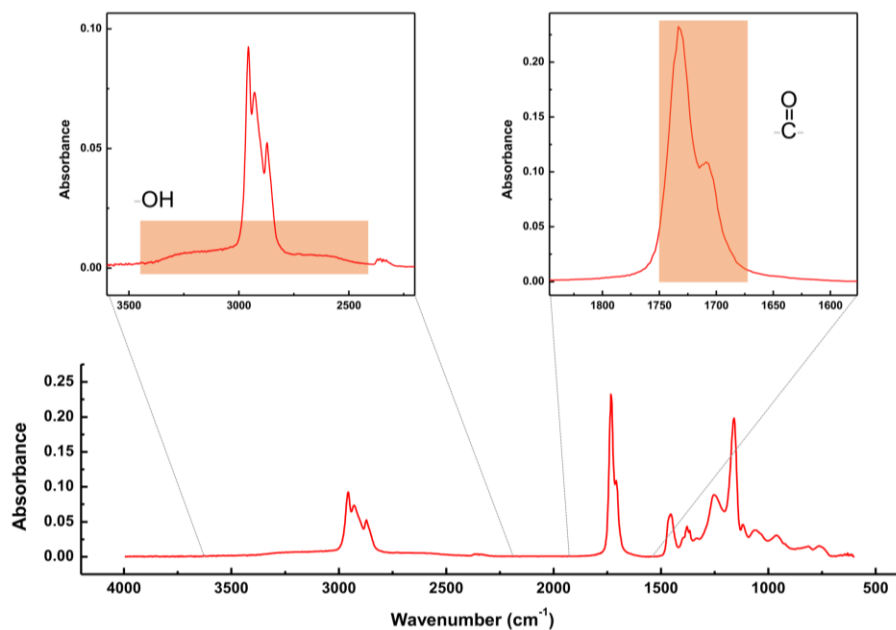


Figure C2 The chemistry of the VHB elastomer. The Fourier-transform infrared spectroscopy (FTIR) shows the VHB elastomer has a sharp peak in the range of 1700-1750 cm⁻¹ and a broad but shallow peak in the range of 2500-3500 cm⁻¹. These peaks correspond to the C=O stretch and O-H stretch, respectively, and indicate the presence of ketone and carboxylic acid groups.

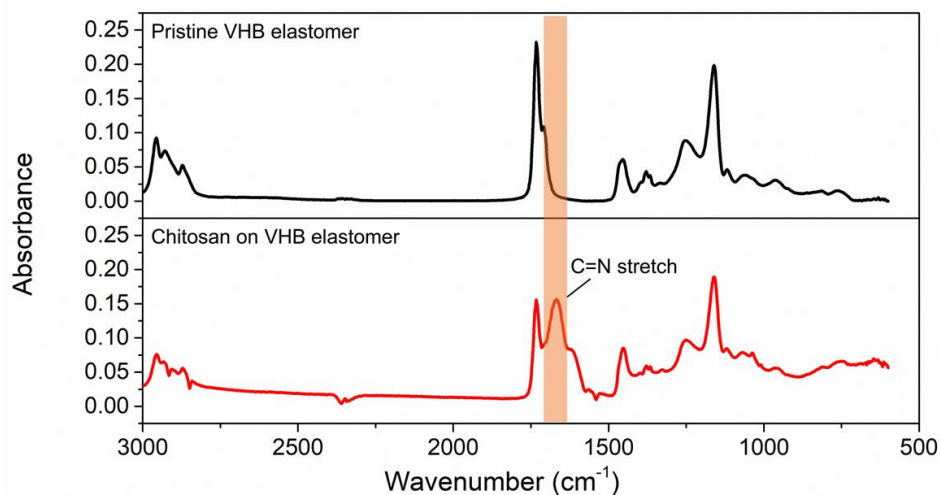


Figure C3 Formation of imine bonds. The FTIR spectrum of chitosan bonded on an VHB elastomer shows a peak in the range of 1640-1690 cm⁻¹, which corresponds to the imine C=N stretch. In contrast, the FTIR spectrum of the pristine VHB elastomer does not show this peak.

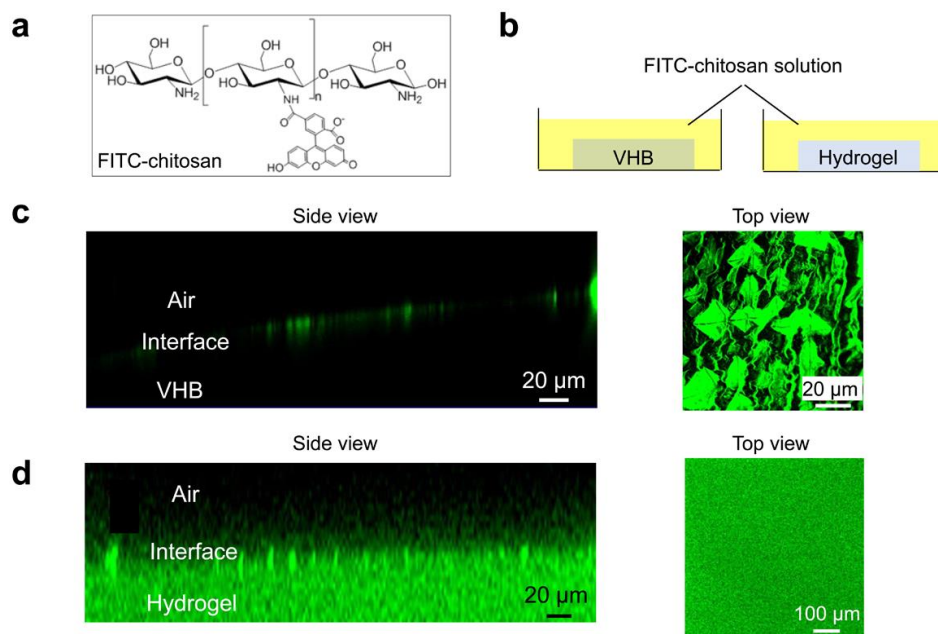


Figure C4 Chitosan chains can diffuse into the PAAM hydrogel, but not into the VHB elastomer. (a) The molecular structure of the FITC-chitosan. (b) A piece of PAAM hydrogel and a piece of VHB are soaked in the FITC-chitosan solution for one day before confocal imaging. (c) Confocal image shows that the FITC-chitosan chains cannot diffuse into the VHB elastomer (side view), but localize on the surface and form an inhomogeneous phase (top view). (d) Confocal image shows that the FITC-chitosan chains can diffuse into the hydrogel (side view), and form a homogeneous phase (top view).

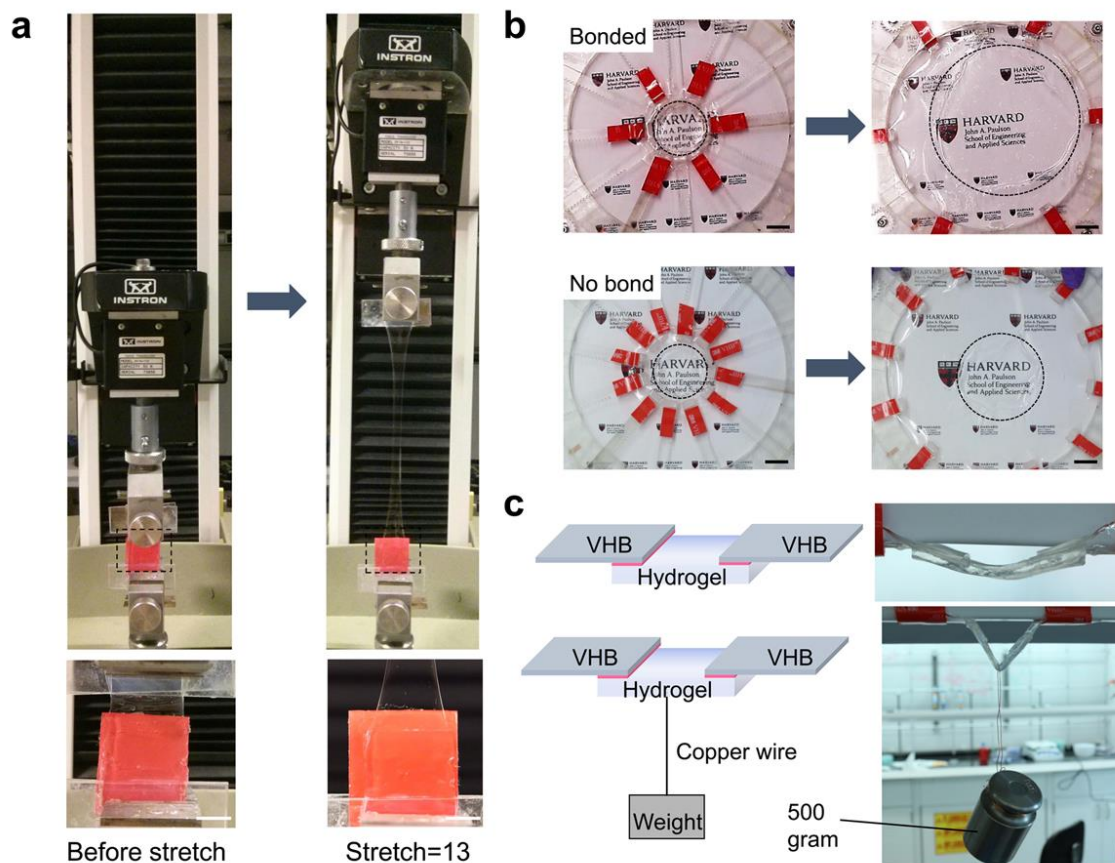


Figure C5 Mechanical robustness of chitosan-bonded PAAM hydrogel and VHB elastomer. (a) Uniaxial stretch of a PAAM hydrogel bonded on a VHB elastomer. The hydrogel is stretched as large as 13 times its initial length without debonding. The scale bar is 1 cm. (b) Top: When a PAAM hydrogel is bonded on a VHB elastomer, the PAAM hydrogel remains strong bonded when the VHB elastomer is equi-biaxially stretched with area change as large as 16 times. Bottom: if no bonding is created between the PAAM hydrogel and the VHB elastomer, the PAAM hydrogel readily detaches from the VHB elastomer at small equi-biaxial stretch of the VHB elastomer. The black dash circle delineates the boundary of the hydrogel. The scale bar is 2 cm. (c) A hybrid of alg-PAAM hydrogel and VHB elastomer can at least sustain a weight of 500 g.

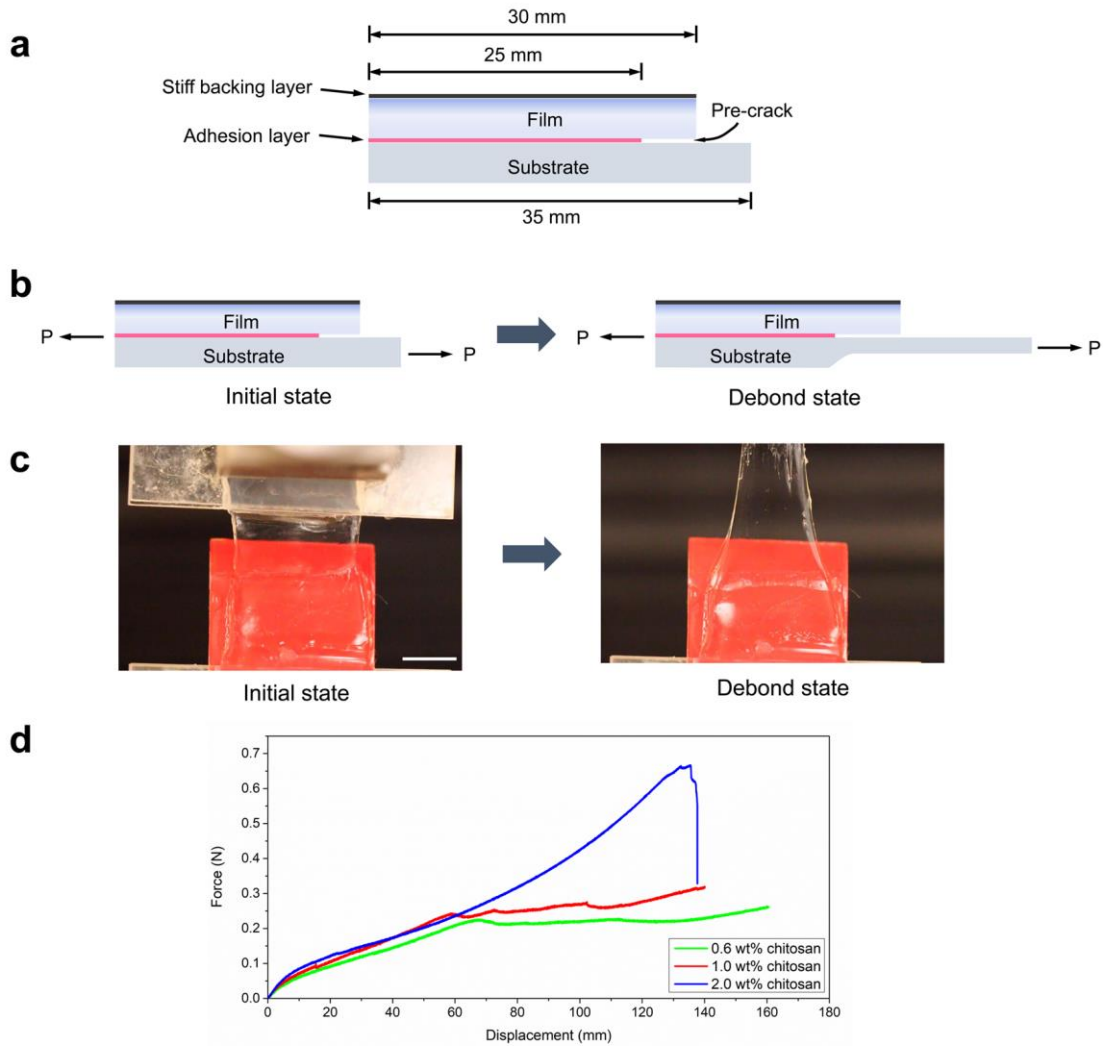


Figure C6 The bilayer adhesion test. (a) Dimensions of a hydrogel-adherend bilayer. (b) Schematics of the bilayer adhesion test. (c) Photos of the bilayer adhesion test. The scale bar is 1 cm. (d) Representative force-displacement curves of the bilayer adhesion test.

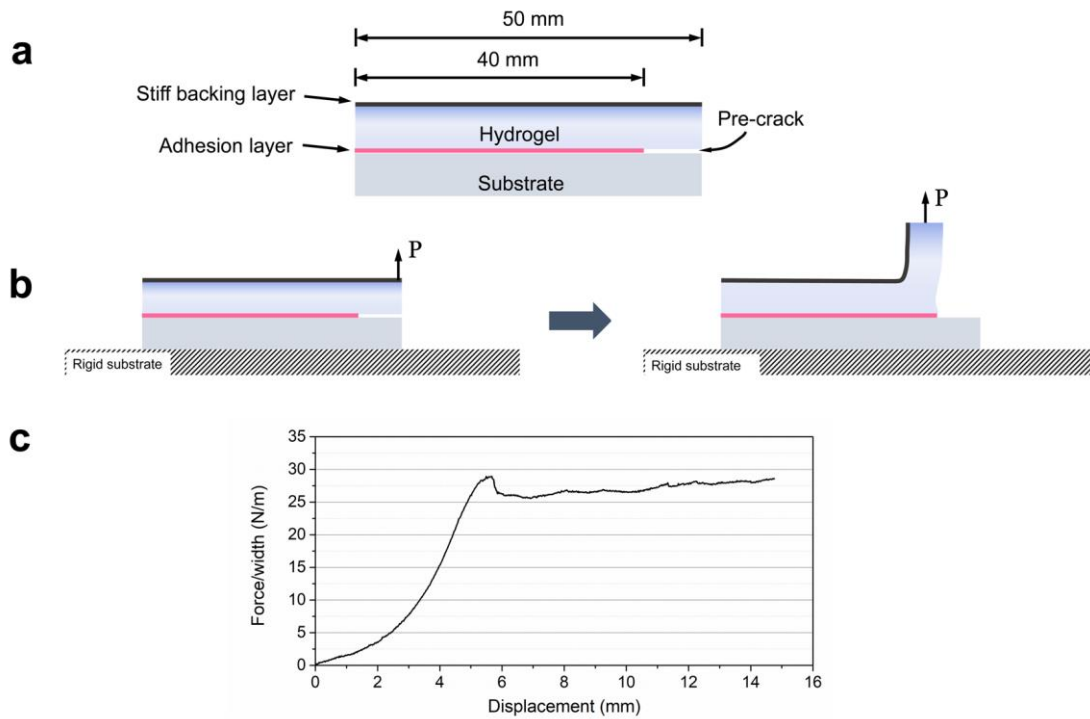


Figure C7 The 90-degree peeling test. (a) Dimensions of a hydrogel-adherend bilayer. (b) Schematics of the 90-degree peeling test. (c) A representative force-displacement curve of the 90-degree peeling test. The adhesion energy is calculated as the average peeling force at plateau divided by the width of the bilayer.

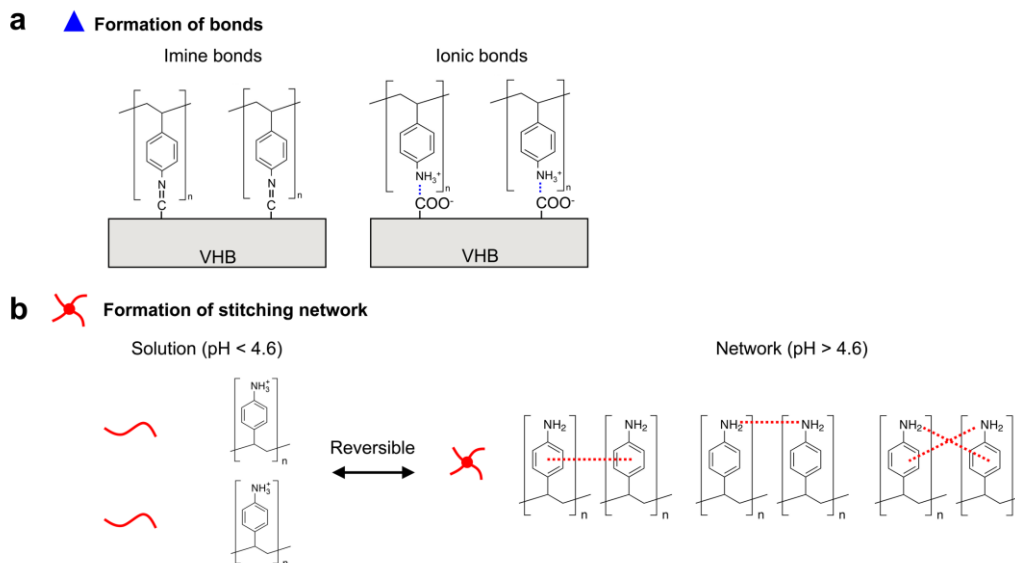


Figure C8 Chemistry of bonds and stitches with poly(4-aminostyrene). (a) Poly(4-aminostyrene) chains form imine bonds and ionic bonds on the VHB elastomer. (b) Poly(4-aminostyrene) chains dissolve in water when pH < 4.6, and crosslink into a network through π - π stacking and hydrogen bonds when pH > 4.6.

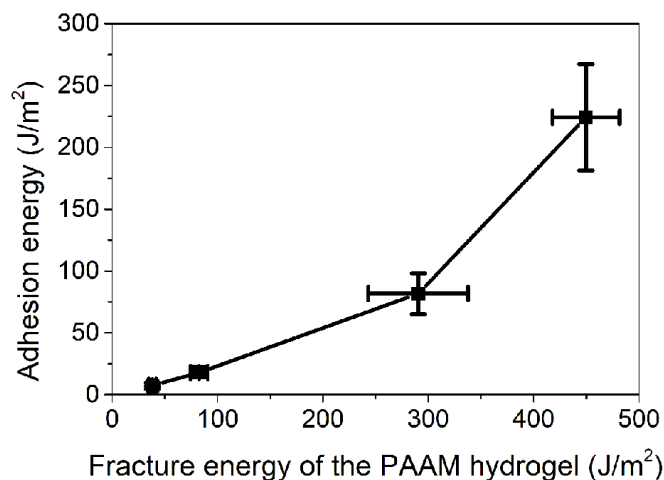


Figure C9 Adhesion energy increases with the fracture energy of the PAAM hydrogel. The fracture energy of the hydrogel is varied by tuning the crosslink density of the PAAM hydrogel. The fracture energies of 450 J/m², 290 J/m², 82.5 J/m² and 38.2 J/m² are measured using PAAM hydrogel with MBAA to acrylamide weight ratio of 0.0006:1, 0.0012:1, 0.0016:1 and 0.002:1, respectively.

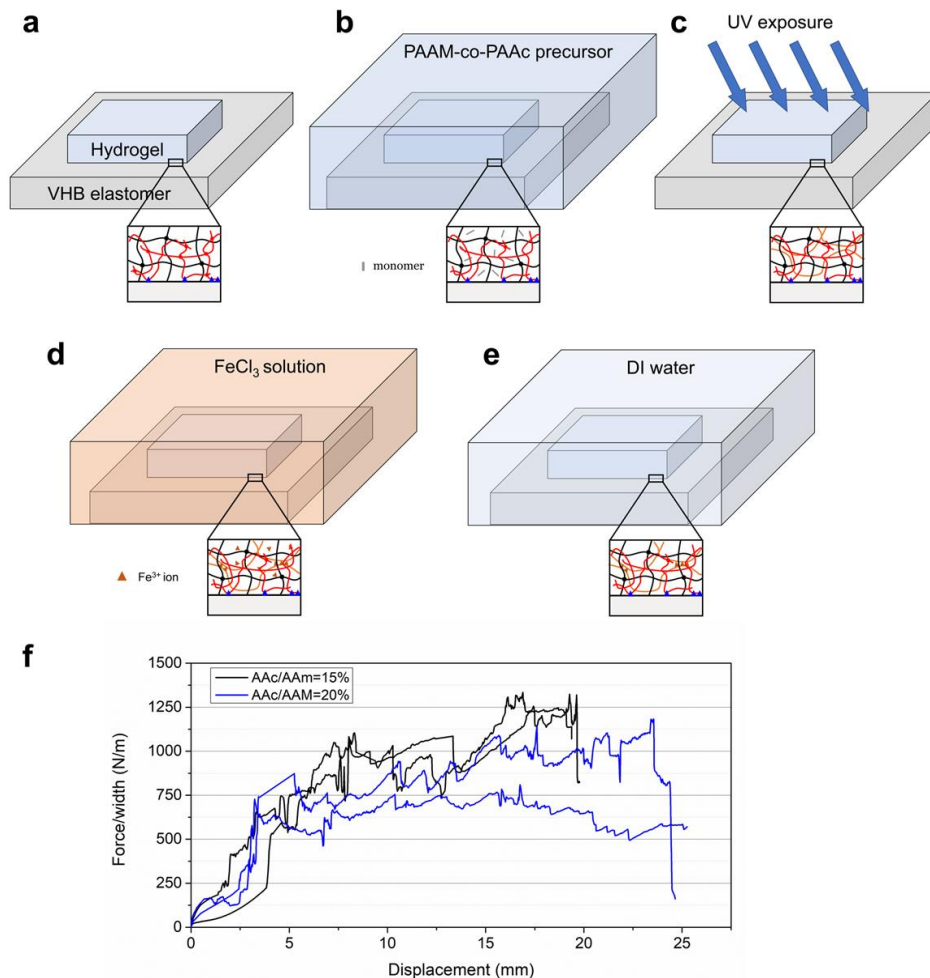


Figure C10 Amplification of adhesion energy using an iron-polyacrylate-PAAM hydrogel. (a) A PAAM hydrogel is bonded on a VHB elastomer with chitosan chains. (b) The bilayer is immersed in a precursor of the PAAM-co-PAAc hydrogel for one day. (c) The precursor polymerizes under UV irradiation, and forms PAAM-co-PAAc copolymers that interpenetrate with the PAAM network. (d) The sample is immersed in FeCl₃ solution for one day. The Fe³⁺ ions form coordination complex with the carboxylic acid groups, and crosslinks PAAM-co-PAAc copolymers into a PAAM-co-PAAc network. The hydrogel turns brown after the crosslinking. (e) The sample is then immersed in DI water for three days to remove the excess Fe³⁺ ions. (f) Force-displacement curves of 90-degree peeling tests. The adhesion energy depends on the AAm/AAc composition, and can reach about 1,000 J/m².

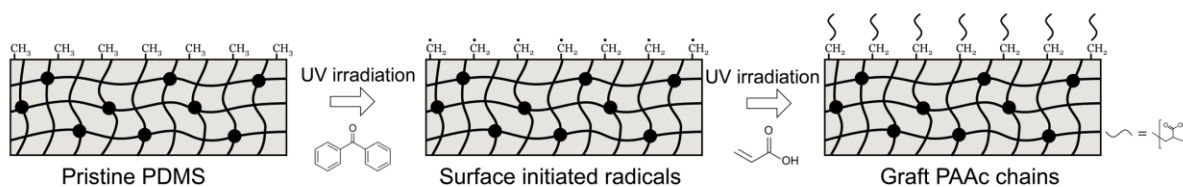


Figure C11 Surface chemical modification of silicone elastomers. A clean silicone elastomer (e.g. PDMS, Ecoflex) is first treated with benzophenone solution for 10 min and dried. Acrylic acid solution (2 M) is subsequently poured on the surface and exposed under UV irradiation for one hour. The acrylic acid monomers polymerize from the surface and grow into poly(acrylic acid) chains, thus modify the surface of silicone elastomer with carboxylic acid groups.

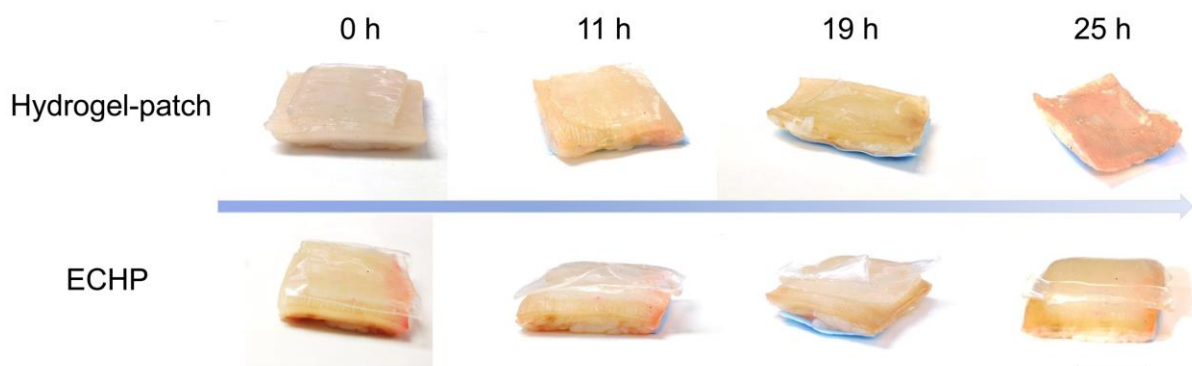


Figure C12 Dehydration of hydrogel and elastomer-coated hydrogel patch (ECHP) over time. For the hydrogel patch, dehydration occurs from both hydrogel and porcine skin. For the ECHP, dehydration is limited by top elastomer coating, and occurs from the periphery of hydrogel and porcine skin. After 25 hours, both the hydrogel patch and the porcine skin are completely dry and become hard, while the ECHP maintains relatively high water-content and is still soft. The scale bar is 1 cm.

Tables

Table C1 Polymer chains used in the tests

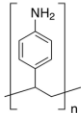
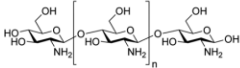
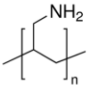
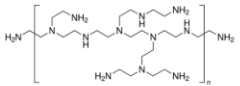
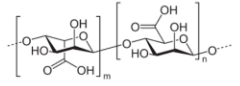
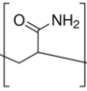
Polymers	Molecular structure	Crosslinks of stitching network	Matching functional groups from adherend
Poly(4-aminestyrene)		<ul style="list-style-type: none"> • NH₂--NH₂ H-bond • NH₂--π H-bond • π-π stacking 	<ul style="list-style-type: none"> • Carboxylic acid • Hydroxyl • Ketone • Epoxide • Phenyl • Negatively charged surface
Chitosan		<ul style="list-style-type: none"> • NH₂--OH H-bond 	<ul style="list-style-type: none"> • Carboxylic acid • Hydroxyl • Ketone • Epoxide • Negatively charged surface
Polyallylamine		NA	<ul style="list-style-type: none"> • Carboxylic acid • Hydroxyl • Ketone • Epoxide • Negatively charged surface
Polyethylenimine		NA	<ul style="list-style-type: none"> • Carboxylic acid • Hydroxyl • Ketone • Epoxide • Negatively charged surface
Alginate		<ul style="list-style-type: none"> • COOH--OH H-bond • COOH--COOH H-bond 	NA
Polyacrylamide		NA	NA

Table C2 Hydrogels used in the tests

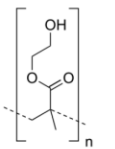
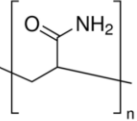
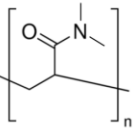
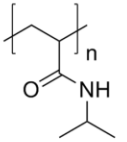
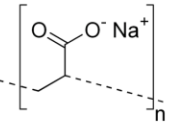
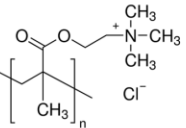
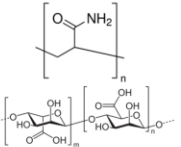
Polymer chain of hydrogel	Molecular structure	Charges on polymer chains	Interaction with chitosan
Poly(hydroxyethylmethacrylate) (PHEMA)		Neutral	Weak hydrogen bond
Poly(acrylamide) (PAAM)		Neutral	Weak hydrogen bond
Poly(dimethylacrylamide) (PDMA)		Neutral	Weak hydrogen bond
Poly(N-isopropylacrylamide) (PNIPAM)		Neutral	Weak hydrogen bond
Sodium polyacrylate (NaPAA)		Negatively charged	Weak hydrogen bond and ionic bond
[2-(Acryloyloxy)ethyl] trimethylammonium chloride (PDMAEA)		Positively charged	Weak hydrogen bond and positive charge repulsion
Polyacrylamide/alginate		Neutral/Negatively charged	Weak hydrogen bond and ionic bond

Table C3 Adherends used in the tests

Adherends	Functional groups	Testing polymer chains	Interfacial bonding
Glass	Hydroxyl	Chitosan	<ul style="list-style-type: none">• O⁻ - NH₃⁺ ionic bond
Surface treated Ecoflex	Carboxylic acid	Chitosan	<ul style="list-style-type: none">• COO⁻ - NH₃⁺ ionic bond
Surface treated PDMS			
VHB elastomer	Ketone Carboxylic acid	Chitosan Poly(4-aminostyrene)	<ul style="list-style-type: none">• COO⁻ - NH₃⁺ ionic bond• Imine bond
Mica	-	Chitosan	<ul style="list-style-type: none">• Ionic bond between negatively charged surface and NH₃⁺
Epoxide-glass	Epoxide	Poly(4-aminostyrene)	<ul style="list-style-type: none">• Covalent bond (NH₂ - epoxide ring opening reaction)
Poly(styrene)	Phenyl	Poly(4-aminostyrene)	<ul style="list-style-type: none">• π-π stacking• NH₂-π hydrogen bond
Aluminum	Hydroxyl	Chitosan	<ul style="list-style-type: none">• NH₂--OH hydrogen bond

Movies

Movie C1 Confocal images of the chitosan distribution in the hydrogel. The PAAM hydrogel was soaked in FITC-chitosan solution for one day before taking images. The fluorescent signals were seen in the entire hydrogel, which indicated chitosan chains can diffuse into the hydrogel.

Movie C2 Confocal images of the chitosan distribution in the VHB elastomer. The VHB elastomer was soaked in FITC-chitosan solution for one day before taking images. The fluorescent signals were seen only in a thin layer, which indicates chitosan chains cannot diffuse into the VHB elastomer, but stay on its surface.

Movie C3 Elastomer-coated hydrogel patch and hydrogel patch adhered *in vivo* on the skin of a rat. After the adhesion procedure, both patches were transparent and bonded well on the skin despite the movements of the rat. After 12 hours, the elastomer-coated hydrogel patch remained transparent and well-bonded, but the hydrogel patch was completely dry and could be easily separated from the skin.

Movie C4 Underwater adhesion. A piece of VHB elastomer was immersed in water. A chitosan solution was directly injected on the surface of the elastomer through water. A hydrogel was immediately placed on top with gentle pressure for an hour. Afterwards, the adhesion was tested by hanging a weight.

Bibliography

1. Ebnesajjad, S. and A.H. Landrock, *Adhesives technology handbook*. Third ed. 2014, United States: William Andrew.
2. Wichterle, O. and D. Lim, *Hydrophilic gels for biological use*. *Nature*, 1960. **185**(4706): p. 117.
3. Zhang, Y.S. and A. Khademhosseini, *Advances in engineering hydrogels*. *Science*, 2017. **356**(6337): p. eaaf3627.
4. Wichterle, O., D. Lim, and M. Dreifus, *On the problem of contact lenses*. *Ceskoslovenska oftalmologie*, 1961. **17**: p. 70.
5. Nicolson, P.C. and J. Vogt, *Soft contact lens polymers: an evolution*. *Biomaterials*, 2001. **22**(24): p. 3273-3283.
6. Dubrovskii, S., et al., *Comprehensive characterization of superabsorbent polymer hydrogels*. *Polymer bulletin*, 1990. **24**(1): p. 107-113.
7. Caliari, S.R. and J.A. Burdick, *A practical guide to hydrogels for cell culture*. *Nature methods*, 2016. **13**(5): p. 405.
8. Tibbitt, M.W. and K.S. Anseth, *Hydrogels as extracellular matrix mimics for 3D cell culture*. *Biotechnology and bioengineering*, 2009. **103**(4): p. 655-663.
9. Bouten, P.J., et al., *The chemistry of tissue adhesive materials*. *Progress in Polymer Science*, 2014. **39**(7): p. 1375-1405.
10. Mehdizadeh, M. and J. Yang, *Design strategies and applications of tissue bioadhesives*. *Macromolecular bioscience*, 2013. **13**(3): p. 271-288.
11. Annabi, N., et al., *Elastic sealants for surgical applications*. *European Journal of Pharmaceutics and Biopharmaceutics*, 2015. **95**: p. 27-39.
12. Lee, K.Y. and D.J. Mooney, *Hydrogels for tissue engineering*. *Chemical reviews*, 2001. **101**(7): p. 1869-1880.
13. Li, J. and D.J. Mooney, *Designing hydrogels for controlled drug delivery*. *Nature Reviews Materials*, 2016. **1**(12): p. 16071.
14. Peppas, N.A., et al., *Hydrogels in biology and medicine: from molecular principles to bionanotechnology*. *Advanced materials*, 2006. **18**(11): p. 1345-1360.
15. Taylor, D.L., *Self-Healing Hydrogels*. *Advanced Materials*, 2016. **28**(41): p. 9060-9093.
16. Phadke, A., et al., *Rapid self-healing hydrogels*. *Proceedings of the National Academy of Sciences*, 2012. **109**(12): p. 4383-4388.
17. Ahn, S.-k., et al., *Stimuli-responsive polymer gels*. *Soft Matter*, 2008. **4**(6): p. 1151-1157.

18. Qiu, Y. and K. Park, *Environment-sensitive hydrogels for drug delivery*. Advanced drug delivery reviews, 2001. **53**(3): p. 321-339.
19. Koetting, M.C., et al., *Stimulus-responsive hydrogels: Theory, modern advances, and applications*. Materials Science and Engineering: R: Reports, 2015. **93**: p. 1-49.
20. Qin, M., et al., *Bioinspired Hydrogel Interferometer for Adaptive Coloration and Chemical Sensing*. Advanced Materials, 2018: p. 1800468.
21. Wang, Q., et al., *Cephalopod-inspired design of electro-mechano-chemically responsive elastomers for on-demand fluorescent patterning*. Nature communications, 2014. **5**: p. 4899.
22. Ionov, L., *Hydrogel-based actuators: possibilities and limitations*. Materials Today, 2014. **17**(10): p. 494-503.
23. Hu, Z., X. Zhang, and Y. Li, *Synthesis and application of modulated polymer gels*. Science, 1995. **269**(5223): p. 525-527.
24. Beebe, D.J., et al., *Functional hydrogel structures for autonomous flow control inside microfluidic channels*. Nature, 2000. **404**(6778): p. 588.
25. Sharifzadeh, G. and H. Hosseinkhani, *Biomolecule-Responsive Hydrogels in Medicine*. Advanced healthcare materials, 2017.
26. Kim, J., J. Yoon, and R.C. Hayward, *Dynamic display of biomolecular patterns through an elastic creasing instability of stimuli-responsive hydrogels*. Nature materials, 2010. **9**(2): p. 159.
27. Ozcelik, B., *Degradable hydrogel systems for biomedical applications*, in *Biosynthetic Polymers for Medical Applications*. 2016, Elsevier. p. 173-188.
28. Liu, J., et al., *Triggerable tough hydrogels for gastric resident dosage forms*. Nature communications, 2017. **8**(1): p. 124.
29. Li, J., et al., *Tough adhesives for diverse wet surfaces*. Science, 2017. **357**(6349): p. 378-381.
30. Keplinger, C., et al., *Stretchable, transparent, ionic conductors*. Science, 2013. **341**(6149): p. 984-987.
31. Sun, J.Y., et al., *Ionic skin*. Advanced Materials, 2014. **26**(45): p. 7608-7614.
32. Yang, C.H., et al., *Ionic cable*. Extreme Mechanics Letters, 2015. **3**: p. 59-65.
33. Yang, C. and Z. Suo, *Hydrogel ionotronics*. Nature Reviews Materials, 2018.
34. Hong, S., et al., *3D printing of highly stretchable and tough hydrogels into complex, cellularized structures*. Advanced materials, 2015. **27**(27): p. 4035-4040.
35. Kolesky, D.B., et al., *3D bioprinting of vascularized, heterogeneous cell-laden tissue constructs*. Advanced materials, 2014. **26**(19): p. 3124-3130.

36. Miller, J.S., et al., *Rapid casting of patterned vascular networks for perfusable engineered three-dimensional tissues*. Nature materials, 2012. **11**(9): p. 768.
37. Duan, B., et al., *3D bioprinting of heterogeneous aortic valve conduits with alginate/gelatin hydrogels*. Journal of biomedical materials research Part A, 2013. **101**(5): p. 1255-1264.
38. Hockaday, L., et al., *Rapid 3D printing of anatomically accurate and mechanically heterogeneous aortic valve hydrogel scaffolds*. Biofabrication, 2012. **4**(3): p. 035005.
39. Tian, K., et al., *3D Printing of Transparent and Conductive Heterogeneous Hydrogel–Elastomer Systems*. Advanced Materials, 2017. **29**(10).
40. Liu, X., et al., *3D Printing of Living Responsive Materials and Devices*. Advanced Materials, 2018. **30**(4).
41. Mescher, A.L., *Junqueira's basic histology: text and atlas*. 2013, United States: Mcgraw-hill.
42. Grinstaff, M.W., *Designing hydrogel adhesives for corneal wound repair*. Biomaterials, 2007. **28**(35): p. 5205-5214.
43. Nonoyama, T., et al., *Double-network hydrogels strongly bondable to bones by spontaneous osteogenesis penetration*. Advanced Materials, 2016. **28**(31): p. 6740-6745.
44. Duflo, S., et al., *Vocal fold tissue repair in vivo using a synthetic extracellular matrix*. Tissue engineering, 2006. **12**(8): p. 2171-2180.
45. Sharma, B., et al., *Human cartilage repair with a photoreactive adhesive-hydrogel composite*. Science translational medicine, 2013. **5**(167): p. 167ra6-167ra6.
46. Lang, N., et al., *A blood-resistant surgical glue for minimally invasive repair of vessels and heart defects*. Science translational medicine, 2014. **6**(218): p. 218ra6-218ra6.
47. Wang, D.-A., et al., *Multifunctional chondroitin sulphate for cartilage tissue–biomaterial integration*. Nature materials, 2007. **6**(5): p. 385.
48. Hoare, T.R. and D.S. Kohane, *Hydrogels in drug delivery: Progress and challenges*. Polymer, 2008. **49**(8): p. 1993-2007.
49. Chin, S.Y., et al., *Additive manufacturing of hydrogel-based materials for next-generation implantable medical devices*. Science Robotics, 2017. **2**(2): p. eaah6451.
50. Meddahi-Pellé, A., et al., *Organ repair, hemostasis, and in vivo bonding of medical devices by aqueous solutions of nanoparticles*. Angewandte Chemie International Edition, 2014. **53**(25): p. 6369-6373.
51. Lloyd, J.D., M.J. Marque, and R.F. Kacprowicz, *Closure techniques*. Emergency Medicine Clinics, 2007. **25**(1): p. 73-81.
52. Tajirian, A.L. and D.J. Goldberg, *A review of sutures and other skin closure materials*. Journal of Cosmetic and Laser Therapy, 2010. **12**(6): p. 296-302.

53. Duarte, A., et al., *Surgical adhesives: systematic review of the main types and development forecast*. Progress in Polymer Science, 2012. **37**(8): p. 1031-1050.
54. Su, J., et al., *Anti-inflammatory peptide-functionalized hydrogels for insulin-secreting cell encapsulation*. Biomaterials, 2010. **31**(2): p. 308-314.
55. Chun, H. and T.D. Chung, *Iontronics*. Annual Review of Analytical Chemistry, 2015. **8**: p. 441-462.
56. Leger, J., M. Berggren, and S. Carter, *Iontronics: Ionic carriers in organic electronic materials and devices*. 2016, United States: CRC Press.
57. Bisri, S.Z., et al., *Endeavor of Iontronics: From Fundamentals to Applications of Ion-Controlled Electronics*. Advanced Materials, 2017.
58. Chen, B., et al., *Stretchable and transparent hydrogels as soft conductors for dielectric elastomer actuators*. Journal of Polymer Science Part B: Polymer Physics, 2014. **52**(16): p. 1055-1060.
59. Xu, C., et al., *A novel dielectric elastomer actuator based on compliant polyvinyl alcohol hydrogel electrodes*. Journal of Materials Science: Materials in Electronics, 2015. **26**(11): p. 9213-9218.
60. Acome, E., et al., *Hydraulically amplified self-healing electrostatic actuators with muscle-like performance*. Science, 2018. **359**(6371): p. 61-65.
61. Kellaris, N., et al., *Peano-HASEL actuators: Muscle-mimetic, electrohydraulic transducers that linearly contract on activation*. Science Robotics, 2018. **3**(14): p. eaar3276.
62. Sarwar, M.S., et al., *Bend, stretch, and touch: Locating a finger on an actively deformed transparent sensor array*. Science advances, 2017. **3**(3): p. e1602200.
63. Lei, Z., et al., *A Bioinspired Mineral Hydrogel as a Self-Healable, Mechanically Adaptable Ionic Skin for Highly Sensitive Pressure Sensing*. Advanced Materials, 2017. **29**(22).
64. Le Floch, P., et al., *Wearable and washable conductors for active textiles*. ACS applied materials & interfaces, 2017. **9**(30): p. 25542-25552.
65. Yang, C.H., et al., *Electroluminescence of giant stretchability*. Advanced Materials, 2016. **28**(22): p. 4480-4484.
66. Wang, J., et al., *Extremely stretchable electroluminescent devices with ionic conductors*. Advanced Materials, 2016. **28**(22): p. 4490-4496.
67. Larson, C., et al., *Highly stretchable electroluminescent skin for optical signaling and tactile sensing*. Science, 2016. **351**(6277): p. 1071-1074.
68. Yang, C.H., et al., *Organic liquid-crystal devices based on ionic conductors*. Materials Horizons, 2017. **4**(6): p. 1102-1109.

69. Kim, C.-C., et al., *Highly stretchable, transparent ionic touch panel*. *Science*, 2016. **353**(6300): p. 682-687.
70. Pu, X., et al., *Ultrastretchable, transparent triboelectric nanogenerator as electronic skin for biomechanical energy harvesting and tactile sensing*. *Science advances*, 2017. **3**(5): p. e1700015.
71. Parida, K., et al., *Highly Transparent, Stretchable, and Self-Healing Ionic-Skin Triboelectric Nanogenerators for Energy Harvesting and Touch Applications*. *Advanced Materials*, 2017. **29**(37).
72. Xu, W., et al., *Environmentally Friendly Hydrogel-Based Triboelectric Nanogenerators for Versatile Energy Harvesting and Self-Powered Sensors*. *Advanced Energy Materials*, 2017. **7**(1).
73. Parada, G.A., et al., *Impermeable Robust Hydrogels via Hybrid Lamination*. *Advanced healthcare materials*, 2017. **6**(19).
74. Yuk, H., et al., *Skin-inspired hydrogel–elastomer hybrids with robust interfaces and functional microstructures*. *Nature communications*, 2016. **7**: p. 12028.
75. Liu, X., et al., *Stretchable living materials and devices with hydrogel–elastomer hybrids hosting programmed cells*. *Proceedings of the National Academy of Sciences*, 2017. **114**(9): p. 2200-2205.
76. Huang, Y., et al., *Energy-Dissipative Matrices Enable Synergistic Toughening in Fiber Reinforced Soft Composites*. *Advanced functional materials*, 2017. **27**(9).
77. Takahashi, R., et al., *Creating Stiff, Tough, and Functional Hydrogel Composites with Low-Melting-Point Alloys*. *Advanced Materials*, 2018.
78. Illeperuma, W.R., et al., *Fiber-reinforced tough hydrogels*. *Extreme Mechanics Letters*, 2014. **1**: p. 90-96.
79. He, Q., et al., *Polymer nanofiber reinforced double network gel composite: Strong, tough and transparent*. *Extreme Mechanics Letters*, 2016. **9**: p. 165-170.
80. Lin, S., et al., *Design of stiff, tough and stretchy hydrogel composites via nanoscale hybrid crosslinking and macroscale fiber reinforcement*. *Soft matter*, 2014. **10**(38): p. 7519-7527.
81. Agrawal, A., N. Rahbar, and P.D. Calvert, *Strong fiber-reinforced hydrogel*. *Acta biomaterialia*, 2013. **9**(2): p. 5313-5318.
82. King, D.R., et al., *Extremely tough composites from fabric reinforced polyampholyte hydrogels*. *Materials horizons*, 2015. **2**(6): p. 584-591.
83. Ragelle, H., et al., *Surface tension-assisted additive manufacturing*. *Nature communications*, 2018. **9**(1).

84. Liao, I.-C., et al., *Composite three-dimensional woven scaffolds with interpenetrating network hydrogels to create functional synthetic articular cartilage*. *Advanced functional materials*, 2013. **23**(47): p. 5833-5839.
85. Thayer, P.S., et al., *Cellularized cylindrical fiber/hydrogel composites for ligament tissue engineering*. *Biomacromolecules*, 2013. **15**(1): p. 75-83.
86. Bakarich, S.E., et al., *Three-dimensional printing fiber reinforced hydrogel composites*. *ACS applied materials & interfaces*, 2014. **6**(18): p. 15998-16006.
87. Mills, N. and A. Gilchrist, *The effectiveness of foams in bicycle and motorcycle helmets*. *Accident Analysis & Prevention*, 1991. **23**(2): p. 153-163.
88. Temenoff, J.S. and A.G. Mikos, *Tissue engineering for regeneration of articular cartilage*. *Biomaterials*, 2000. **21**(5): p. 431-440.
89. Cheng, H., et al., *Mussel-inspired multifunctional hydrogel coating for prevention of infections and enhanced osteogenesis*. *ACS applied materials & interfaces*, 2017. **9**(13): p. 11428-11439.
90. LaPorte, R.J., *Hydrophilic polymer coatings for medical devices*. 1997, New York: CRC Press.
91. Wirthl, D., et al., *Instant tough bonding of hydrogels for soft machines and electronics*. *Science advances*, 2017. **3**(6): p. e1700053.
92. Yuk, H., et al., *Tough bonding of hydrogels to diverse non-porous surfaces*. *Nature materials*, 2016. **15**(2): p. 190.
93. Lin, S., et al., *Stretchable hydrogel electronics and devices*. *Advanced Materials*, 2016. **28**(22): p. 4497-4505.
94. Liu, Q., et al., *Bonding dissimilar polymer networks in various manufacturing processes*. *Nature communications*, 2018. **9**(1): p. 846.
95. Liu, W., et al., *Rapid continuous multimaterial extrusion bioprinting*. *Advanced Materials*, 2017. **29**(3).
96. Gladman, A.S., et al., *Biomimetic 4D printing*. *Nature materials*, 2016. **15**(4): p. 413.
97. Yang, S.Y., et al., *A bio-inspired swellable microneedle adhesive for mechanical interlocking with tissue*. *Nature communications*, 2013. **4**: p. 1702.
98. Rose, S., et al., *Nanoparticle solutions as adhesives for gels and biological tissues*. *Nature*, 2014. **505**(7483): p. 382.
99. Tang, J., et al., *Adhesion between highly stretchable materials*. *Soft Matter*, 2016. **12**(4): p. 1093-1099.
100. Yang, J., R. Bai, and Z. Suo, *Topological Adhesion of Wet Materials*. *Advanced Materials*, 2018: p. 1800671.

101. Jiawei Yang, R.B., Jianyu Li, Canhui Yang, Xi Yao, Qihan Liu, Joost J. Vlassak, David J. Mooney, and Zhigang Suo, *Topologies of hydrogel adhesion*. Submitted, 2018.
102. Brown, H.R., *Effects of chain pull-out on adhesion of elastomers*. *Macromolecules*, 1993. **26**(7): p. 1666-1670.
103. Reichert, W.F. and H.R. Brown, *Effect of a polystyrene-polyisoprene diblock layer on the adhesion between polystyrene and polyisoprene*. *Polymer*, 1993. **34**(11): p. 2289-2296.
104. Léger, L. and C. Creton, *Adhesion mechanisms at soft polymer interfaces*. *Philosophical Transactions of the Royal Society of London A: Mathematical, Physical and Engineering Sciences*, 2008. **366**(1869): p. 1425-1442.
105. Creton, C., et al., *Adhesion and fracture of interfaces between immiscible polymers: from the molecular to the continuum scal*, in *Molecular Simulation Fracture Gel Theory*. 2001, Springer. p. 53-136.
106. Levinson, P., et al., *The spreading of macroscopic droplets*. *Revue de Physique Appliquee*, 1988. **23**(6): p. 1009-1016.
107. Gong, J.P., et al., *Double-network hydrogels with extremely high mechanical strength*. *Advanced Materials*, 2003. **15**(14): p. 1155-1158.
108. Sun, J.Y., et al., *Highly stretchable and tough hydrogels*. *Nature*, 2012. **489**(7414): p. 133-136.
109. Griffith, A., *The phenomena of flow and rupture in solids: Phil. Trans. Roy. Soc. Lond. Ser. A*, 1920. **221**: p. 163-198.
110. Lake, G. and A. Thomas, *The strength of highly elastic materials*. *Proc. R. Soc. Lond. A*, 1967. **300**(1460): p. 108-119.
111. Orowan, E., *Fracture and strength of solids*. *Reports on progress in physics*, 1949. **12**(1): p. 185.
112. Irwin, G.R., *Fracture dynamics*. *Fracturing of metals*, 1948. **152**.
113. Evans, A.G., *Perspective on the development of high-toughness ceramics*. *Journal of the American Ceramic society*, 1990. **73**(2): p. 187-206.
114. Tvergaard, V. and J.W. Hutchinson, *The relation between crack growth resistance and fracture process parameters in elastic-plastic solids*. *Journal of the Mechanics and Physics of Solids*, 1992. **40**(6): p. 1377-1397.
115. Bao, G. and Z. Suo, *Remarks on crack-bridging concepts*. *Applied Mechanics Reviews*, 1992. **45**(8): p. 355-366.
116. Du, J., M. Thouless, and A. Yee, *Effects of rate on crack growth in a rubber-modified epoxy*. *Acta materialia*, 2000. **48**(13): p. 3581-3592.

117. Baumberger, T., C. Caroli, and D. Martina, *Solvent control of crack dynamics in a reversible hydrogel*. Nature materials, 2006. **5**(7): p. 552.
118. Zhao, X., et al., *Stress-relaxation behavior in gels with ionic and covalent crosslinks*. Journal of applied physics, 2010. **107**(6): p. 063509.
119. Bai, R., et al., *Fatigue Fracture of Self-Recovery Hydrogels*. ACS Macro Letters, 2018. **7**: p. 312-317.
120. Tanaka, Y., K. Fukao, and Y. Miyamoto, *Fracture energy of gels*. The European Physical Journal E, 2000. **3**(4): p. 395-401.
121. Sanderson, R.T., *Chemical bonds and bond energy*. 1976, New York: Academic Press.
122. Holyst, R., *Some features of soft matter systems*. Soft Matter, 2005. **1**(5): p. 329-333.
123. Steiner, T., *The hydrogen bond in the solid state*. Angewandte Chemie International Edition, 2002. **41**(1): p. 48-76.
124. Braccini, I. and S. Pérez, *Molecular basis of Ca²⁺-induced gelation in alginates and pectins: the egg-box model revisited*. Biomacromolecules, 2001. **2**(4): p. 1089-1096.
125. Berg, J.M., et al., *Biochemistry*. 2002, WH Freeman: New York.
126. Israelachvili, J. and R. Pashley, *The hydrophobic interaction is long range, decaying exponentially with distance*. Nature, 1982. **300**(5890): p. 341-342.
127. Jorgensen, W.L. and D.L. Severance, *Aromatic-aromatic interactions: free energy profiles for the benzene dimer in water, chloroform, and liquid benzene*. Journal of the American Chemical Society, 1990. **112**(12): p. 4768-4774.
128. Houk, K., et al., *Binding affinities of host-guest, protein-ligand, and protein-transition-state complexes*. Angewandte Chemie International Edition, 2003. **42**(40): p. 4872-4897.
129. Annabi, N., et al., *Engineering a highly elastic human protein-based sealant for surgical applications*. Science translational medicine, 2017. **9**(410): p. eaai7466.
130. Liang, S., et al., *Paintable and Rapidly Bondable Conductive Hydrogels as Therapeutic Cardiac Patches*. Advanced Materials, 2018: p. 1704235.
131. Jackson, M.R., *Fibrin sealants in surgical practice: an overview*. The American journal of surgery, 2001. **182**(2): p. S1-S7.
132. Ahmed, T.A., E.V. Dare, and M. Hincke, *Fibrin: a versatile scaffold for tissue engineering applications*. Tissue Engineering Part B: Reviews, 2008. **14**(2): p. 199-215.
133. Martinowitz, U. and R. Saltz, *Fibrin sealant*. Current opinion in hematology, 1996. **3**(5): p. 395-402.
134. Janmey, P.A., J.P. Winer, and J.W. Weisel, *Fibrin gels and their clinical and bioengineering applications*. Journal of the Royal Society Interface, 2009. **6**(30): p. 1-10.

135. Budzynski, A.Z. and J.R. Shainoff, *Fibrinogen and fibrin: biochemistry and pathophysiology*. Critical reviews in oncology/hematology, 1986. **6**(2): p. 97-146.
136. Sierra, D.H., *Fibrin sealant adhesive systems: a review of their chemistry, material properties and clinical applications*. Journal of Biomaterials Applications, 1993. **7**(4): p. 309-352.
137. Elvin, C., et al., *Evaluation of photo-crosslinked fibrinogen as a rapid and strong tissue adhesive*. Journal of Biomedical Materials Research Part A, 2010. **93**(2): p. 687-695.
138. Elvin, C.M., et al., *The development of photochemically crosslinked native fibrinogen as a rapidly formed and mechanically strong surgical tissue sealant*. Biomaterials, 2009. **30**(11): p. 2059-2065.
139. Schek, R., A. Michalek, and J. Iatridis, *Genipin-crosslinked fibrin hydrogels as a potential adhesive to augment intervertebral disc annulus repair*. European cells & materials, 2011. **21**: p. 373.
140. Ono, K., et al., *Photocrosslinkable chitosan as a biological adhesive*. Journal of Biomedical Materials Research Part A, 2000. **49**(2): p. 289-295.
141. Ishihara, M., et al., *Photocrosslinkable chitosan as a dressing for wound occlusion and accelerator in healing process*. Biomaterials, 2002. **23**(3): p. 833-840.
142. Liu, G., et al. *Synthesis and Characterization of Chitosan/Dextran-Based Hydrogels for Surgical Use*. in *Macromolecular symposia*. 2009. Wiley Online Library.
143. Lih, E., et al., *Rapidly curable chitosan-PEG hydrogels as tissue adhesives for hemostasis and wound healing*. Acta biomaterialia, 2012. **8**(9): p. 3261-3269.
144. Nie, W., et al., *Rapidly in situ forming chitosan/ε-polylysine hydrogels for adhesive sealants and hemostatic materials*. Carbohydrate polymers, 2013. **96**(1): p. 342-348.
145. Bhatia, S.K., et al., *Polysaccharide-based tissue adhesives for sealing corneal incisions*. Current eye research, 2007. **32**(12): p. 1045-1050.
146. Li, Q., et al., *Photocrosslinkable polysaccharides based on chondroitin sulfate*. Journal of biomedical materials research Part A, 2004. **68**(1): p. 28-33.
147. Reyes, J.M., et al., *A modified chondroitin sulfate aldehyde adhesive for sealing corneal incisions*. Investigative ophthalmology & visual science, 2005. **46**(4): p. 1247-1250.
148. Strehin, I., et al., *Synthesis and characterization of a chondroitin sulfate-polyethylene glycol corneal adhesive*. Journal of Cataract & Refractive Surgery, 2009. **35**(3): p. 567-576.
149. Smeds, K.A. and M.W. Grinstaff, *Photocrosslinkable polysaccharides for in situ hydrogel formation*. Journal of Biomedical Materials Research Part A, 2001. **54**(1): p. 115-121.

150. Caliceti, P. and F.M. Veronese, *Pharmacokinetic and biodistribution properties of poly (ethylene glycol)–protein conjugates*. *Advanced drug delivery reviews*, 2003. **55**(10): p. 1261-1277.
151. Knop, K., et al., *Poly (ethylene glycol) in drug delivery: pros and cons as well as potential alternatives*. *Angewandte chemie international edition*, 2010. **49**(36): p. 6288-6308.
152. Sawhney, A.S., C.P. Pathak, and J.A. Hubbell, *Bioerodible hydrogels based on photopolymerized poly (ethylene glycol)-co-poly (. alpha.-hydroxy acid) diacrylate macromers*. *Macromolecules*, 1993. **26**(4): p. 581-587.
153. Nivasu, V.M., T.T. Reddy, and S. Tammishetti, *In situ polymerizable polyethyleneglycol containing polyesterpolyol acrylates for tissue sealant applications*. *Biomaterials*, 2004. **25**(16): p. 3283-3291.
154. Preul, M.C., et al., *Toward optimal tissue sealants for neurosurgery: use of a novel hydrogel sealant in a canine durotomy repair model*. *Neurosurgery*, 2003. **53**(5): p. 1189-1199.
155. Wallace, D., et al., *A tissue sealant based on reactive multifunctional polyethylene glycol*. *Journal of Biomedical Materials Research Part A*, 2001. **58**(5): p. 545-555.
156. Gokgol, C., C. Basdogan, and D. Canadinc, *Estimation of fracture toughness of liver tissue: Experiments and validation*. *Medical engineering & physics*, 2012. **34**(7): p. 882-891.
157. Pereira, B.P., P.W. Lucas, and T. Swee-Hin, *Ranking the fracture toughness of thin mammalian soft tissues using the scissors cutting test*. *Journal of Biomechanics*, 1997. **30**(1): p. 91-94.
158. Kord Forooshani, P. and B.P. Lee, *Recent approaches in designing bioadhesive materials inspired by mussel adhesive protein*. *Journal of Polymer Science Part A: Polymer Chemistry*, 2017. **55**(1): p. 9-33.
159. Rahimnejad, M. and W. Zhong, *Mussel-inspired hydrogel tissue adhesives for wound closure*. *RSC Advances*, 2017. **7**(75): p. 47380-47396.
160. Lee, H., et al., *Mussel-inspired surface chemistry for multifunctional coatings*. *Science*, 2007. **318**(5849): p. 426-430.
161. Waite, J.H., *Mussel adhesion—essential footwork*. *Journal of Experimental Biology*, 2017. **220**(4): p. 517-530.
162. Barrett, D.G., G.G. Bushnell, and P.B. Messersmith, *Mechanically robust, negative-swelling, mussel-inspired tissue adhesives*. *Advanced healthcare materials*, 2013. **2**(5): p. 745-755.
163. Liao, M., et al., *Wearable, Healable, and Adhesive Epidermal Sensors Assembled from Mussel-Inspired Conductive Hybrid Hydrogel Framework*. *Advanced Functional Materials*, 2017. **27**(48).

164. Hammond, R., *The proboscis mechanism of Acanthocephalus ranae*. Journal of Experimental Biology, 1966. **45**(2): p. 203-213.
165. Shin, K., et al., *Multifunctional nanoparticles as a tissue adhesive and an injectable marker for image-guided procedures*. Nature communications, 2017. **8**: p. 15807.
166. Cao, Z. and A.V. Dobrynin, *Nanoparticles as adhesives for soft polymeric materials*. Macromolecules, 2016. **49**(9): p. 3586-3592.
167. Maw, J. and J. Quinn, *Cyanoacrylate tissue adhesives*. The American Journal of Cosmetic Surgery, 1997. **14**(4): p. 413-416.
168. Singer, A.J., J.V. Quinn, and J.E. Hollander, *The cyanoacrylate topical skin adhesives*. The American journal of emergency medicine, 2008. **26**(4): p. 490-496.
169. Leonard, F., *The n-alkylalphacyanoacrylate tissue adhesives*, in *Biomaterials*. 1969, Springer. p. 15-30.
170. Klemarczyk, P. and J. Guthrie, *Advances in anaerobic and cyanoacrylate adhesives*, in *Advances in Structural Adhesive Bonding*. 2010, Elsevier. p. 96-131.
171. Shantha, K., S. Thennarasu, and N. Krishnamurti, *Developments and applications of cyanoacrylate adhesives*. Journal of adhesion science and technology, 1989. **3**(1): p. 237-260.
172. Melody, D.P., *Advances in room temperature curing adhesives and sealants—a review*. Polymer International, 1989. **21**(2): p. 175-179.
173. Leggat, P.A., D.R. Smith, and U. Kedjarune, *Surgical applications of cyanoacrylate adhesives: a review of toxicity*. ANZ journal of surgery, 2007. **77**(4): p. 209-213.
174. Vinters, H., et al., *The histotoxicity of cyanoacrylates*. Neuroradiology, 1985. **27**(4): p. 279-291.
175. Robello, D.R., T.D. Eldridge, and M.T. Swanson, *Degradation and stabilization of polycyanoacrylates*. Journal of Polymer Science Part A: Polymer Chemistry, 1999. **37**(24): p. 4570-4581.
176. Nakajima, N. and Y. Ikada, *Mechanism of amide formation by carbodiimide for bioconjugation in aqueous media*. Bioconjugate chemistry, 1995. **6**(1): p. 123-130.
177. Gilles, M.A., A.Q. Hudson, and C. Borders Jr, *Stability of water-soluble carbodiimides in aqueous solution*. Analytical biochemistry, 1990. **184**(2): p. 244-248.
178. Ladet, S., L. David, and A. Domard, *Multi-membrane hydrogels*. Nature, 2008. **452**(7183): p. 76.
179. Okuyama, K., et al., *Molecular and crystal structure of hydrated chitosan*. Macromolecules, 1997. **30**(19): p. 5849-5855.
180. Pharr, M., J.-Y. Sun, and Z. Suo, *Rupture of a highly stretchable acrylic dielectric elastomer*. Journal of Applied Physics, 2012. **111**(10): p. 104114.

181. Efimenko, K., W.E. Wallace, and J. Genzer, *Surface modification of Sylgard-184 poly (dimethyl siloxane) networks by ultraviolet and ultraviolet/ozone treatment*. Journal of colloid and interface science, 2002. **254**(2): p. 306-315.
182. Hegemann, D., H. Brunner, and C. Oehr, *Plasma treatment of polymers for surface and adhesion improvement*. Nuclear instruments and methods in physics research section B: Beam interactions with materials and atoms, 2003. **208**: p. 281-286.
183. Bodas, D. and C. Khan-Malek, *Hydrophilization and hydrophobic recovery of PDMS by oxygen plasma and chemical treatment—An SEM investigation*. Sensors and Actuators B: Chemical, 2007. **123**(1): p. 368-373.
184. Béfahy, S.p., et al., *Thickness and elastic modulus of plasma treated PDMS silica-like surface layer*. Langmuir, 2009. **26**(5): p. 3372-3375.
185. Bowden, N., et al., *The controlled formation of ordered, sinusoidal structures by plasma oxidation of an elastomeric polymer*. Applied Physics Letters, 1999. **75**(17): p. 2557-2559.
186. Mills, K., et al., *The mechanical properties of a surface-modified layer on polydimethylsiloxane*. Journal of materials research, 2008. **23**(1): p. 37-48.
187. Lawton, R.A., et al., *Air plasma treatment of submicron thick PDMS polymer films: effect of oxidation time and storage conditions*. Colloids and Surfaces A: Physicochemical and Engineering Aspects, 2005. **253**(1-3): p. 213-215.
188. Plueddemann, E.P., *Silane adhesion promoters in coatings*. Progress in Organic Coatings, 1983. **11**(3): p. 297-308.
189. Witucki, G.L., *A silane primer: chemistry and applications of alkoxy silanes*. Journal of coatings technology, 1993. **65**: p. 57-57.
190. Plueddemann, E.P., *Chemistry of silane coupling agents*, in *Silane coupling agents*. 1991, Springer. p. 31-54.
191. Cha, C., et al., *Tailoring hydrogel adhesion to polydimethylsiloxane substrates using polysaccharide glue*. Angewandte Chemie International Edition, 2013. **52**(27): p. 6949-6952.
192. Zhang, H., et al., *Fabrication of robust hydrogel coatings on polydimethylsiloxane substrates using micropillar anchor structures with chemical surface modification*. ACS applied materials & interfaces, 2014. **6**(12): p. 9126-9133.
193. Schneider, M.H., Y. Tran, and P. Tabeling, *Benzophenone absorption and diffusion in poly (dimethylsiloxane) and its role in graft photo-polymerization for surface modification*. Langmuir, 2011. **27**(3): p. 1232-1240.
194. Deng, J., et al., *Developments and new applications of UV-induced surface graft polymerizations*. Progress in Polymer Science, 2009. **34**(2): p. 156-193.
195. Okamoto, Y. and P.T. Klemarczyk, *Primers for bonding polyolefin substrates with alkyl cyanoacrylate adhesive*. The Journal of Adhesion, 1993. **40**(2-4): p. 81-91.

196. Gutowski, W., D.Y. Wu, and S. Li, *Surface silanization of polyethylene for enhanced adhesion*. The Journal of Adhesion, 1993. **43**(1-2): p. 139-155.
197. Wu, D.Y., et al., *Ammonia plasma treatment of polyolefins for adhesive bonding with a cyanoacrylate adhesive*. Journal of adhesion science and technology, 1995. **9**(4): p. 501-525.
198. Mandolino, C., et al., *Improving adhesion performance of polyethylene surfaces by cold plasma treatment*. Meccanica, 2014. **49**(10): p. 2299-2306.
199. Gobble, K., A. Stark, and S.P. Stagon, *Improved bond strength of cyanoacrylate adhesives through nanostructured chromium adhesion layers*. Nanoscale research letters, 2016. **11**(1): p. 416.
200. Scheller, P.N., et al., *Imine Reductase-Catalyzed Intermolecular Reductive Amination of Aldehydes and Ketones*. ChemCatChem, 2015. **7**(20): p. 3239-3242.
201. Layer, R.W., *The Chemistry of Imines*. Chemical Reviews, 1963. **63**(5): p. 489-510.
202. Kurokawa, T., et al., *Formation of a strong hydrogel-porous solid interface via the double-network principle*. Acta biomaterialia, 2010. **6**(4): p. 1353-1359.
203. Dugas, V. and Y. Chevalier, *Surface hydroxylation and silane grafting on fumed and thermal silica*. Journal of colloid and interface science, 2003. **264**(2): p. 354-361.
204. Metters, A., K. Anseth, and C. Bowman, *Fundamental studies of a novel, biodegradable PEG-b-PLA hydrogel*. Polymer, 2000. **41**(11): p. 3993-4004.
205. Boonthekul, T., H.-J. Kong, and D.J. Mooney, *Controlling alginate gel degradation utilizing partial oxidation and bimodal molecular weight distribution*. Biomaterials, 2005. **26**(15): p. 2455-2465.
206. West, J.L. and J.A. Hubbell, *Polymeric biomaterials with degradation sites for proteases involved in cell migration*. Macromolecules, 1999. **32**(1): p. 241-244.
207. Huebsch, N., et al., *Ultrasound-triggered disruption and self-healing of reversibly cross-linked hydrogels for drug delivery and enhanced chemotherapy*. Proceedings of the National Academy of Sciences, 2014. **111**(27): p. 9762-9767.
208. Boateng, J.S., et al., *Wound healing dressings and drug delivery systems: a review*. Journal of Pharmaceutical Sciences, 2008. **97**(8): p. 2892-2923.
209. Dagdeviren, C., et al., *Conformal piezoelectric energy harvesting and storage from motions of the heart, lung, and diaphragm*. Proceedings of the National Academy of Sciences, 2014. **111**(5): p. 1927-1932.
210. Minev, I.R., et al., *Electronic dura mater for long-term multimodal neural interfaces*. Science, 2015. **347**(6218): p. 159-163.
211. Vakalopoulos, K.A., et al., *Mechanical strength and rheological properties of tissue adhesives with regard to colorectal anastomosis: an ex vivo study*. Annals of surgery, 2015. **261**(2): p. 323-331.

212. Tamagawa, H. and Y. Takahashi, *Adhesion force behavior between two gels attached with an electrolytic polymer liquid*. *Materials Chemistry and Physics*, 2008. **107**(1): p. 164-170.
213. Dragan, E.S., *Design and applications of interpenetrating polymer network hydrogels. A review*. *Chemical Engineering Journal*, 2014. **243**: p. 572-590.
214. Ducrot, E., et al., *Toughening elastomers with sacrificial bonds and watching them break*. *Science*, 2014. **344**(6180): p. 186-189.
215. Okumura, Y. and K. Ito, *The polyrotaxane gel: A topological gel by figure-of-eight cross-links*. *Advanced Materials*, 2001. **13**(7): p. 485-487.
216. Jia, D., Y. Pang, and X. Liang, *Mechanism of adhesion of polyurethane/polymethacrylate simultaneous interpenetrating networks adhesives to polymer substrates*. *Journal of Polymer Science Part B: Polymer Physics*, 1994. **32**(5): p. 817-823.
217. Kim, I.-Y., et al., *Chitosan and its derivatives for tissue engineering applications*. *Biotechnology advances*, 2008. **26**(1): p. 1-21.
218. Rubinstein, M. and R.H. Colby, *Polymer Physics*. 2003, New York: Oxford University Press.
219. Zavitsas, A.A., *Quantitative relationship between bond dissociation energies, infrared stretching frequencies, and force constants in polyatomic molecules*. *Journal of Physical Chemistry*, 1987. **91**(22): p. 5573-5577.
220. Hu, X., et al., *Weak hydrogen bonding enables hard, strong, tough, and elastic hydrogels*. *Advanced Materials*, 2015. **27**(43): p. 6899-6905.
221. Yang, Y., et al., *A universal soaking strategy to convert composite hydrogels into extremely tough and rapidly recoverable double-network hydrogels*. *Advanced Materials*, 2016. **28**(33): p. 7178-7184.
222. Li, J., Z. Suo, and J.J. Vlassak, *Stiff, strong, and tough hydrogels with good chemical stability*. *Journal of Materials Chemistry B*, 2014. **2**(39): p. 6708-6713.
223. Sherwood, L., *Human Physiology: from cells to systems*. 7 ed. 2010, Belmont: Brooks/Cole.
224. Zhang, T., et al., *Predicting fracture energies and crack-tip fields of soft tough materials*. *Extreme Mechanics Letters*, 2015. **4**: p. 1-8.
225. Long, R. and C.-Y. Hui, *Crack tip fields in soft elastic solids subjected to large quasi-static deformation—a review*. *Extreme Mechanics Letters*, 2015. **4**: p. 131-155.
226. Bai, R., et al., *Fatigue fracture of tough hydrogels*. *Extreme Mechanics Letters*, 2017. **15**: p. 91-96.
227. Zhao, X., *Multi-scale multi-mechanism design of tough hydrogels: building dissipation into stretchy networks*. *Soft Matter*, 2014. **10**(5): p. 672-687.

228. Mao, Y., et al., *A large deformation viscoelastic model for double-network hydrogels*. Journal of the Mechanics and Physics of Solids, 2017. **100**: p. 103-130.
229. Lu, T., et al., *A constitutive model for soft materials incorporating viscoelasticity and Mullins effect*. Journal of Applied Mechanics, 2017. **84**(2): p. 021010.
230. Budhlall, B.M., M. Marquez, and O.D. Velev, *Microwave, Photo-and Thermally Responsive PNIPAm– Gold Nanoparticle Microgels*. Langmuir, 2008. **24**(20): p. 11959-11966.
231. Prausnitz, M.R. and R. Langer, *Transdermal drug delivery*. Nature Biotechnology, 2008. **26**(11): p. 1261-1268.
232. Ghobril, C., et al., *A dendritic thioester hydrogel based on thiol–thioester exchange as a dissolvable sealant system for wound closure*. Angewandte Chemie, 2013. **125**(52): p. 14320-14324.
233. Roche, E.T., et al., *A bioinspired soft actuated material*. Advanced Materials, 2014. **26**(8): p. 1200-1206.
234. Feiner, R., et al., *Engineered hybrid cardiac patches with multifunctional electronics for online monitoring and regulation of tissue function*. Nature materials, 2016. **15**(6): p. 679.
235. Dastjerdi, A.K., et al., *Cohesive behavior of soft biological adhesives: experiments and modeling*. Acta Biomaterialia, 2012. **8**(9): p. 3349-3359.
236. Moretti, M., et al., *Structural characterization and reliable biomechanical assessment of integrative cartilage repair*. Journal of biomechanics, 2005. **38**(9): p. 1846-1854.
237. Pawlicki, J., et al., *The effect of molluscan glue proteins on gel mechanics*. Journal of Experimental Biology, 2004. **207**(7): p. 1127-1135.
238. Wilks, A.M., et al., *Double network gels and the toughness of terrestrial slug glue*. Journal of Experimental Biology, 2015: p. jeb. 128991.
239. Braun, M., et al., *The relative contribution of calcium, zinc and oxidation-based cross-links to the stiffness of Arion subfuscus glue*. Journal of Experimental Biology, 2013. **216**(8): p. 1475-1483.
240. Fernandez, J.G., et al., *Direct bonding of chitosan biomaterials to tissues using transglutaminase for surgical repair or device implantation*. Tissue Engineering Part A, 2017. **23**(3-4): p. 135-142.
241. Gent, A., *Adhesion and strength of viscoelastic solids. Is there a relationship between adhesion and bulk properties?* Langmuir, 1996. **12**(19): p. 4492-4496.
242. Hutchinson, J.W. and Z. Suo, *Mixed mode cracking in layered materials*, in *Advances in applied mechanics*. 1991, Elsevier. p. 63-191.

243. Stefanov, T., et al., *Mechanical bulk properties and fracture toughness of composite-to-composite joints of an elastomer-toughened ethyl cyanoacrylate adhesive*. International Journal of Adhesion and Adhesives, 2016. **68**: p. 142-155.
244. Sun, M., et al., *Hydrogel Interferometry for Ultrasensitive and Highly Selective Chemical Detection*. Advanced Materials, 2018: p. 1804916.
245. Macron, J., et al., *Equilibrium and Out-of-Equilibrium Adherence of Hydrogels against Polymer Brushes*. Macromolecules, 2018.
246. Sudre, G., et al., *Reversible adhesion between a hydrogel and a polymer brush*. Soft Matter, 2012. **8**(31): p. 8184-8193.
247. Fessenden, R.J. and J.S. Fessenden, *Organic Chemistry*. 2nd ed. 1982, Boston: Willard Grant Press.
248. Thoumie, P. and E. Mevellec, *Relation between walking speed and muscle strength is affected by somatosensory loss in multiple sclerosis*. Journal of Neurology, Neurosurgery & Psychiatry, 2002. **73**(3): p. 313-315.
249. McKee, C.T., et al., *Indentation versus tensile measurements of Young's modulus for soft biological tissues*. Tissue Engineering Part B: Reviews, 2011. **17**(3): p. 155-164.
250. Truby, R.L., et al., *Soft Somatosensitive Actuators via Embedded 3D Printing*. Advanced Materials, 2018: p. 1706383.
251. Bai, R., et al., *Slow crack of hydrogels with complex rheology*. In preparation.
252. Yang, J., et al., *Slow debonding of soft layered materials*. In preparation.
253. Tang, J., et al., *Fatigue fracture of hydrogels*. Extreme Mechanics Letters, 2017. **10**: p. 24-31.
254. Zhang, E., et al., *Fatigue fracture of nearly elastic hydrogels*. Soft matter, 2018. **14**(18): p. 3563-3571.
255. Wiederhorn, S., *Influence of Water Vapor on Crack Propagation in Soda-Lime Glass*. Journal of the American Ceramic Society, 1967. **50**(8): p. 407-414.
256. Wiederhorn, S. and L. Bolz, *Stress corrosion and static fatigue of glass*. Journal of the American Ceramic Society, 1970. **53**(10): p. 543-548.
257. Michalske, T.A. and S.W. Freiman, *A molecular interpretation of stress corrosion in silica*. Nature, 1982. **295**(5849): p. 511.
258. Cai, J. and L. Zhang, *Rapid dissolution of cellulose in LiOH/Urea and NaOH/Urea aqueous solutions*. Macromolecular Bioscience, 2005. **5**(6): p. 539-548.
259. Rivlin, R. and A. Thomas, *Rupture of rubber. I. Characteristic energy for tearing*. Journal of Polymer Science, 1953. **10**(3): p. 291-318.

260. Kong, H.J., et al., *Controlling rigidity and degradation of alginate hydrogels via molecular weight distribution*. *Biomacromolecules*, 2004. **5**(5): p. 1720-1727.
261. Nemir, S., H.N. Hayenga, and J.L. West, *PEGDA hydrogels with patterned elasticity: Novel tools for the study of cell response to substrate rigidity*. *Biotechnology and bioengineering*, 2010. **105**(3): p. 636-644.
262. Qaqish, R.B. and M.M. Amiji, *Synthesis of a fluorescent chitosan derivative and its application for the study of chitosan-mucin interactions*. *Carbohydrate Polymers*, 1999. **38**(2): p. 99-107.
263. Li, J., et al., *Hybrid hydrogels with extremely high stiffness and toughness*. *ACS Macro Letters*, 2014. **3**(6): p. 520-523.
264. Roche, E.T., et al., *Comparison of biomaterial delivery vehicles for improving acute retention of stem cells in the infarcted heart*. *Biomaterials*, 2014. **35**(25): p. 6850-6858.
265. Morgan, C.E., et al., *Development and validation of 4 different rat models of uncontrolled hemorrhage*. *JAMA surgery*, 2015. **150**(4): p. 316-324.
266. Gaharwar, A.K., et al., *Shear-thinning nanocomposite hydrogels for the treatment of hemorrhage*. *ACS nano*, 2014. **8**(10): p. 9833-9842.
267. Chollakup, R., et al., *Phase behavior and coacervation of aqueous poly (acrylic acid)-poly (allylamine) solutions*. *Macromolecules*, 2010. **43**(5): p. 2518-2528.
268. Nagy, P.I. and P.W. Erhardt, *On the interaction of aliphatic amines and ammonium ions with carboxylic acids in solution and in receptor pockets*. *The Journal of Physical Chemistry B*, 2012. **116**(18): p. 5425-5436.